HIGH PERFORMANCE CONCRETE IN WASHINGTON STATE SR18/SR516 OVERCROSSING:

FINAL REPORT ON GIRDER MONITORING

Paul Barr
Marc Eberhard
John Stanton
Bijan Khaleghi
J.C. Hsieh

Washington State Transportation Center (TRAC)
University of Washington, JD-10
The University District Building
1107 N.E. 45th Street, Suite 535
Seattle, Washington 98105-4631

Washington State Department of Transportation
Technical Monitors
Tom Roper and Myint Lwin
Bridges and Structures Engineer

Prepared for

Washington State Transportation Commission
Department of Transportation
and in cooperation with
U.S. Department of Transportation
Federal Highway Administration

December 2000

Table of Contents

List of figures

Number Page

List of TABLES

Number Page

Acknowledgments

The authors wish to thank the Washington Department of Transportation and the Federal Highway Administration for providing funding for this project. Central Pre-mix Co. provided valuable logistical assistance and provided access to their fabrication plant. The authors also wish to thank Barry Brecto (FHWA), Myint Lwin (WSDOT), Tom Roper (WSDOT), Ray Shaefer (WSDOT), Keith Anderson (WSDOT), Chuck Ruth (WSDOT) and Chuck Prussack (Central Pre-Mix Co.) for all the support during the project.

SUMMARY

The Federal Highway Administration has developed a program to encourage the use of High-Performance Concrete (HPC) in bridges. As part of that program, the University of Washington and the Washington State Department of Transportation investigated the long-term behavior of a High-Performance Concrete (HPC) pretensioned concrete girder bridge. This report provides results from the program of girder design, and three years of monitoring and evaluation. A companion report provides results of the materials testing program (Barr et al. 2000a).

The Washington State Department of Transportation (WSDOT) builds many precast, pretensioned concrete girders, largely because this form of construction is very economical, thanks to the excellent aggregates that are available locally, and the competitive nature of the precast industry. Pretensioned girders can be made stronger by using more prestressing steel, but this in turn necessitates that the concrete be stronger. The stronger girders offer several potential benefits, such as shallower girders for a given span, longer spans with a given girder size, or fewer girder lines in a bridge of given size. In the latter case, the cost per girder may increase slightly, but the total initial cost of the bridge is expected to decrease compared with bridges made of conventional concrete.

The prestressing force in a girder under service conditions is significantly lower than the initial jacking force, because losses occur due to elastic shortening, creep, shrinkage and relaxation. Accurate prediction of these losses, and thus the final prestressing force, is an important step in the design of any prestressed concrete girder; this prediction assumes even greater importance in a highly stressed HPC girder.

The bridge used for this study is located near Kent, WA, and carries the eastbound lanes of SR 18 over SR 516. The bridge has three spans, of 24, 42 and 24 m (80, 137 and 80 ft), five lines of girders and a skew of 40°. The girders are WSDOT W74MG pretensioned I-girders, and the deck is 190-mm (7.5-inch) thick, cast-in-place composite. The prestressing force was supplied by forty 15-mm (0.6-in.) diameter strands in the longer girders (Span 2) and by fourteen strands in the shorter ones (Spans 1

and 3). The girders were designed as simply supported, but significant continuity steel was supplied at the interior pier supports. The girders were designed for zero bottom tension under full service load. WSDOT engineers believed that the small incremental cost of this conservative design easily warranted its adoption.

Using seven girders, WSDOT could have satisfied all of the design requirements with conventional concrete. To meet the design requirements for the long span using only five girders, it was necessary for WSDOT to specify a nominal concrete compressive strength of 51 MPa (7400 psi) at release of prestress and 69 MPa (10,000 psi) at 56 days. A suitable mix was developed by the precast fabricator, Central Premix Prestress Co. of Spokane, Washington.

A 6-m (20-ft) long test girder was cast in December 1996 in order to provide the fabricator with experience in handling the HPC. The test girder casting also provided the researchers with an opportunity to evaluate various specimen preparation procedures and to install instrumentation under field conditions. The test girder was designed so that the stress conditions at midspan would be the same as those at midspan of a long bridge girder. The bridge girders were cast during March and April of 1997. They were transported and erected in May 1997, and the deck was cast in September 1997. The time between the girder erection and deck casting was longer than had been scheduled, but it provided an opportunity to take relatively long-term strain and deflection readings on the bare girders.

The primary instrumentation was designed to record temperatures, strains and cambers in the girders. During casting, additional instrumentation was used to measure strand slip-back, from which the transfer length of the strands could be estimated. Two stress gages were installed in the test girder on an experimental basis, but their subsequent use was rejected, because they were too sensitive to temperature variations.

Embedded Vibrating-Wire Strain Gages (VWSGs) were used to measure concrete strains. They were chosen on the basis of their long-term stability and durability, and the fact that they contain an integral thermistor for measuring temperature as well as strains. They were installed in a standard pattern at ten locations on the bridge; the midspan and

at 1.5 m (5 ft) from one end of each of the instrumented girders. The standard pattern consisted of six gages over the height of the girder and two more in the slab above the girder. Several gages were also installed at other selected locations.

Midspan cambers were recorded using two methods. An automatic recording system, based on a wire stretched between the girder ends and a midspan displacement sensor (an LVDT), was developed and installed on three long girders and three short ones. Supplementary readings were taken with a surveyor's level in the fabricator's yard and, when possible, at the bridge site. The automatic system was plagued by damage in the fabricator's yard and by vandalism on site. Thus the records from that system are far from complete. However, a modified, more robust system worked well on site. The surveyor's level readings provided an independent measure of camber, but these measurements were inevitably intermittent. Both methods provide approximately ± 1 mm. (0.04") accuracy on site and somewhat worse in the yard.

Results suggest that the general performance of the HPC Bridge is similar to that expected of comparable bridges made from conventional concrete. The bridge is performing well under service loads.

The slip-back of the strands showed considerable scatter but implied a transfer length between 50 and 100 strand diameters, compared with the 60 predicted by the AASHTO equations (1994). Nineteen of the twenty-four measurements exceeded the transfer length estimated with the AASHTO equation. The slip-back readings could only be taken over a period of about one hour during destressing, so they do not include the effects of "creep slipback," which has been reported by others. Thus, the true transfer length probably exceeds that reported here.

The thermistors in the VWSGs showed that the concrete temperature during curing varied by approximately 25 °C (45°F) over the girder height. The concrete was coldest, and therefore presumably weakest, at the bottom. The reason for this variation is believed to be that the girders were cast out of doors during the winter when the freezing ground acted as a heat sink. The fabricator installed at mid-height of the girder a thermocouple that was connected to a "sure-cure" cylinder curing system. This

observation is significant, because the prestressing release time was based on the strength of concrete at mid-height, rather than at the bottom flange of the girder, where the stress was highest and the concrete was weakest.

In general, strains recorded in the field are frequently susceptible to errors and to large scatter. However, those recorded here are believed to be reliable, because they satisfy several consistency criteria. They are similar in similar girders, and they vary consistently over the height of the girders. Moreover, the relative magnitudes of the strains among the girders are consistent with the relative magnitudes among the measured cambers.

Several methods for estimating prestress losses have been proposed in the literature. The total losses computed from the measured strains are, in general, similar to those implied by the AASHTO and PCI equations for prestress losses. However, this agreement is not a result of the methods accurately predicting each individual component. Instead, the total changes compared well, because some predictions were too low (e.g., elastic shortening) and others were too high (e.g., creep and shrinkage, relaxation and deck casting).

The prestress losses due to some sources that are not usually accounted for, such as deck casting and differential shrinkage, were also considered in the predictions made here. In particular, the effect of shrinkage of the deck concrete on available prestressing force is more complex than usually assumed. For example, girder-to-girder continuity can reverse the direction of the prestress force change due to deck shrinkage.

CHAPTER 1

INTRODUCTION

1.1 CONTEXT

The American Concrete Institute defines High-Performance Concrete (HPC) as "concrete that meets special performance and uniformity requirements that cannot always be obtained using conventional ingredients, normal mixing procedures, and typical curing practices" (Goodspeed et al., 1996). These requirements may include the following enhancements: (1) easier placement and consolidation, (2) high early strength, (3) better long-term mechanical properties, (4) increased resistance to abrasion, (5) better volume stability and (6) longer life in severe environments.

The use of High-Performance Concrete can be a step towards further improving the durability of our nation's bridges. Of the 596,047 bridges listed in the National Bridge Inventory (NBI) in 1997, 18% were identified as structurally deficient (NBI 1997). It was estimated that more than 400 billion dollars would be needed just to replace the existing deteriorated bridges in the United States highway system (NBI 1997). Some bridges built with conventional concrete and located in severe environments have not proven to be durable. The use of HPC for the deck and substructure of future bridges would increase durability, resulting in longer life and decreased-long term maintenance costs.

In the case of precast, prestressed girder bridges, the availability of high-strength concrete would enable engineers to design longer span lengths, increased girder spacings and therefore, fewer girders and shallower sections. The longer spans would permit the use of fewer supports, which could improve traffic safety, especially where the bridge is built at locations that are already congested. Increased girder spacings would decrease fabrication, transportation and erection costs. If girders were shallower, it would be possible to increase underpass clearances or lower embankment heights.

1.2 CHALLENGES TO THE IMPLEMENTATION OF HPC

Despite the apparent benefits of using High Performance Concrete, there are reasons why it has not yet been widely used in prestressed members.

Current methods for calculating prestress losses, such as those advocated by the American Association of State Highway and Transportation Officials (AASHTO 1994) and the Precast Prestressed Concrete Institute (PCI 1975), were based on the observed behavior of conventional concrete, with strengths usually below 41.4 MPa (6000 psi). In particular, several equations for calculating prestress losses are empirically related to concrete strength. Because incorrect calculations of prestress losses can lead to unacceptable service performance, these losses need to be predicted accurately.

The appropriateness of applying current design methods to High-Performance Concrete needs to be evaluated. For example, elastic shortening and creep are two major components of the total prestress loss. Because an HPC girder will almost certainly be more highly stressed than one made with conventional concrete, those components will probably be higher. It is unknown whether this difference in prestress loss is adequately predicted by present methods of analysis.

The use of larger-diameter strand with HPC has also been an area of concern for designers. Compared with lower strength concrete, the use of HPC permits additional prestressing force to be used. To obtain this force in a standard girder shape with standard strand spacing without inducing excess congestion, larger-diameter strands must often be used. However, in 1988 the Federal Highway Administration (FHWA) placed a moratorium on the use of 15 mm (0.6 inch) diameter strand for pretensioned applications because of uncertainties in its bond properties. In May 1996, based on preliminary studies at the University of Texas (Russel and Burns 1997) on the transfer and development length of the 15 mm (0.6 inch) strand, the FHWA permitted the use of 15 mm (0.6 inch) diameter strands at 51 mm (2 inch) spacings. The current design equations for transfer and development length were based on smaller, 13 mm (0.5 inch) diameter

strands. Whether they are universally applicable for the 15 mm (0.6 inch) diameter strands remains an open question.

Precast fabricators also have concerns about the economics of HPC. They prefer to produce girders on a 24-hour cycle in order to make the most efficient use of their casting beds and to provide an orderly schedule for their work force. The higher the prestressing force in the girder, the larger must be the concrete compressive strength at release of the prestressing strands. To achieve this higher strength, the precast plants must use a combination of various materials, longer curing times and increased curing rates. Each of these options is likely to increase costs, and some may negatively affect the long-term concrete strength. Many plants already steam-cure conventional concrete to increase the curing rate and remain on a 24-hour cycle. A better understanding of the effects of this heating on HPC is needed.

This report and its companion report (Barr et al. 2000) document a study undertaken to evaluate the benefits and concerns of using HPC.

1.3 SR18/SR516 OVERCROSSING

The FHWA has been encouraging the states to use HPC in bridge applications. Since the Washington State Department of Transportation (WSDOT) was also interested in expanding the use of HPC to structural applications, WSDOT (with sponsorship from the FHWA) designed a new bridge to carry the eastbound lanes of State Route 18 (SR 18) over State Route 516 (SR 516). This HPC bridge has three spans with lengths of 24.4 m, 41.7 m and 24.4 m (80 ft, 137 ft and 80 ft) respectively. The girders were designed to have a release strength of 51 MPa (7,400 psi) and a 56-day compressive strength of 68.9 MPa (10,000 psi). As a result of specifying HPC, WSDOT was able to reduce the number of lines of girders from seven to five.

The roadway deck has a width of 11.6 m (38 ft). The design strength of the deck concrete is only 27.6 MPa (4000 psi), but it has enhanced durability properties due to the use of fly ash and the requirement of a 14-day water cure. The HPC bridge is described

further in Chapter 3. The design and construction of the bridge provided the opportunity to assess the benefits and drawbacks of using HPC.

1.4 RESEARCH OBJECTIVES

In general, the use of HPC in bridge applications is considered an innovative concept. Therefore, the bridges built under the FHWA HPC programs are being monitored and evaluated for satisfactory performance. The research phase of the study focuses on evaluating the effectiveness of using HPC in prestressed precast concrete girders. Specific objectives include:

- Documenting the prestress losses of five bridge girders made with HPC.
- Documenting the camber growth for five bridge girders made with HPC.
- Comparing measured field behavior with that expected according to current design methods.
- Estimating the transfer length for 15 mm (0.6 in.) diameter strands based on slipback displacements measured during fabrication.
- Evaluating the material properties of the HPC.

The first four bulleted items are addressed in this report, while the last item is addressed in a separate report (Barr et al. 2000).

1.5 SCOPE AND ORGANIZATION OF REPORT

The report is organized as follows:

- Chapter 2 describes several methods for calculating prestress losses: the AASHTO, PCI and Modified Rate of Creep methods. In addition to these methods, procedures for calculating changes in prestress due to deck casting, differential shrinkage and intrinsic relaxation are also presented.
- In Chapter 3, the design and fabrication of a 6.1 m (20 foot) long test girder and five HPC bridge girders are described.

- Chapter 4 describes the instrumentation program used to monitor the test girder and bridge girders. The monitoring program for the instrumentation is also presented in this chapter.
- Chapter 5 presents the measured data for the bridge girders. The measurements include strain, camber and temperature time histories. Also presented are the estimates of transfer length, and a chronology of important events during fabrication of the test girder and bridge.
- Chapter 6 focuses on documenting the prestress losses, which were estimated using the measured change in concrete strain of the girders. Creep, shrinkage and elastic shortening losses were calculated from measured strain data at the prestressing centroid. Intrinsic relaxation values were taken from the manufacturer's test data and then converted to prestress loss by a procedure described by Ghali (1994).
- Chapter 7 evaluates the accuracy of a variety of prestress loss equations in predicting the observed prestress losses. Specific methods discussed include the AASHTO and PCI recommended methods.
- Chapter 8 documents the measured camber growth in the bridge girders, and compares this behavior with calculated estimates.
- Chapter 9 summarizes the report and its conclusions.

CHAPTER 2
METHODS FOR ESTIMATING PRESTRESS LOSSES

2.1 INTRODUCTION

The prestressing force in a girder during service is lower than at initial stressing, because losses occur. These stress losses must be estimated when the girder is designed so that, once they are subtracted from the initial prestress force, the remaining strand force will be sufficient to provide the allowable concrete stress during service. The primary sources of these losses are relaxation of the steel, elastic shortening of the concrete when the prestress is applied, and creep and shrinkage of the concrete during the life of the girder. Stress is regained with the addition of load, caused for example, by casting of the deck.

Several methods of estimating prestress losses have been proposed, but many of them were developed in the 1970s. The methods described in this chapter are the PCI General method (PCI 1975), the three AASHTO LRFD methods (AASHTO 1994) and the Modified Rate of Creep Method (Lwin and Khaleghi 1996). These methods are subsequently used in Chapter 3 (girder design), and in Chapter 6 (comparison of observed and measured prestress losses).

Methods for predicting prestress losses can be classified into four groups according to their complexity (Fekete 1997). True lump-sum methods are the crudest and require no knowledge of material properties. Single equation methods use a single equation to predict the ultimate loss, but the coefficients in the equation vary with the material properties and girder geometry. Component methods predict the ultimate loss by calculating explicitly the components of loss due to various causes, such as elastic shortening or creep, based on knowledge of the material properties. Time-step methods use a similar methodology to component methods, but compute the loss at user-selected time intervals. Such methods require as input the time-dependence of the material properties, for which approximations are provided in the absence of material-specific data.

According to this classification system, the AASHTO Lump-Sum Method is a single equation method. AASHTO's description of it as a lump sum method is unfortunate and confusing, since previous editions of the AASHTO Specifications contained a method that is a true lump sum method. The AASHTO Refined Method contains a more detailed estimate of the time-dependent components of loss but does so only for the ultimate condition, and it is therefore a component method. The equations in the AASHTO Refined Method can be made time-dependent by multiplying the ultimate loss by the ratio of loss at any time to total loss at service. This time-dependent approach is not explicitly contained in the AASHTO Specifications, but it was used in this report to investigate the rate of loss throughout time and is identical to the official AASHTO Refined Method at service. It is referred to here as the AASHTO Refined Method. The Modified Rate of Creep Method and the PCI General Method are also related to the AASHTO methods, and are also time-step methods.

None of these methods was developed specifically for HPC. One of the goals of this research was to evaluate the actual prestress losses and to determine the accuracy of current prediction methods. The methods are described in this chapter, but specific values of losses are computed in chapters 3 and 6.

Also discussed in this chapter are procedures for calculating changes in strand stress due to deck casting (Section 2.7) and differential shrinkage (Section 2.8). A procedure to convert relaxation test data at constant strain to relaxation loss in prestressed concrete girders is also presented (Section 2.9). Each of the procedures will be used in subsequent chapters to help compare measured and predicted prestress losses.

2.2 AASHTO LUMP-SUM METHOD

According to the AASHTO LRFD Specification (AASHTO 1994), the total stress loss, Δf_{pTOT}, is given by

$$\Delta f_{pTOT} = \Delta f_{pES} + \Delta f_{pTD} \tag{2.1}$$

where Δf_{pES} = prestress loss due to elastic shortening
Δf_{pTD} = total time-dependent prestress loss.

The elastic shortening loss is given by

$$\Delta f_{pES} = \frac{E_p}{E_{ci}}\left(f_{cgp}\right) \tag{2.2}$$

where E_p = modulus of elasticity of prestressing strand

E_{ci} = modulus of elasticity of concrete at release

f_{cgp} = concrete stress at the center of gravity of the prestressing strand (cgp) directly after transfer

$$= \frac{P_i}{A_g} + P_i \frac{e_p{}^2}{I_g} - \frac{M_g e_p}{I_g} \tag{2.3}$$

P_i = initial prestressing force directly after transfer

$$= A_{ps} 0.7 f_{pu} \tag{2.4}$$

A_g = gross-cross sectional area of girder

e_p = eccentricity of center of gravity of prestressing strand

I_g = gross-section moment of inertia of girder

M_g = self-weight moment of girder

$$= \frac{w_g L^2}{8} \tag{2.5}$$

A_{ps} = cross-sectional area of sum of prestressing strand

f_{pu} = specified tensile strength of prestressing steel

w_g = girder self weight per unit length

L = length of girder

The value of the initial prestressing force, P_i, is really unknown because it depends on the girder and strand properties. The AASHTO Specification (1994) requires the designer to approximate the initial stress (Equation 2.4).

For I-shaped girders that are prestressed with 1860 MPa (270 ksi) grade low-relaxation strands, that contain no mild reinforcement and that have a concrete strength above 41 MPa (6 ksi), the time-dependent losses in Equation 2.1 (creep, shrinkage and relaxation) are approximated by Equation 2.6. This equation predicts a slight reduction in time-dependent losses as concrete strength increases.

$$\Delta f_{pTD} = 230 \, [1 - 0.15 \, (f'_c - 41) / 41] \quad \text{(MPa)} \tag{2.6}$$

2.3 AASHTO REFINED METHOD

The AASHTO Refined Method (AASHTO 1994) is a more detailed procedure than the AASHTO lump-sum method. This method provides procedures to obtain the losses only at service. However, the stress loss throughout time can be obtained by multiplying the individual loss components by the ratio of loss that has occurred at any time over the total loss at the end of service life. This ratio is obtained using the creep and shrinkage coefficients in the AASHTO LRFD Specification (AASHTO 1994) and the procedure for doing so is outlined below.

According to the AASHTO Refined Method, the total stress loss is given by

$$\Delta f_{pTOT} = \Delta f_{pES} + \Delta f_{pRE} + \Delta f_{pSH} + \Delta f_{pCR} \tag{2.7}$$

where the components of the loss are

Δf_{pES} = prestress loss due to elastic shortening

Δf_{pRE} = prestress loss due to relaxation

Δf_{pSH} = prestress loss due to shrinkage

Δf_{pCR} = prestress loss due to creep

The prestress loss due to elastic shortening, Δf_{pES}, is calculated using Equation 2.2. Prestress loss due to shrinkage during service is given by

$$\Delta f_{pSH} = (117.0 - 1.035 \, H) \quad \text{(MPa)} \tag{2.8}$$

where H = relative humidity (%)
Δf_{pSH} = shrinkage loss in MPa

According to Equation 2.8, the stress loss due to shrinkage can range from 117 MPa (17.0 ksi) at 0% humidity to 13.8 MPa (2 ksi) at 100% humidity. Western Washington, where the SR18/SR516 Bridge is located, has an average humidity value of 80% which corresponds to a predicted ultimate stress loss due to shrinkage of 34.5 MPa (5 ksi).

The ultimate shrinkage loss in Equation 2.8 can be made time-dependent by using the relationship in Equation 2.9.

$$\Delta f_{pSH}(t) = \Delta f_{pSH}\left(\frac{\varepsilon sh(t=ti)}{\varepsilon sh(t=\infty)}\right) \tag{2.9}$$

where ε_{sh}= strain due to shrinkage of concrete

$$= -k_s * k_h * \left(\frac{t}{55.0+t}\right) * 0.56x10^{-3}$$

k_s = volume-to-surface ratio factor

$$= \left[\frac{\frac{t}{26*e^{0.36*(v/s)}+t}}{\frac{t}{45+t}}\right]\left[\frac{1064-94*(v/s)}{923}\right]$$

$$= \left[\frac{45+t}{26*e^{(0.36v/s)}+t}\right]\left[1.153+0.102(v/s)\right]$$

t = time in days

v/s = volume-to-surface ratio of girder (76.5 mm for W74MG)

k_h = humidity factor (0.80 for Western Washington)

The time-dependent shrinkage strain is taken from Section 5.4.2.3.3 of the AASHTO LRFD Specifications (AASHTO 1994). The prestress loss due to creep is given by

$$\Delta f_{pCR} = 12.0\, f_{cgp} - 7.0\, \Delta f_{cdp} \quad > 0.0 \tag{2.10}$$

where f_{cgp} = sum of the concrete stresses due to prestressing and the self weight of the girder at the center of gravity of the prestressing strands at mid-span. This stress is considered constant over time.

Δf_{cdp} = change in the concrete stress at the level of the prestressing strands due to the weight of the concrete deck slab, diaphragms and barriers. The term $7.0\, \Delta f_{cdp}$ in Equation 2.10 is an approximate estimate of prestress gain due to dead load of slab, diaphragm and barriers.

The ultimate creep loss in Equation 2.10 can be made time dependent by using the relationship in Equation 2.11, which is taken from Section 5.4.2.3.2 of the AASHTO LRFD Specifications (AASHTO 1994).

$$\Delta f_{pCR}(t) = \Delta f_{pCR} * \left(\frac{\Psi(t)}{\Psi(t = \infty)} \right) \tag{2.11}$$

where $\Delta f_{pCR}(t)$ = prestress loss due to creep at time t

$\Psi(t)$ = creep coefficient

$$= 3.5 * k_c * k_f * \left(1.58 - \frac{H}{120}\right) t_i^{-0.118} \left(\frac{(t - t_i)^{0.6}}{\left(10.0 + (t - t_i)^{0.6}\right)} \right)$$

k_c = factor for volume to surface ratio

$$= \left[\frac{t}{\frac{26 * e^{0.36(v/s)} + t}{\frac{t}{45+t}}} \right] \left[\frac{1.80 + 1.77 * e^{-0.54(v/s)}}{2.587} \right]$$

$$= \left[\frac{45+t}{26 * e^{(0.36 v/s)+t}} \right] \left[0.696 + 0684 * e^{(-0.54 v/s)} \right]$$

k_f = factor for the effect of concrete strength

$$= \frac{1}{0.67 + \left(\frac{f'c}{62} \right)}$$

f'_c = concrete strength at 28 days (MPa)

H = relative humidity in % (80 for Western Washington)

t_i = age of concrete when load is initially applied (days)

t = age of concrete of time interval (days)

v/s = volume-to-surface ratio

The relaxation loss, Δf_{pRE}, is divided into two components. The one that occurs before transfer is given by

$$\Delta f_{pRE} = \log(24*t)/40.0 \, [f_{Pj}/f_{Py} - 0.55] f_{Pj} \qquad (2.12)$$

where t = time in days from stressing to transfer

f_{Pj} = stress in steel directly before transfer

f_{py} = yield strength of the prestressing steel

After transfer, the relaxation is given by

$$\Delta f_{pRE} = 0.30 \, [\, 138 - 0.4 \, \Delta f_{pES} - 0.2(\Delta f_{pSH} + \Delta f_{pCR})] \quad \text{(MPa)} \qquad (2.13)$$

Equation 2.13 is intended to account for the fact that the strand is under continuously decreasing strain, due to creep and shrinkage in the concrete, rather than the constant strain that exists prior to transfer and is considered in Equation 2.12.

2.4 AASHTO TIME-STEP METHOD

The AASHTO Time-Step Method (AASHTO 1994) is similar to the AASHTO Refined Method except that the time-step method is iterative. Although this method is not an official AASHTO Method, it has been proposed as an alternative method (Lwin and Khaleghi 1996). The calculation for the first iteration is exactly the same as the refined method, in which prestress loss values are obtained throughout time. These prestress losses are then used to calculate the prestress force throughout time for the next iteration. The prestressing force is then used to calculate concrete stresses due to prestressing and the self weight of the girder at the center of gravity of the prestressing strands at mid-span (f_{cgp}), except that now, this stress will change over time (Equation 2.3). The prestressing force is calculated at the end of the previous iteration and used in the beginning of the next iteration. Losses generally converge after a few cycles (Lwin and Khaleghi 1996).

2.5 MODIFIED

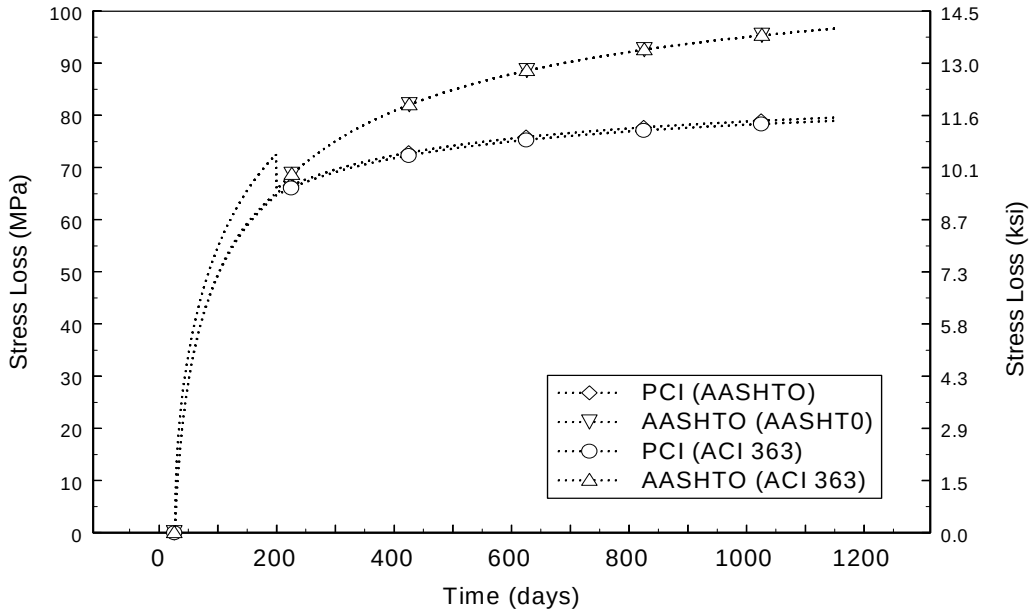

RATE OF CREEP METHOD

The Modified Rate of Creep Method (Lwin and Khaleghi 1996) is another time-step method that takes into account the instantaneous and time-dependent effect of slab casting, and the transition from non-composite to composite cross-section properties. It also includes provision for the effects of differential shrinkage between the slab and girders, and allows for different creep rates before and after slab casting. The rate after slab casting is a weighted average of the slab and girder concrete properties. As with the AASHTO Methods the elastic shortening loss is computed using Equation 2.2. Time-dependent prestress losses using the Modified Rate of Creep Method are given by

$$\Delta f_{pTD} = \Delta f_{pSH} + \Delta f_{pCR1} + \Delta f_{pCR2} + \Delta f_{pRE} - \Delta f_{pEG} - \Delta f_{pCRG} - \Delta f_{pDSH} \qquad (2.14)$$

where Δf_{pTD} = total prestress loss

Δf_{pSH} = prestress loss due to shrinkage

Δf_{pCR1} = prestress loss due to creep of concrete before slab casting

Δf_{pCR2} = prestress loss due to creep of concrete at any time after slab casting

Δf_{pRE} = prestress loss due to relaxation

Δf_{pEG} = prestress gain due to dead load of slab

Δf_{pCRG} = prestress gain due to creep effect of slab casting

Δf_{pDSH} = prestress gain due to differential shrinkage between slab and concrete girder

For non-composite girders, Equation 2.14 may be simplified, and the time-dependent prestress losses may be taken as

$$\Delta f_{pTD} = \Delta f_{pSH} + \Delta f_{pCR1} + \Delta f_{pRE} \qquad (2.15)$$

The prestress loss due to girder shrinkage is computed using Equation 2.9. The prestress loss due to creep is calculated in two stages. Stage 1 is the creep loss between time of transfer and slab casting is given by

$$\Delta f_{pCR1} = n\, f_{cgp}\, \Psi_{t,tisc}\, (1-\Delta F_{SC}/2F_o) \qquad (2.16)$$

Stage 2 is the creep loss for any time after slab casting, which is expressed as

$$\Delta f_{pCR2} = n\, f_{cgp}\, (\Psi_{t,ti}-\Psi_{t,tisc})\, (1-(\Delta F_{SC}+\Delta F_t)/2F_o)\, I_g/I_c \qquad (2.17)$$

where $\Psi_{t,ti}$ = creep coefficient of girder at any time

$\Psi_{t,tisc}$ = creep coefficient of girder at the time of slab casting

ΔF_{SC} = total loss of force at the time of slab casting minus initial elastic shortening loss

F_o = prestressing force at transfer after elastic losses

ΔF_t = total prestressing loss at any time minus initial elastic shortening loss

I_g/I_c = ratio of moment of inertia of prestressed girder to composite girder

n = modular ratio (E_P/E_C)

E_p = modulus of elasticity of prestressing strand

E_c = modulus of elasticity of concrete at 28 days

In the above equations, the terms $\Psi_{t,tisc}(1-\Delta F_{SC}/2F_o)$ and $(\Psi_{t,ti}-\Psi_{t,tisc})(1-\Delta F_{SC}+\Delta F_t)/2F_o)$ take into account the effects of variable stress history from the time of transfer to the time of slab casting, and from slab casting to final conditions, respectively. The term I_g/I_c represents the effect of composite section properties after slab casting.

The AASHTO LRFD Specifications recognize the prestress gain due to the deck weight by the term 7.0 Δf_{cdp} in Equation 2.10. In the Modified Rate of Creep Method, the creep response to slab and diaphragm dead load is treated as a prestress gain. Part of the initial compressive strain induced in the concrete immediately after transfer is reduced by the tensile strain resulting from permanent loads. The prestress gain due to slab dead load consists of two parts. The first part is due to instantaneous elastic

prestress gain. The second part is a time-dependent creep effect. Prestress gain due to elastic and creep effect of slab casting is given as

$$\Delta f_{pEG} = n_{SC}\, f_{S+D} \tag{2.18}$$

$$\Delta f_{pCRG} = n_{SC}\, f_{S+D}\, (\Psi_{t,ti} - \Psi_{t,tisc})\, I_g/I_c \tag{2.19}$$

where Δf_{pEG} = gain in prestress from elastic response to superimposed dead load.

Δf_{pCRG} = gain in prestress from to creep response to superimposed dead load.

n_{SC} = modular ratio at the time of slab casting;

f_{S+D} = stress in concrete at the level of prestressing strands due to dead load of slab and diaphragms.

In composite prestressed girders bridges, the concrete in the girder is steam-cured while the concrete in the slab is usually cast-in-place and moist-cured. Slab concrete is also cast at a later time, when the girders are already in place. Due to differences in the concrete properties, curing processes and times of casting, the Modified Rate of Creep Method predicts a prestress gain due to differential shrinkage. This gain in prestressing force is given by

$$\Delta f_{pDS} = n_{SC}\, f_{CD} \tag{2.20}$$

where f_{CD} = concrete stress at the level of prestressing strands

$=[\Delta\varepsilon_{S\text{-}G}\, A_{cSLAB}\, E_{cSLAB} / (1 + \Psi_{t,ti})]\, (y_{CS}\, e_c / I_c)$

$\Delta\varepsilon_{S\text{-}G}$ = differential shrinkage strain;

A_{cSLAB} = area of concrete deck slab;

E_{cSLAB} = modulus of elasticity of slab;

y_{CS} = distance between the c.g. of composite section to the c.g. of slab;

e_c = eccentricity of prestressing strands in composite section;

I_c = moment of inertia of composite section.

The denominator $(1 + \Psi_{t,ti})$ is meant to approximate the long-term creep effect.

2.6 PCI GENERAL METHOD

The Precast Concrete Institute (PCI) Committee on Prestress Losses (PCI 1975) recommends two methods for calculating the change in prestress. The General Method is a time-stepping method that computes the total loss in stress in the prestressing strand as the sum of the separate components, over discrete time steps.

$$\Delta f_{pTOT} = \Delta f_{pANC} + \Delta f_{pES} + \sum_{t} (\delta f_{pSH} + \delta f_{pCR} + \delta f_{pRE}) \tag{2.21}$$

where Δf_{pANC} = change in prestress due to anchorage slip

Δf_{pES} = change in prestress due to elastic shortening

δf_{pCR} = incremental change due to creep of concrete

δf_{pSH} = incremental change due to shrinkage of concrete

δf_{pRE} = incremental change due to relaxation of prestressing steel

Δf_{pANC} and Δf_{pES} are one-time changes, whereas δf_{pCR}, δf_{pSH} and δf_{pRE} are time-dependent and are calculated for each time step. In pretensioned construction, Δf_{pANC} is not applicable and Equation 2.21 is reduced to Equation 2.22.

$$\Delta f_{pTOT} = \Delta f_{pES} + \sum_{t} (\delta f_{pSH} + \delta f_{pCR} + \delta f_{pRE}) \tag{2.22}$$

Instantaneous elastic shortening loss is calculated by

$$\Delta f_{pES} = (E_p/E_{ci})*f_{cgp} \tag{2.23}$$

where f_{cgp} = concrete stress at the center of gravity of the prestressing strand (cgp) directly after transfer.

E_P = modulus of elasticity of prestressing strand

E_{ci} = initial modulus of elasticity of concrete

This equation is identical to that contained in the AASHTO LRFD Specification (AASHTO 1994), but PCI does not approximate the prestressing force after transfer (Equation 2.4). The PCI General Method (PCI 1975) uses an iterative calculation to

compute f_{cgp} and Δf_{pES}. However a direct calculation is also possible which can be used in place of the iterative procedure (Equation 2.24).

$$f_{cgp} = +\frac{f_{pj}A_{ps}}{A_t}\left[1+\frac{e_{pt}^{\,2}}{r_t^{\,2}}\right]-\frac{M_{sw}e_{pt}}{I_t} \tag{2.24}$$

where f_{pj} = stress in prestressing strand immediately before transfer

A_{ps} = area of prestressing strand

A_t = transformed cross-sectional area of girder

e_{pt} = eccentricity of center of gravity of prestressing strand (c.g.p.) using transformed section properties

r_t = radius of gyration of girder using transformed cross section

$$= \sqrt{\frac{I_t}{A_t}}$$

I_t = gross-section moment of inertia of girder using transformed section

M_{sw} = self-weight moment of girder

$$= \frac{w_g L^2}{8}$$

The incremental change of prestress due to shrinkage over any time interval is described by

$$\delta_{pSH} = (USH)(SSF)(PSH) \tag{2.25}$$

where USH = ultimate change in stress due to shrinkage

SSF = size and shape factor

PSH = portion of ultimate shrinkage during a given time interval

The ultimate change in stress due to shrinkage is

$$USH = 186 - 0.003E_c \leq 83 \qquad (2.26)$$

where E_c is the 28-day elastic modulus of the concrete in MPa.

Equation 2.26 is illustrated in Figure 2.1. The equation suggests a link between the ultimate shrinkage stress and the elastic modulus rather than the concrete strength. A possible explanation lies in the fact that both shrinkage and elastic modulus depends on the paste content of the concrete. The lowest value of stress loss due to shrinkage that may be obtained, prior to the application of the volume-to-surface ratio, is 83 MPa (12 ksi).

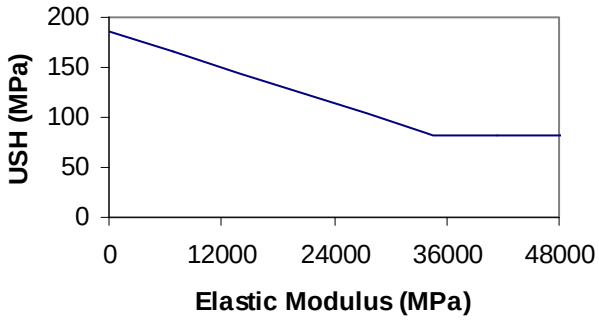

Figure 2.1 Ultimate Prestress Change Due to Shrinkage (USH)

The size and shape factor is determined using Table 2.1 (PCI 1975). SSF has the value 1.0 for a 152 x 304 mm (6 x 12 inch) cylinder with sealed ends, which has a volume-to-surface ratio of 38 mm (1.5 inches). The use of the factor SSF implies that the volume-to-surface (v/s) ratio influences the total shrinkage at infinite time, rather than the rate of shrinkage. The concept of shrinkage caused by diffusion and evaporation of moisture from the sample suggests the opposite. The reasons for the apparently anomalous choice in the PCI General Method are unknown.

Table 2.1. Size and Shape Factor for Shrinkage (SSF)

V/S (mm)	SSF
25	1.04
50	0.96
75	0.86
100	0.77
125	0.69
150	0.60

The portion of ultimate shrinkage during a given time step is calculated using Equation 2.27.

$$PSH = (AUS)_t - (AUS)_{t_1} \tag{2.27}$$

AUS is the variation of shrinkage with time provided in Table 2.2. Linear interpolation should be used for values between those listed. Times t_1 and t are the beginning and end of the interval, respectively, in days. The fact that AUS is based on the time since the end of curing suggests that it addresses only drying shrinkage and ignores basic shrinkage. Tabular values are inconvenient for automation of the procedure. A good fit to the tabulated data is given by Equation 2.28 and a comparison is listed in Table 2.2.

$$AUS(t) = 1.0 - e^{-0.0918t^{0.5159}} \tag{2.28}$$

Table 2.2. Shrinkage Coefficients (AUS)

Time after curing (Days)	AUS (PCI)	AUS (Eq. 2.31)
1	0.08	0.09
3	0.15	0.15
5	0.20	0.19
7	0.22	0.22
10	0.27	0.26
20	0.36	0.35
30	0.42	0.41
60	0.55	0.53
90	0.62	0.61
180	0.68	0.74
365	0.86	0.85
End of Service life	1.00	1.00

The incremental change in prestress due to creep over a time interval, δf_{pCR} , is directly related to the stress in the concrete at the end of the previous time interval.

$$\delta f_{p,CR} = (UCR)(SCF)(MCF) \times (PCR)(f_c) \tag{2.29}$$

where UCR = ultimate change in prestress due to creep
SCF = size and shape factor for creep
MCF = factor for age of moist cured concrete at transfer
PCR = portion of ultimate creep during a given time interval
f_c = net concrete compressive stress at the c.g.p. at the end of the previous time interval

The ultimate change in prestress due to creep for accelerated-cured concrete is given by

$$UCR = 434 - 0.002E_C \geq 76 \quad \text{(MPa)} \tag{2.30}$$

The size and shape factor for creep is provided in Table 2.3 as a function of the volume-to-surface ratio of the member in millimeters (PCI 1975). The values vary from those given for shrinkage by a maximum of 0.01. That such a difference is considered

justifiable is surprising in the light of the scatter and sensitivity commonly found in creep and shrinkage tests.

Table 2.3. Size and Shape Factor for Creep

V/S (mm)	SCF
25	1.05
50	0.96
75	0.87
100	0.77
125	0.68

The portion of the ultimate creep during a given time step is

$$PCR = (AUC)_t - (AUC)_{t_1} \tag{2.31}$$

AUC is the variation of creep with time after application of the prestress force, given in Table 2.4. The 7-day data point of 0.23 does not lie on a smooth curve with the other data and is probably a mis-print. Linear interpolation is used to determine the value for times between those listed. Times t_1 and t are as described above. Again, an equation to express the data in Table 2.4 is desirable for automation purposes. Equation 2.32 provides an acceptable curve fit.

$$AUC = 1.0 - e^{-0.1t^{0.438}} \tag{2.32}$$

Table 2.4. Variation of Creep (AUC) with Time

Time after prestress (Days)	AUC (PCI)	AUC (Eq. 2.36)
1	0.08	0.09
3	0.15	0.15
5	0.18	0.18
7	0.23	0.21
10	0.24	0.24
20	0.30	0.31
30	0.35	0.36
60	0.45	0.45
90	0.51	0.51
180	0.61	0.62
365	0.74	0.73
End of Service life	1.00	1.0

The relaxation contribution to the total change in prestress for low-relaxation steel is

$$\delta f_{pRE} = f_p \left\{ \left[\frac{\log 24t - \log 24t_1}{45} \right] \times \left[\frac{f_p}{f_{py}} - 0.55 \right] \right\} \qquad (2.33)$$

where $\frac{f_p}{f_{py}} \geq 0.60$

f_p = stress in the prestressing steel at the end of the previous interval taking into account all previous changes in stress

f_{py} = the yield strength of the prestressing steel

= 0.90 f_{pu}

f_{pu} = the ultimate strength of the prestressing steel

If the ratio of applied stress to yield strength of the prestressing strand is less than 0.60, it is assumed that no relaxation occurs, and the incremental change in prestress for that time interval is equal to zero. For the first interval, the time of anchorage, t_1, is

assumed to be 1/24 day (1 hour). It should also be noted that Equation 2.33 leads to different ultimate values of change in stress due to relaxation if time steps, rather than a single calculation over the lifetime of the girder, are used. However, the total change due to relaxation is typically so small in low-relaxation strand that the difference has little practical importance.

2.7 DECK CASTING

The preceding sections have described methods for calculating prestress losses that have been formalized in codes or in the technical literature. These methods fail to address issues associated with the deck, such as the moment due to self weight of the deck and differential shrinkage. These issues are discussed in sections 2.7 and 2.8. For a simply supported girder, the expected change in strand stress due to deck casting can be calculated as

$$\Delta f_{pDECK} = \Delta f_{cDECK}\left(\frac{E_p}{E_c}\right) \tag{2.34}$$

where Δf_{pDECK} = change in strand stress due to deck casting

Δf_{cDECK} = change in concrete stress due to deck casting

$$= \frac{M_{DC} e_{pt}}{I_t}$$

M_{DC} = moment due to self weight of deck

$$= \frac{w_{DC} L^2}{8}$$

e_{pt} = distance from neutral axis to centroid of the prestressing strand using transformed properties

w_{DC} = self weight of deck

L = length of girder

I_t = moment of inertia of girder of transformed section (girder and reinforcement)

E_p = modulus of elasticity of the prestressing strand

E_c = modulus of elasticity of concrete

Here the subscript 't' refers to properties of the transformed concrete section, calculated taking into account the transformed area of the prestressing strands but without the deck. For simplicity, the gross section properties are usually used in place of the transformed-section properties.

At the time of deck casting, the SR18/SR516 Bridge was not truly simply supported. A one-foot high strip of concrete was placed over each of the pier caps connecting the bottom flanges of the girders from the various spans. A two-degree-of-freedom model of a typical, symmetric, three-span bridge was developed to investigate whether this strip of concrete could partially restrain the girders. This model is shown in Figure 2.2.

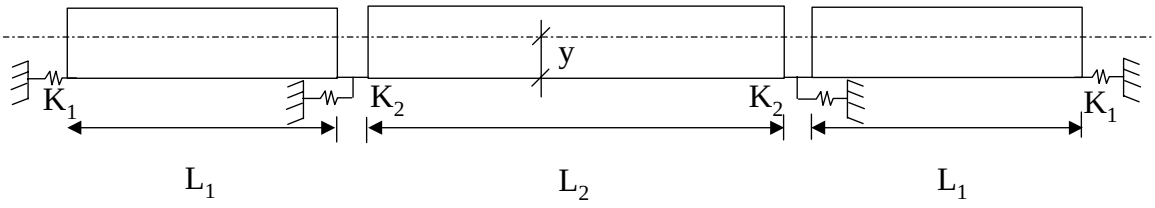

Figure 2.2. Two-Degree-of-Freedom Model of Bridge

L_1 and L_2 in Figure 2.2 are the span lengths of the girders. The horizontal stiffnesses of the bearing and column are K_1 and K_2 respectively. The symbol y represents the distance from the cgc of the girder to the location about which the girders rotate. If the two-degree-of-freedom system is solved for a uniform load on all three spans, the midspan moments caused by deck casting can be calculated using Equation 2.35, in which underlined properties represent matrices.

$$\underline{M} = \underline{M_o} - y^2 \underline{K}\underline{B}\underline{A}^{-1}\underline{\theta}_o \qquad (2.35)$$

where $\underline{M}$ = the midspan moments in girders 1 and 2

$$= \begin{bmatrix} M_1 \\ M_2 \end{bmatrix}$$

$\underline{M}_o$ = the simply supported moments due to the self weight of the slab

$$= \begin{bmatrix} \frac{wL_1^2}{8} \\ \frac{wL_2^2}{8} \end{bmatrix}$$

$$\underline{K} = \begin{bmatrix} K_1 & 0 \\ K_1 & K_2 \end{bmatrix} = \begin{bmatrix} \frac{GA_b}{h_b} & 0 \\ \frac{GA_b}{h_b} & \frac{3E_{col}I_{col}}{L^3_{col}} \end{bmatrix}$$

$$\underline{B} = \begin{bmatrix} 2 & 1 \\ 0 & 1 \end{bmatrix}$$

$$\underline{A} = \begin{bmatrix} 1+\frac{K_1L_1y^2}{3E_gI_g} & \frac{K_1L_1y^2}{2E_gI_g} \\ \frac{K_1L_2y^2}{2E_gI_g} & 1+\frac{(K_1+K_2)L_2y^2}{2E_gI_g} \end{bmatrix}$$

$$\underline{\theta}_o = \begin{bmatrix} \frac{w_{DC}L_1^3}{24E_gI_g} \\ \frac{w_{DC}L_2^3}{24E_gI_g} \end{bmatrix}$$

y = distance from the neutral axis to the location about which the girder rotates

w_{DC} = weight of the deck

G = shear modulus of elasticity of bearing

A_b = cross sectional area of bearing

h_b = thickness of rubber in bearing

E_{col} = modulus of elasticity of column

E_g = modulus of elasticity of girder

I_{col} = moment of inertia of column

I_g = moment of inertia of girder

L_{col} = length of column

2.8 DIFFERENTIAL SHRINKAGE

Stress loss due to shrinkage of composite, prestressed concrete girders comes from two sources: (1) shrinkage of the girder concrete and (2) shrinkage of the deck concrete. The deck concrete is usually placed a few months after the girder concrete has already been cast, so the rate of creep and shrinkage of the girder concrete has significantly decreased at this time. However, the deck concrete has yet to experience its shrinkage. The effect of differences between the shrinkage strain of the deck concrete and the shrinkage strain of the girder concrete is termed differential shrinkage. The effects of differential shrinkage for a simply supported girder and a continuous girder are illustrated in Figure 2.3 and are explained in this section.

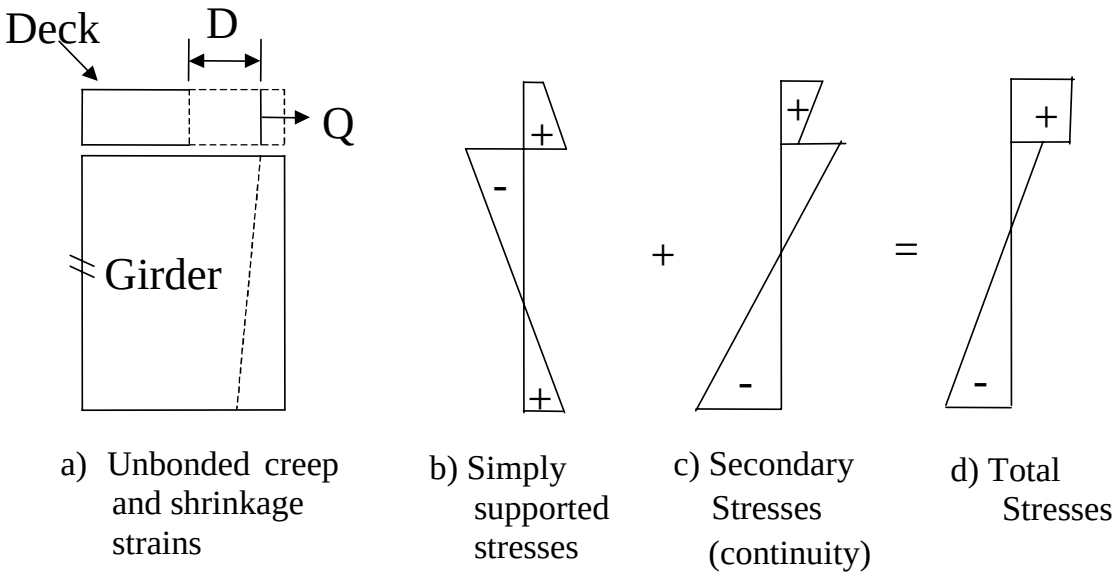

Figure 2.3. Differential Shrinkage Stresses

The effect of differential shrinkage on concrete stress is first calculated for the basic case of elastic assumptions and a statically determinate girder (Section 2.8.1). The calculations are then extended to account for creep and for continuity (Section 2.8.2). The procedure followed to calculate the change in prestress due to differential shrinkage is described in Section 2.8.3.

2.8.1 Statically-Determinate Girders

The effect of differential shrinkage can be estimated by superimposing two load cases. In the first case, fictitious restraint forces are applied to the deck (at its centroid) to inhibit shrinkage-induced displacements. This fictitious force is calculated as

$$Q_d = -A_d E_d \varepsilon_{sh} \tag{2.36}$$

where Q_d = restraint force

A_d = cross-sectional area of deck

E_d = modulus of elasticity of deck concrete

ε_{sh} = free shrinkage strain

In this case, the strain is zero in the deck and girder, but the stress in the deck is equal to $-\varepsilon_{sh} E_d$. The deck and girder are assumed to be attached in shear, without slip, prior to any deck shrinkage. The total shrinkage of the girder may be ignored for these purposes, because it causes only a shortening of the composite system and, in the case of a girder that is not restrained by its supports from translating, no forces are introduced. Thus only the difference in shrinkage strains between the deck and girder concrete needs to be applied to the deck.

This restraint force (Q_d) cannot exist in practice so in the second load case, an equal and opposite force is applied to the composite deck and girder system at the level of the centroid of the deck. This force causes an axial strain at the composite centroid and a curvature given by

$$\varepsilon_a = \frac{-Q_d}{(EA)_{comp}} \tag{2.37}$$

$$\phi = \frac{-Q_d e_d}{(EI)_{comp}} \tag{2.38}$$

where ε_a = axial strain at centroid of composite system caused by differential shrinkage

$(EA)_{comp}$ = axial stiffness of composite system

ϕ = curvature of composite system caused by differential shrinkage

e_d = distance from centroid of composite system to centroid of deck

$(EI)_{comp}$ = flexural stiffness of composite system

By superimposing the two load cases, the stress in the deck at a vertical location y is

$$f_c(y) = E_d(-\varepsilon_{sh} + \varepsilon_a + \phi y) \tag{2.39}$$

and the stress in the girder is

$$f_c(y) = E_g(\varepsilon_a + \phi y) \tag{2.40}$$

where E_g = Young's modulus of girder concrete

$f_c(y)$ = stress at vertical location y due to deck shrinkage

y = vertical coordinate

The sign convention used in Equations 2.36 to 2.40 is that all distances are measured positive downwards from the centroid of the composite system, and that tension stress and strain are positive. Thus, for example, e_d and ε_{sh} are both negative quantities. The stress distribution for the simply supported girder is shown in Figure 2.3b.

In the previous calculations, girder shrinkage was neglected, because in general, it will be small. Most of this shrinkage has already occurred by the time the deck was cast. One could include girder shrinkage by replacing ε_{sh} with $\varepsilon_{sh} - \varepsilon_{shgirder}$, where $\varepsilon_{shgirder}$ is the girder shrinkage.

In practice, some creep will occur over time and will reduce the stresses induced by the differential shrinkage. The stresses are induced in the girder when the concrete in it is relatively old, so the girder creep is likely to be significantly less than the deck creep. If the girder creep is ignored, the calculations in Equations 2.36 to 2.39 can be modified to account for deck creep by using an age-adjusted modulus, E_{adj}, in place of E_d, where $E_{adj} = E_d/(1+C_c)$, and C_c = creep coefficient.

2.8.2 Secondary Stresses

If the girder is continuous, additional stresses are induced as a result of the secondary moments that are generated in the girder. The secondary moment in a three-span girder (with equal end spans) can be calculated as follows

$$M'_{DS} = \lambda Q_d e_d \tag{2.41}$$

where M'_{DS} = secondary moment

$$\lambda = \frac{L_1 + L_2}{\left(\frac{2}{3}L_1 + L_2\right)}$$

= 1.14 for the SR18/SR516

L_1 = length of spans 1 and 3

L_2 = length of Span 2

The secondary stresses (f_{csec}) in the deck, shown in Figure 2.3c, at a vertical location y are

$$f_{c\,sec}(y) = \frac{M'_{DS}\, y}{I_c}\left(\frac{E_{adj}}{E_g}\right) \tag{2.42}$$

and the secondary stress in the girder is

$$f_{c\,sec}(y) = \frac{M'_{DS}\, y}{I_c} \tag{2.43}$$

where f_{csec} = stress due to secondary moment

I_c = moment of inertia of composite section

The total change in concrete stress resulting from differential shrinkage that is induced in a composite girder is the sum of the simply supported stresses (Equations 2.39 and 2.40) and the secondary moment stresses (Equations 2.42 and 2.43) respectively.

2.8.3 Change in Prestress

The change in prestress due to differential shrinkage is calculated as

$$\Delta f_{pDS} = \Delta f_{cgpDF}\frac{E_p}{E_g} \tag{2.44}$$

where Δf_{pDS} = change in prestress due to differential shrinkage

Δf_{cgpDS} = change in concrete stress at cgp due to differential shrinkage

$$= E_g\left(\varepsilon_a + \phi e_p\right) + \frac{M'_{DS}\, e_p}{I_c}$$

e_p = distance from neutral axis to center of gravity of prestressing strand

E_p = modulus of elasticity of prestressing strand

ϕ = curvature (Equation 2.38)

2.9 REDUCED RELAXATION COEFFICIENT

In a prestressed girder, the strain in the prestressing strand reduces due to creep and shrinkage in the girder concrete. This reduction in strain leads to a reduction in strand stress. Therefore the relaxation in a prestressed girder should therefore be smaller than the intrinsic relaxation of the strand. This reduced relaxation value can be estimated using Equation 2.45 (Ghali 1994).

$$\Delta \bar{f}_{p,RE} = \chi_r \Delta f_{p,RE} \tag{2.45}$$

where $\Delta \bar{f}_{p,RE}$ = reduced relaxation value

χ_r = reduction coefficient

$$= \int_0^1 (1 - \Omega\xi) \left(\frac{\lambda(1 - \Omega\xi) - 0.4}{\lambda - 0.4} \right)^2 d\xi$$

$$\Omega = \frac{\Delta f_{p,CRSH}(t) - \Delta f_{p,RE}}{f_{pe}}$$

Δf_{pCRSH} = change in strand stress due to creep and shrinkage

f_{pe} = effective prestressing force

$$\lambda = \frac{f_{pe}}{f_{pu}}$$

f_{pu} = characteristic tensile strength of prestressing strand

The concept for this reduction coefficient was developed in 1978 (Ghali et al. 1978) when low-relaxation strand was not readily available and relaxation represented a significant proportion of the total loss. The low-relaxation strand that is widely used today leads to lower relaxation losses, in which case, the reduction coefficient is less important.

CHAPTER 3
DESIGN AND CONSTRUCTION OF THE HPC GIRDERS FOR THE SR18/SR516 BRIDGE

3.1 TEST GIRDER

Prior to fabricating the girders for the SR18/SR516 Bridge, which was to be monitored, a 6.1-m (20-ft) long test girder was fabricated, both for the precaster to gain experience with using the new HPC concrete mix and for the researchers to gain experience installing the instrumentation under field conditions. The Washington W74MG girder cross-section was selected for the test girder in order to match the bridge girders. Its cross-section is shown in Figure 3.1. Table 3.1 lists the cross-sectional properties of the W74MG test girder.

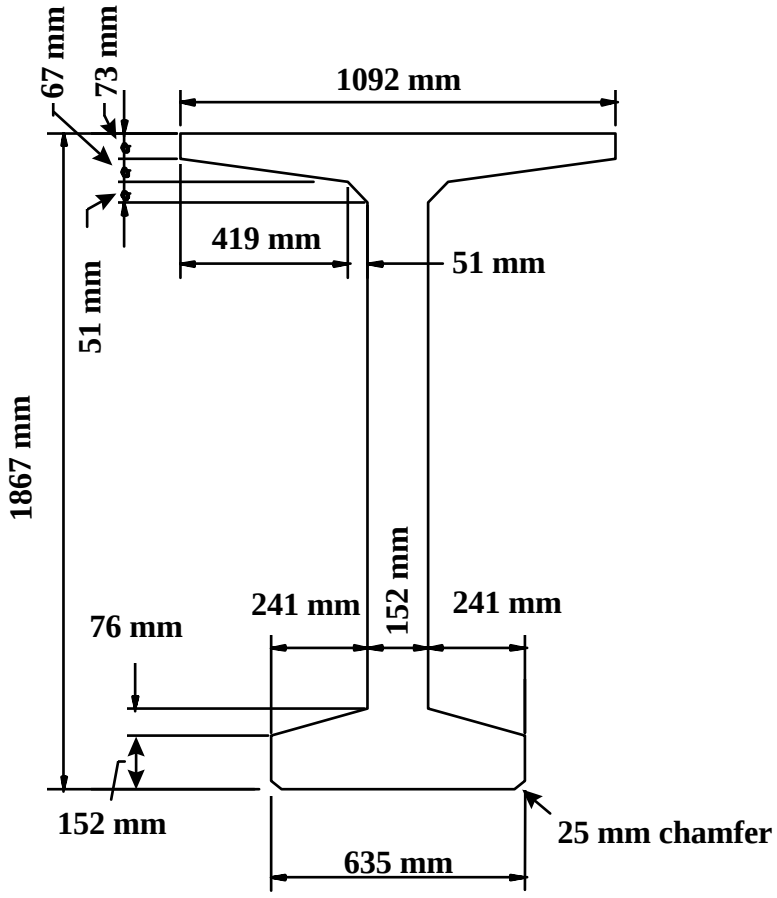

Figure 3.1. W74MG Girder Dimensions

Table 3.1. W74G Cross-Section Properties

Property	I (mm^4)	A (mm^2)	Y_t (mm.)	Y_b (mm)	S_{top} (mm^3)	S_{bot} (mm^3)
Value	227.5 (10^9)	485300	895	970	254.3 (10^6)	234.4 (10^6)

The test girder was prestressed with 15 mm (0.6 inch) diameter, 1860 MPa (270 ksi) strands. The tendon profile was designed so that the midspan stress profiles of the test girder and the long bridge girders would be the same at release. The strands were straight in the test girder because the self-weight moment was less than 1% of the prestressing moment. Table 3.2 lists the design details for the test girder. The distances from the bottom of the girder to the center of gravity of the web strands and the bottom flange strands are labeled $W_{C.G.}$ and $B_{C.G.}$ respectively. Figure 3.2 provides an elevation view of the test girder, showing the centroids of the web and flange prestressing strands.

Table 3.2. HPC Test Girder Design Details

Property	Skew	Length (m)	56-day f'c (MPa)	Release f'c (Mpa)	No. of Web Strands	Jacking Force (KN)	No. of Bot. Strands	Jacking Stress (MPa)	$W_{C.G.}$ (mm)	$B_{C.G.}$ (mm)
Value	0°	6.10	68.9	51.0	14	2710	26	1400	851	85.7

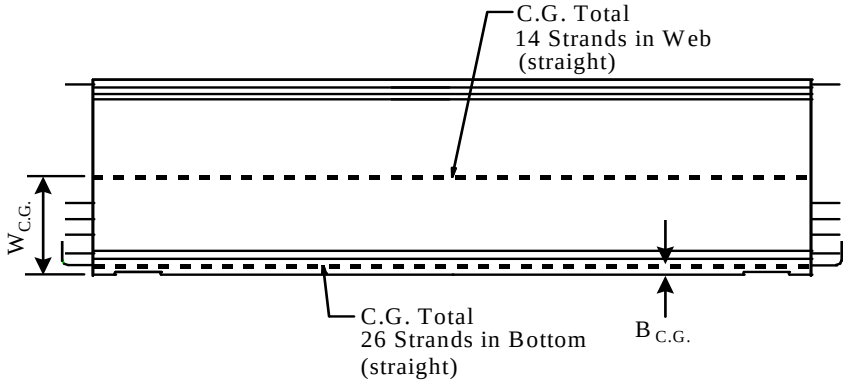

Figure 3.2. Elevation of Test Girder

The Grade 60 (420 MPa) mild reinforcing steel in the test girder was placed in the same locations as in the bridge girders. This placement provided the researchers with the

opportunity to practice installing the instrumentation in a region containing tightly-spaced reinforcing steel. Figure 3.3 shows the mild steel reinforcement for the test girder. In this figure, dimensions are shown in US Customary Units (1 in. = 25.4 mm).

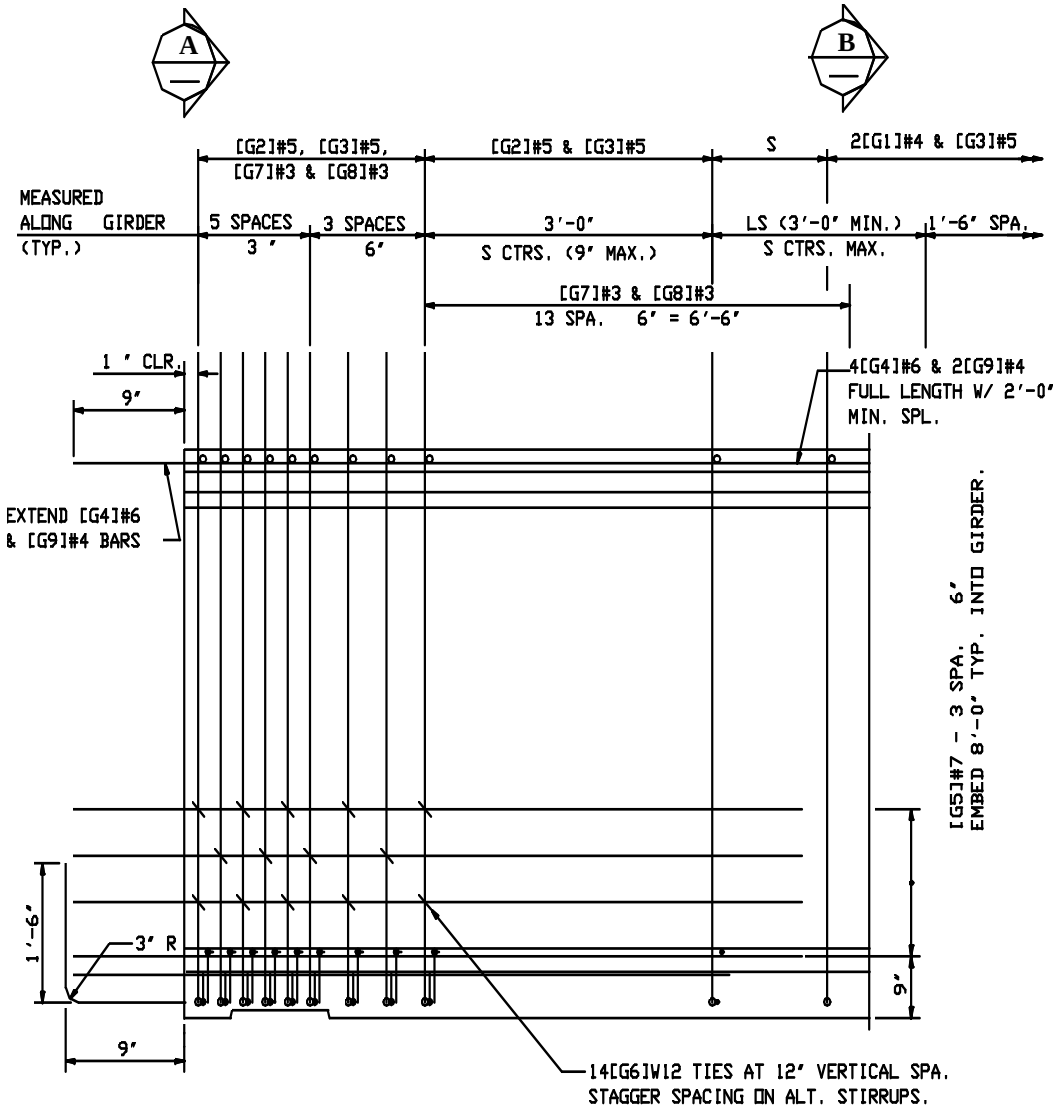

Figure 3.3. Test Girder Mild Reinforcing Steel

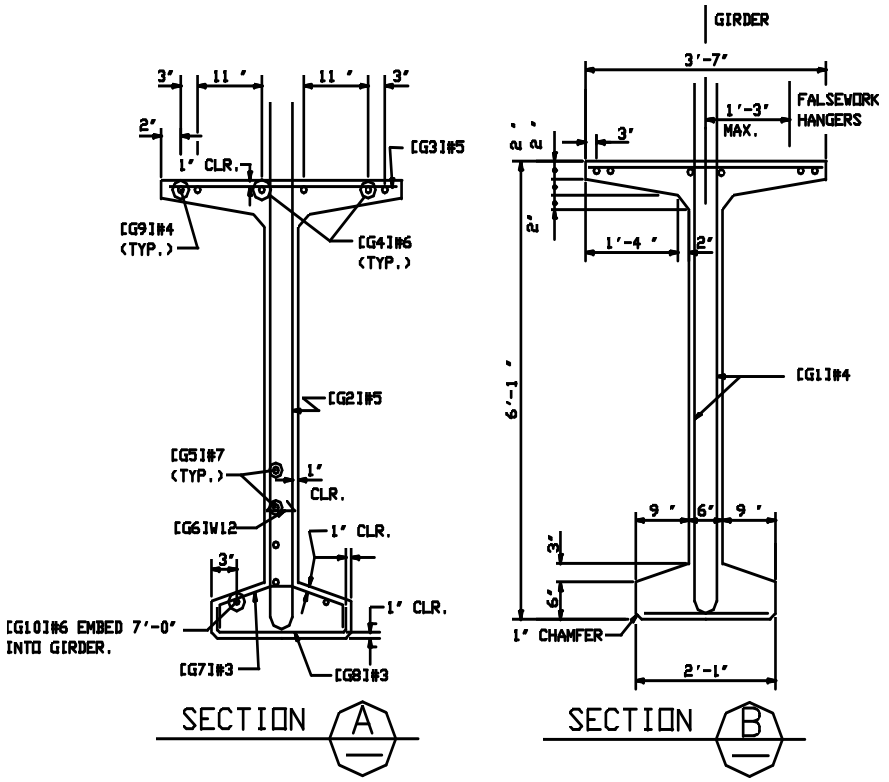

BENDING DIAGRAM

ALL DIMENSIONS ARE OUT TO OUT

MARK	LOCATION	SIZE	
G1	GIRDER STIRRUPS	4	
G2	GIRDER END STIRRUPS	5	
G3	GIRDER TOP FLANGE	5	STR.
G4	GIRDER LONGIT. FULL LENGTH	6	STR.
G5	GIRDER END LONGIT.	7	STR.
G6	GIRDER END TIES	W12	
G7	GIRDER END TIES	3	
G8	GIRDER END TIES	3	
G9	GIRDER LONGIT. FULL LENGTH	4	STR.
G10	GIRDER LONGIT.	6	STR.

= VARIES FOR SKEWED SPANS

#3 OR #4 MAY BE SUBSTITUTED FOR W12, FIELD BENDING IS OPTIONAL.

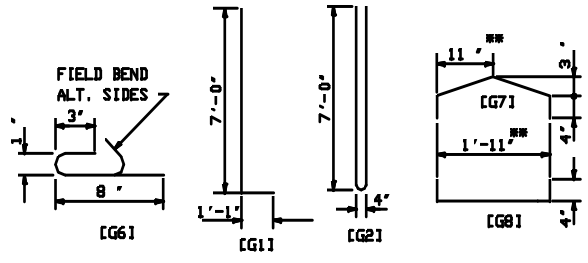

Figure 3.3. Test Girder Mild Reinforcement Steel (cont.)

The test girder was cast outside in a casting yard at Central Premix Prestress Co, Spokane, WA. The strand for the test girder was stressed during the afternoon of Dec 11, 1996. The instrumentation was installed that night, and the concrete was cast on the morning of December 12, 1996. The ambient temperature lay in the range -5°C to +5°C during the stressing and casting. After casting the concrete, an insulating blanket was placed over the girder form to contain the heat generated by hydration and added steam. The fabricator embedded a thermocouple 1.52 meters (5 feet) from one end at approximately midheight of the girder, in order to regulate the application of steam to the girder. The concrete was allowed to cure for 29 hours, after which the forms were removed and the strands were destressed.

After destressing, the test girder was placed on timber blocks until it was shipped to the University of Washington campus on January 4, 1997. The Test Girder was stored outside the Structural Research Laboratory on the north side of the building, in order to replicate, as closely as possible, the environmental conditions of the bridge girders.

3.2 BRIDGE GIRDERS

Figure 3.4 shows a layout of the bridge and the girder numbering system. Each girder line is denoted by a letter (A-E), and each span, by a number (1-3). Figure 3.5 shows a section through the bridge at Pier 2.

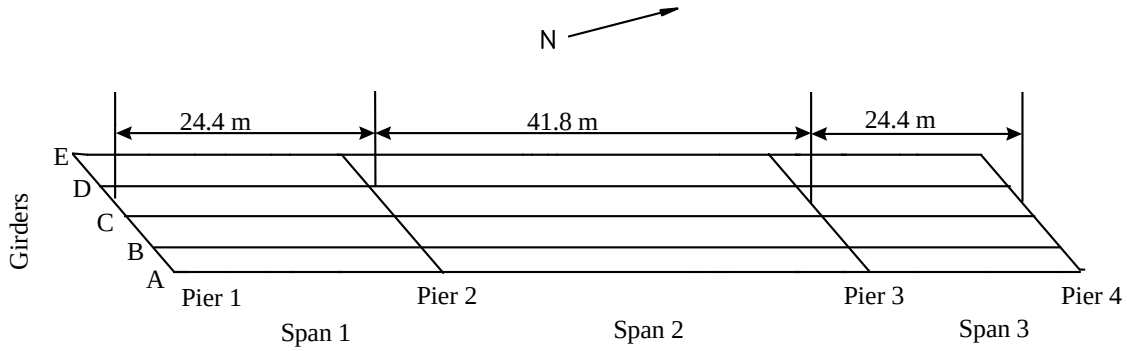

Figure 3.4. Bridge Layout

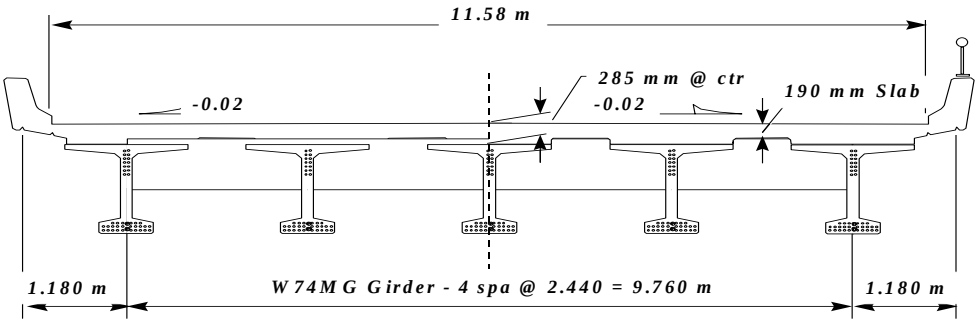

Figure 3.5. Bridge Cross-Section at Pier 2 (looking north)

Fifteen bridge girders were fabricated for the three-span bridge. Ten had spans of 24.4 m (80 ft), and five had spans of 41.8 m (137 ft). The Washington W74MG cross-section, shown in Figure 3.1, was used for all girders. In the field, the girders were made composite with the 190 mm (7.5 in.) deck slab, which included a 10 mm (0.4 in.) integral wearing surface. Table 3.3 lists section properties for the girder and for the girder-slab composite section. The composite properties were computed assuming that the slab lay directly on the top of the girder. In fact, WSDOT made provisions for a pad up to 95 mm (2.75 inches) thick, as shown in Figure 3.5, between the girder and slab to accommodate differential camber between girders. Thus the true composite properties were in most cases larger than the minimum values given in Table 3.3. The arrangement of mild reinforcing steel for the bridge girders was similar to that of the test girder, shown in Figure 3.3.

Table 3.3. Cross-Section Properties

	W74MG Girder	Composite Section
depth, mm	1865	2055
Area, mm^2	485300	765100
I, mm^4	227.5×10^9	400.4×10^9
y_b, mm	970	1 330
S_b, mm^3	234.4×10^6	301.0×10^6
y_t girder, mm	895	535
S_t girder, mm^3	254.3×10^6	748.8×10^6
y_t slab, mm	-	715
S_t slab, mm^3	-	560.2×10^6

Each bridge girder contained both harped web strands and straight bottom flange strands. The web strands were harped at a distance of 0.4 times the length from each end. Figure 3.6 shows an elevation of one half of one of a bridge girder with the tendon strand profile. The web strands were splayed from the harping point, where they were bundled, and the strands were spaced vertically at 51 mm (2 inches) at the girder end.

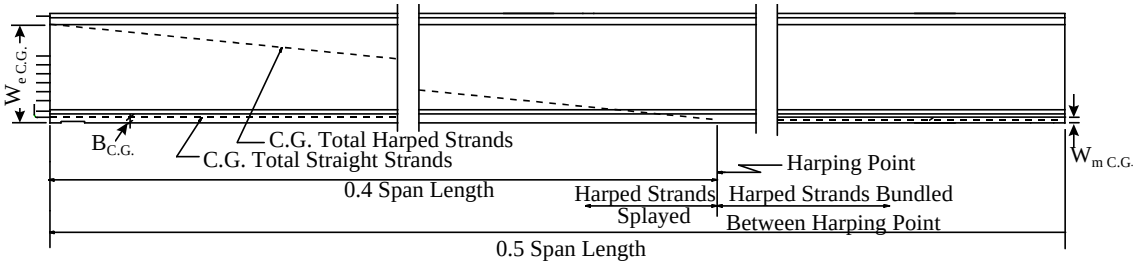

Figure 3.6. Elevation of Bridge Girders

Table 3.4 lists the design details for the bridge girders. The distances from the bottom of the girder to the center of gravity of the harped web strands at the end and at midspan are labeled $W_{e\ C.G.}$ and $W_{m\ C.G.}$ respectively. The location of the center of gravity of the bottom strands is labeled $B_{C.G.}$. For the long girders, 14 harped and 26 straight strands were used.

Table 3.4. HPC Bridge Girders Design Details

Girder	Skew	Length (m)	56-day f'c (MPa)	Release f'c (MPa)	No. of Harped Strands	No. of Straight Strands	Jacking Stress (MPa)	$W_{m\ C.G.}$ (mm)	$W_{e\ C.G.}$ (mm)	$B_{C.G.}$ (mm)
Span 1	40°	23.3	68.9	34.5	6	8	1400	76.2	1360	47.6
Span 2	40°	40.6	68.9	51.0	14	26	1400	85.7	1130	85.7
Span 3	40°	23.3	68.9	34.5	6	8	1400	76.2	1360	47.6

Table 3.5 summarizes time-dependent prestress losses at midspan for the interior long girders predicted by various AASHTO and Modified Rate of Creep methods discussed in Chapter 2, assuming that $f_{pi} = 0.7f_{pu}$. The elastic losses are identical, because they are all calculated with Equation 2.2. The long-term losses from the AASHTO Time-Step method are lower than the ones obtained from the AASHTO LRFD Refined Method, because the Time-Step method is based on effective prestress force rather than the initial force at transfer. Prestress losses computed from the Modified Rate of Creep Method are lower than those obtained from other methods. The WSDOT selected the Modified Rate of Creep Method as the basis for the design.

Table 3.5. Predicted Time-Dependent Prestress Losses (MPa)

	AASHTO Lump Sum	AASHTO Refined	AASHTO Time-step	Modified Rate of Creep
Transfer	159.2	159.2	159.2	159.2
Before Slab Cast.	-	238.5	227.3	197.3
After Slab Cast.	-	232.5	214.2	175.8
Final	348.2	376.1	327.5	283.5

The final midspan and harping point service stresses at the top (f_t) and bottom (f_b) of the girder predicted using the Modified Rate of Creep Method are summarized in Table 3.6. The concrete stresses at transfer are not shown, but they also satisfy the requirements of the AASHTO Specifications. Girder deflections predicted by the

Modified Rate of Creep Method are presented in Table 3.7. WSDOT does not allow any tension in its girders under service conditions.

Table 3.6. Summary of Predicted Concrete Stresses at Service

	At Midspan			At Harping Point		
Stress Type (MPa)	f_b	f_t(girder)	f_t(slab)	f_b	f_t(girder)	f_t(slab)
Girder	10.15	-9.35	-	9.74	-8.98	-
Slab + haunch	12.26	-11.30	-	11.77	-10.85	-
Diaphragm	1.41	-1.30	-	1.27	-1.17	-
Traffic barrier	1.85	-0.74	-0.99	1.77	-0.71	-0.95
ΣDL	25.67	-22.69	-0.99	24.55	-21.71	-0.95
LL - Service I	-	-4.73	-6.33	-	-4.58	-6.12
LL - Service III	9.42	-	-	9.11	-	-
Prestressing	-35.98	8.66	-	-35.98	8.66	-
Total Stress under permanent load	-	-14.03	-0.99	-	-13.04	-0.95
Allowable	-	-31.05	-12.60	-	-31.05	-12.60
Total Stress under all loads	-0.89	-18.76	-7.32	-2.32	-17.62	-7.07
Allowable	0.00	-41.40	-16.80	0.00	-41.40	-16.80

Note: Tension (+)

Table 3.7. Predicted Girder Deflection

	Total Deflection (mm)
At Transfer	-80
Before Slab Casting	-107
After Slab Casting	-56
Final	-44

The long girders were cast individually on a 61.0 m (200 ft) long casting bed. After they were cast, the bed was reconfigured and the short girders were cast in it, end-to-end, in pairs. The steam curing arrangements were the same as in the Test Girder except that, in Girder 2B, the thermocouple was located approximately 508 mm

(20 inches) above the bottom. The curing time varied among the instrumented girders. Table 3.8 lists the critical events and times for each of the instrumented bridge girders.

Table 3.8. Fabrication Schedule for Bridge Girders

Girder	Instrumentation Installation Date	Casting Date	Destressing Date	Time to Start of Destress (Hours)
2A	3/5/97	3/6/97	3/7/97	28.25
2B	3/9/97	3/10/97	3/11/97	25
2C	3/11/97	3/12/97	3/13/97	24
1A	4/1/97	4/2/97	4/3/97	24.25
1C	4/1/97	4/2/97	4/3/97	24.25

After destressing, the girders were placed on timber supports in the yard, where they remained until the shipping date. During this time, finishing work was performed on the girders. Strain and camber readings were taken automatically and without interruption until April 29 when the instrumentation was removed for shipping. The girders for spans 1 and 2 were shipped on May 7, and the girders for Span 3 were shipped on May 8.

The girders were erected during the night following the day they were shipped. During the next five months, work was done on the bridge at the contractor's convenience. During this time, the forms for the intermediate diaphragms, pier caps and soffit were erected. The intermediate diaphragms were cast over a 10-day period between July 14 and July 23, and the deck was cast on September 23, 1997.

CHAPTER 4
INSTRUMENTATION PROGRAM

Instrumentation was installed in both the Test Girder (Section 4.1) and in bridge girders 1A, 1C, 2A, 2B and 2C (Section 4.2). The instrumentation measured strains, temperature, strand slipback, camber and strand stress.

4.1 TEST GIRDER

The Test Girder was instrumented and monitored to gain experience installing the instrumentation. Results from the Test Girder's instrumentation helped finalize the locations and types of instrumentation that would be used for the bridge girders. Figure 4.1 shows the cross-section of the Test Girder and individual strand locations.

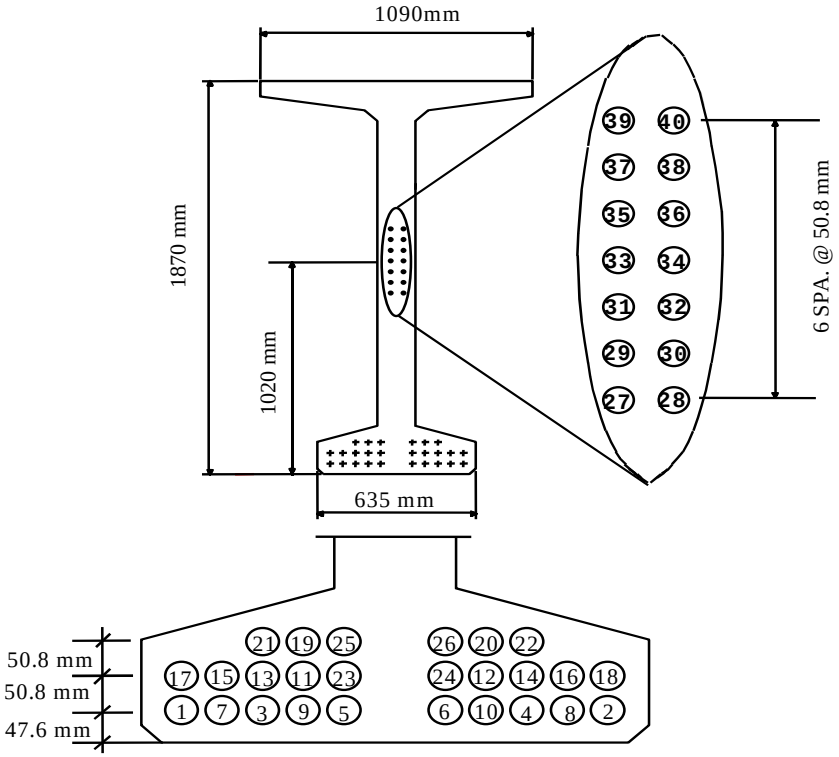

Figure 4.1. Strand Pattern in W74MG Test Girder

4.1.1 Concrete Strains and Temperatures

Vibrating-wire strain gages were embedded in the Test Girder to monitor both temperatures and longitudinal strains. They were selected because of their history of long-term reliability. These gages (Geokon model VCE-4200, 152 mm (6 inch) gage length) were embedded at midspan and 1.52 meters (5 feet) from one end. The layout of the midspan gages is shown in Figure 4.2. The instrumentation layout at the 1.52 meter (5 foot) location was identical to the one at midspan except that the LW and UW gages were omitted. In addition, a vibrating-wire strain gage was embedded in each of two 152 x 305 mm (6 x 12 inch) cylinders to monitor curing temperatures and for gage calibration.

Two vibrating-wire strain gages (BL and BR) were embedded in the bottom flange of the girder. To secure the gages in place, they were attached with nylon cable ties to a 9.53 mm (3/8 inch) diameter U-shaped section of reinforcement. Before casting, the U-shaped reinforcement was tied to the existing prestressed strands within the girder.

At midspan, three gages (LW, MW and UW) were placed at the quarter points over the height of the girder. The gages at midheight of the girder (MW), both at midspan and near the end, were attached to a U-shaped piece of reinforcement and then tied to the prestressing strand in the web of the girder. The remaining two gages (LW and UW) were attached to a welded grid of four pieces of #3 reinforcing bar. Figure 4.3 shows the dimensions of the welded rebar grid. The grids were tied to the vertical stirrups in the girder. The grids made it possible for researchers to attach the gages accurately and fast.

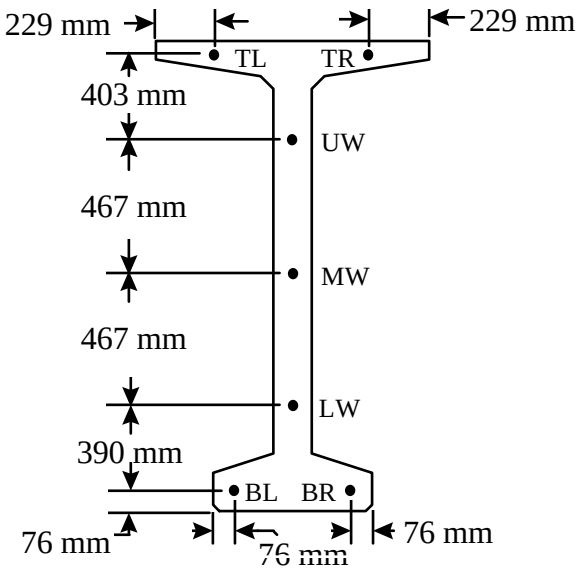

Figure 4.2. Vibrating Wire Strain Gage Nominal Locations

Two vibrating-wire strain gages (TL and TR) were placed in the top flange of the girder at both instrumentation sites. These gages were attached to grids similar to those used in the web (Figure 4.3). The steel grids and gages were placed in the girder by tying them to the girder's horizontal top reinforcement.

After installing the gages, all gage locations were measured to the nearest 3 mm (1/8 inch). The lead wires were then gathered into a bundle, inserted into a section of garden hose for protection, and brought out of the top of the girder. A blockout was formed in the top flange with a section of a 76 mm (3 inch) diameter PVC tube. After the forms were removed, the lead wires from the gages were passed down through the tube and connected to a multiplexer.

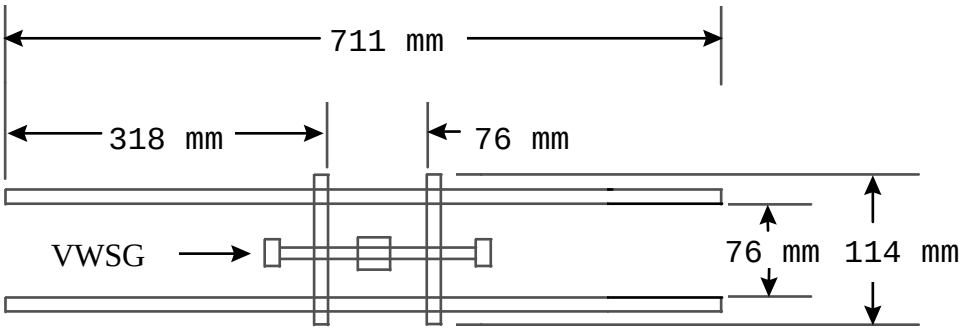

Figure 4.3. Welded Grid Rebar Cage

4.1.2 Strand Slipback

Potentiometers were used to measure the strand slipback as the strand force was transferred to the Test Girder. The goal of this slipback monitoring was to estimate the transfer length. Strand slip measurements were made only at the jacking end, where the strand was released gradually. The slipback could not be measured at the dead end, where the strand was flame cut, without damaging the instruments. After the girder end forms were removed, potentiometers were attached to ten strands, namely strands 1, 2, 13, 14, 25, 26, 27, 32, 35 and 40 (Figure 4.1).

Each potentiometer was preattached to a wooden block that had a 15 mm (0.6 inch) diameter hole drilled longitudinally through the block as shown in Figure 4.4. The block was cut in half, which allowed it to be placed over the prestressing strand, and then the two halves were bolted together. To provide a flat and smooth bearing surface for the potentiometer pistons, a 25.4 mm (1 inch) square piece of sheet metal was attached with epoxy to the face of the Test Girder next to the instrumented strand. The potentiometer, which was attached to the top of the block, read the relative displacement between the strand and the sheet metal. Each potentiometer was wired to a central patch board. Voltage readings were taken after each destressing stage using a digital voltage meter. The voltage readings were then converted into slipback measurements.

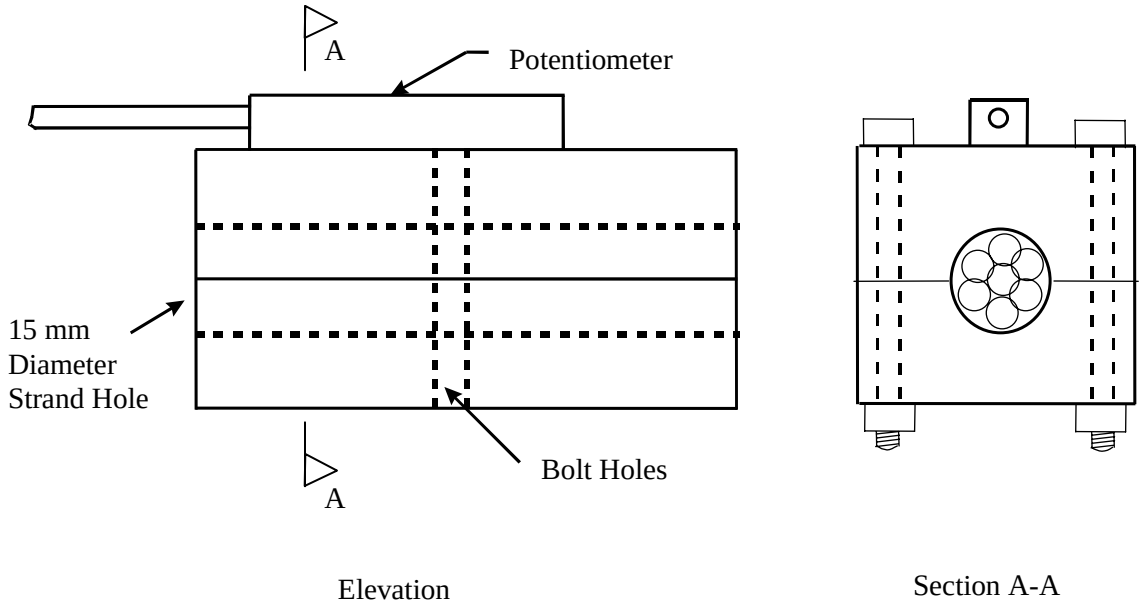

Figure 4.4. Potentiometer and Wooden Block

4.1.3 Girder Camber

A stretched-wire system was used to measure the camber in the Test Girder (Figure 4.5). A bearing pulley was fitted over a bolt through the web at one end of the girder. At the opposite end, a high-strength wire was fixed to another bolt through the girder web. The wire was then placed over the pulley and stressed by hanging a 155 N (35 pound) weight on the wire. At midspan a light trolley ran on two pulley wheels on the stretched wire. The trolley was prevented from falling by a third pulley wheel below the wire and by the fact that its center of gravity lay below the wire. An LVDT attached to a board on the girder web measured the relative vertical displacement between the trolley and the girder web. The trolley was constrained to move only vertically with respect to the girder by installing a drawer-glide vertically on the board and connecting the trolley to the gliding end.

The drawer glide was not really necessary on the Test Girder, but it was installed in order to verify that it would work on the bridge girders, where it would be needed to

prevent horizontal movement of the wire away from the web. Such motion could damage the LVDT plunger, which might subsequently bind.

During design of the stretched-wire system, it was found that pulley friction controlled the accuracy of the system. Only if the pulley were perfectly frictionless would the tension, and thus the midspan sag in the wire, remain constant. High-quality pulleys with sealed roller bearings were thus used in all cases. Figure 4.5 shows an elevation of the Test Girder with the stretched-wire system.

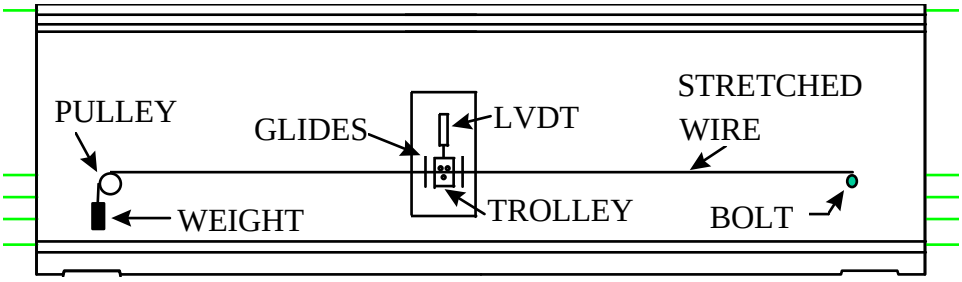

Figure 4.5. Test Girder Stretched Wire System

4.1.4 Concrete Stress

Vibrating-wire stress gages, also supplied by Geokon (VCE 4800), were installed to measure the concrete stress. Two stress gages were placed at midspan, one in the top of the girder and one in the bottom (Figure 4.6). Each stress gage was attached to the vertical stirrups using tie wire. Unfortunately, the gage readings were so strongly influenced by the large change in concrete temperature during curing that they were useless. As a result, such gages were not installed in the bridge girders.

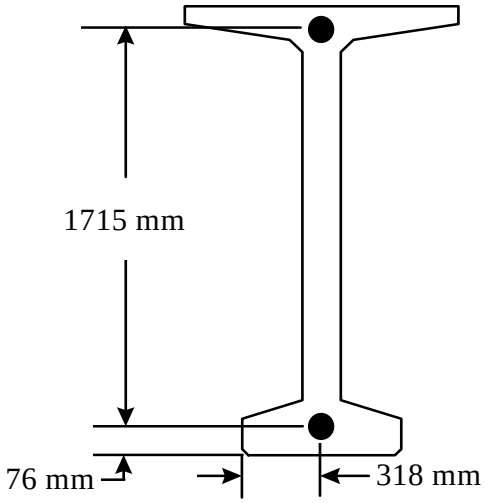

Figure 4.6. Locations of Vibrating Wire Stress Gages

4.1.5 Strand Stress

A load cell was installed by the precaster on strand number 29 (Figure 4.1) to measure the strand stress during fabrication. The load cell was located at the dead end anchorage. Unfortunately, the readings proved unreliable and so were not used in the subsequent analysis.

4.2 BRIDGE GIRDERS

Experience gained during the instrumentation of the Test Girder was used to design the instrumentation in the bridge girders. The system used was similar, but not identical, to that used in the Test Girder.

4.2.1 Concrete Strains and Temperatures

VWSGs were embedded in five of the W74MG bridge girders. In these instrumented girders, gages were embedded both at 1.52 m (5 feet) from the end nearest Pier 2 and 457 mm (18 inches) from midspan towards Pier 2. The gages could not be placed exactly at midspan due to dowel-ducts at midspan, but they were placed within 460 mm (18 inches). Figure 4.7 shows plan and elevation views of the bridge, with the

instrumentation sites marked. Each instrumentation site can be identified by span (1 or 2), girder (A, B or C) and span location (E or M).

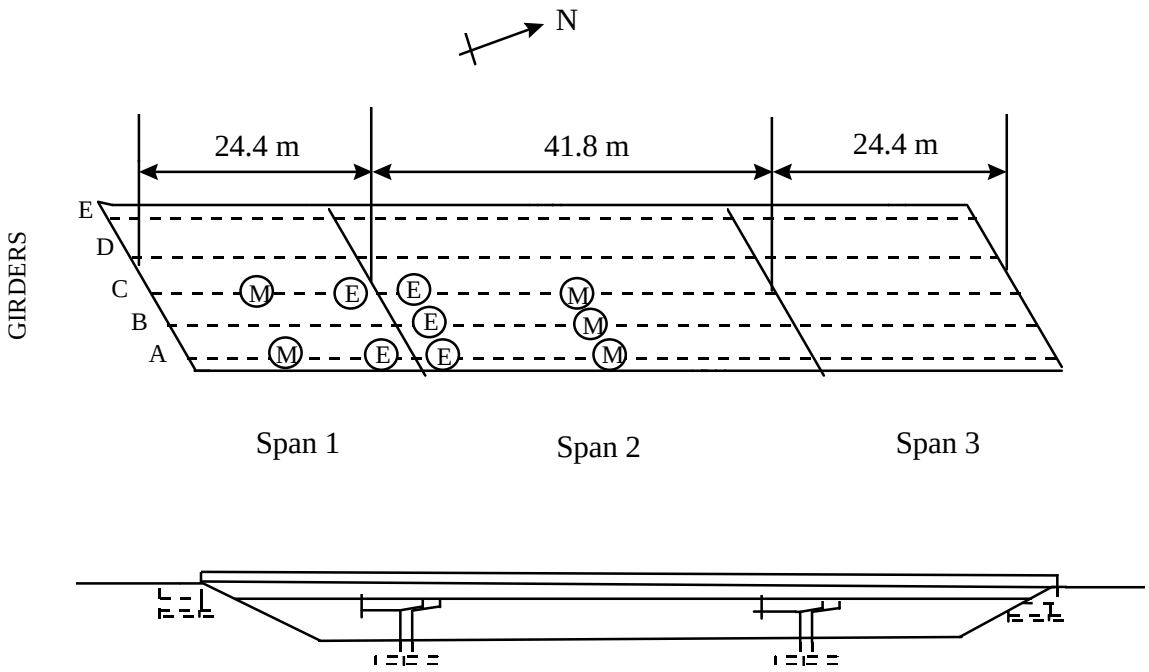

Figure 4.7. Instrumentation Sites in HPC Bridge

Each site was instrumented in the same manner. Figure 4.7 shows the VWSG locations at a typical instrumentation site. In order to speed installation, the gages were pre-attached to welded rebar grids. In the last girders cast, gages LW, MW, UW and TG were all attached to a single grid. This led to fast, accurate gage placement. Two gages were placed in the slab (LS and US). Each of these gages was attached to the deck reinforcing steel. All lead wires were gathered, protected in a short section of garden hose, and run out of the top of the girder. At each instrumentation site, a section of PVC pipe was placed through the top flange to allow lead wires to be passed down through the flange after the girder forms had been stripped.

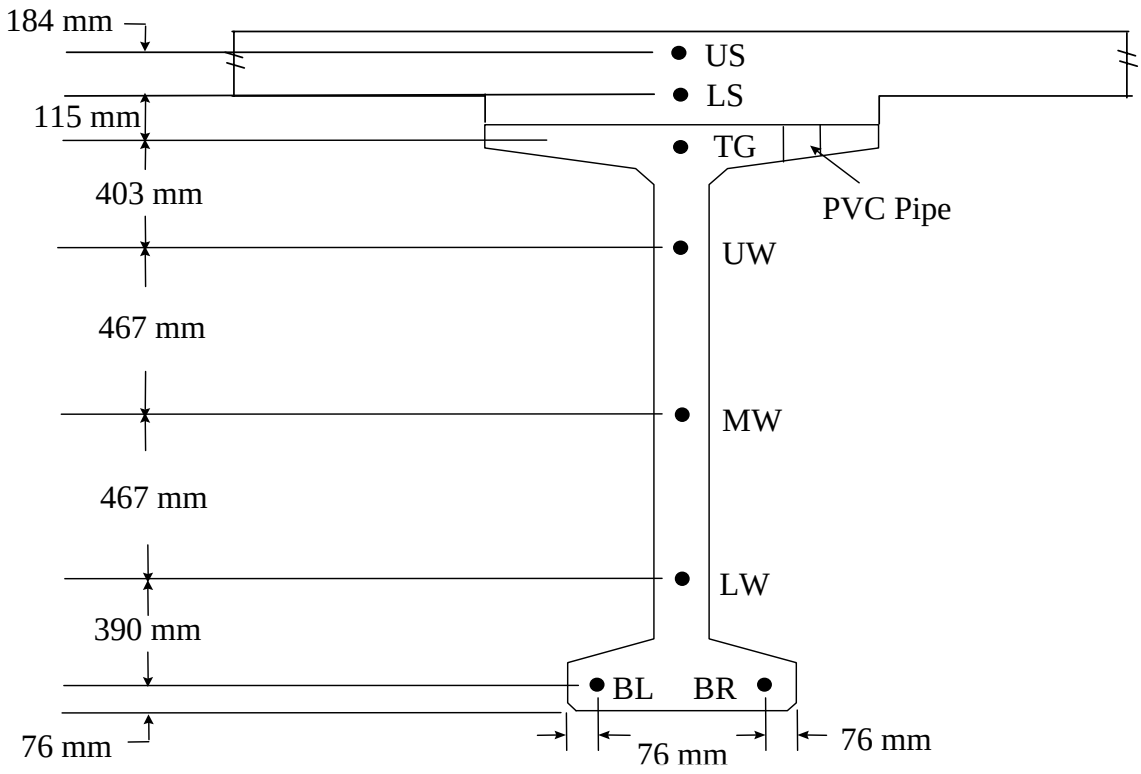

Figure 4.8. Cross Section of Typical Instrumentation Site

After the forms were removed, a multiplexer was attached to the web of each girder at sites 1A-E, 1C-E, 2A-E, 2B-E and 2C-E. Here, the symbol 1A-E indicates the end instrumentation site in girder A of Span 1. The cables from the gages at these sites ran down through the flange blockouts and were connected to the multiplexers. Cables from the midspan gages sites (1A-M, 1C-M, 2A-M, 2B-M and 2C-M) were fed through their respective PVC pipes and ran along the length of the girder to the multiplexers at sites 1A-E, 1C-E, 2A-E, 2B-E and 2C-E, respectively. At the bridge site, each multiplexer was connected to a datalogger located near Pier 2 on Girder B in Span 1 (1B). To support the cables, cable trays made from 50.8 mm (2 inch) diameter plastic pipe, split longitudinally, were bolted to the web of each of the five instrumented girders.

The trays were bolted every 1.52 meters (5 feet) between midspan and the instrumentation site near Pier 2.

4.2.2 Strand Slipback

Strand slipback was measured on girders 1-A, 2-A and 2-B (Figure 4.7). The method for installing the potentiometers and measuring the strand slipback in the bridge girders was the same as for the Test Girder, except that a wooden block, cut to the same skew as the bridge, was used to provide a flat reference surface perpendicular to the strand. The strand pattern at the end of the long bridge girders (Span 2) was the same as the strand pattern in the Test Girder (Figure 4.1).

On the first girder instrumented, the wooden blocks were attached with epoxy but dropped off the girder, which led to delays. This was unfortunate, because the precaster was anxious to stress the concrete quickly before it cooled and cracked. Installation time was particularly critical because the blocks could not be attached before the end forms were removed. The problem was caused by the fact that the epoxy would not adhere to the hot, moist concrete. In subsequent girders hot glue was used instead and gave good results.

Table 4.1 lists the locations at which strand slipback measurements were taken. The strand locations for the short girders (spans 1 and 3) are shown in Figure 4.9.

Table 4.1. Instrumented Slipback Strands

Girder	Strands Monitored
1A	1,4,5,8,9,10,13,14
2A	5,6,13,14,25,26,27,32,35,40
2B	6,13,14,25,26,27,32,35,40

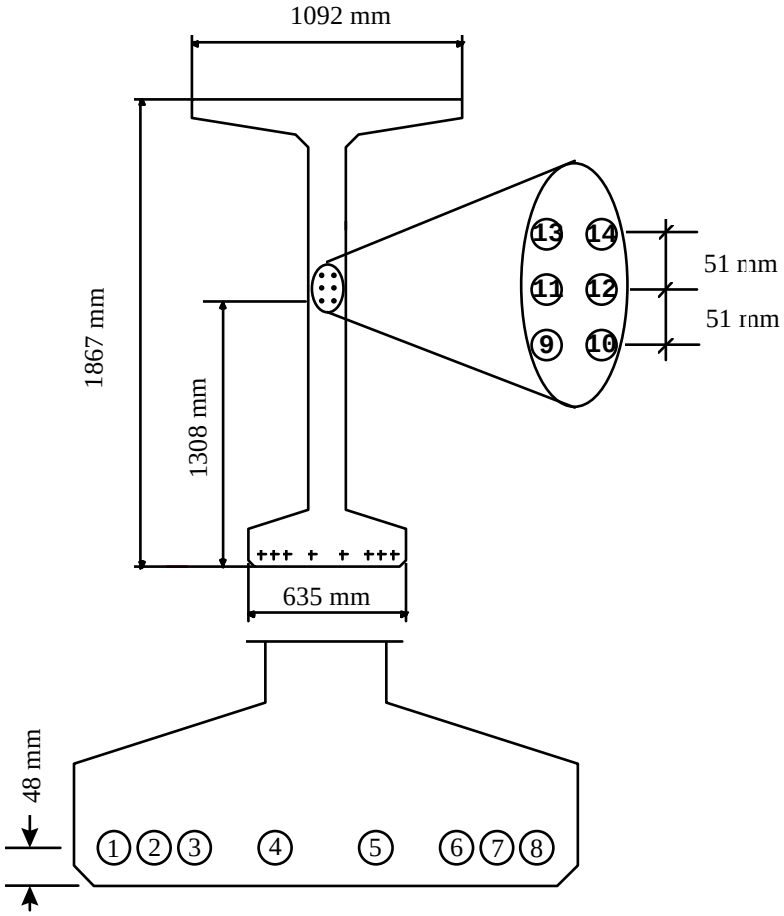

Figure 4.9. Strand Pattern for Spans 1 and 3

4.2.3 Girder Camber

A stretched-wire system was used to measure the camber of the bridge girders. The stretched-wire setup was identical to the setup for the Test Girder (Figure 4.4), except that the magnitude of the weights at midspan was increased to force the wire to pass below the intermediate diaphragms. The LVDTs were connected to a multiplexer, and displacements were recorded using a datalogger.

The drawer glides on the stretched-wire-system suffered damage in the precast yard, because their bearings had been contaminated with cement powder during the finishing. Cleaning them sufficiently proved impossible. They were replaced by a pair of oil-impregnated plastic blocks with vertical slots that allowed the stretched wire to

move freely vertically, but prevented horizontal motion (Figure 4.10). That system worked well and led to an accuracy of approximately ± 1.5 mm (± 0.06 inches). The weight of the trolley was effective in minimizing vibrations. Additional protection against accidental damage at the bridge site was provided by enclosing the trolley and LVDT in a plywood box.

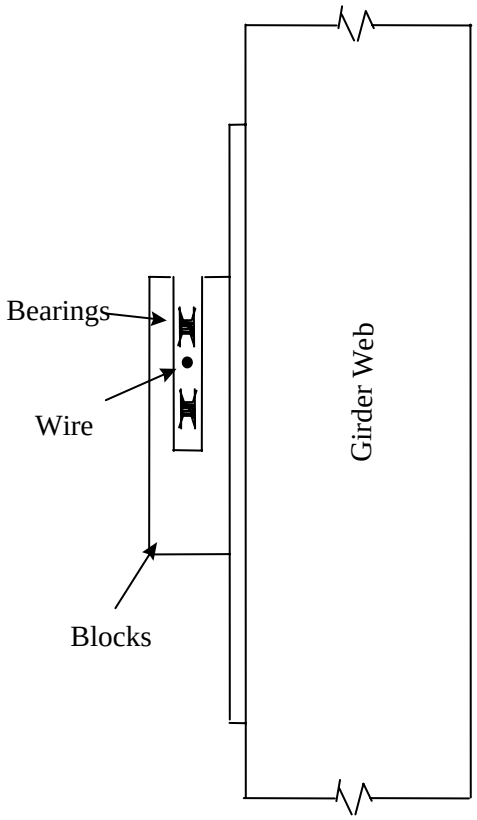

Figure 4.10. Guides for Bridge Stretched-Wire System

To complement the stretched-wire system, level readings were obtained in the production yard by reading rulers that were attached to the webs of the girders at midspan and 0.914 m (3 feet) from each end. At the bridge site, level readings were taken by placing a titanium rod vertically at marked locations along the bottom of the girders. A ruler, which was attached to the rod, was then read with the level. The values of camber

calculated from these readings were adjusted using the girder's deflection curve to compensate for the fact that the readings were not taken exactly at the end of the girders. Readings at the bridge site were always taken between 6 A.M. and 8 A.M. in order to minimize the effects of temperature.

At the bridge site, the level produced readings that were repeatable to ± 1 mm (± 0.04 inches). In the casting yard, access to the girders was more difficult and, particularly for the readings taken at destressing, the accuracy was almost certainly not as good.

4.2.4 Strand Stress

A load cell was used by the fabricator to measure the strand stress during fabrication. One load cell was attached to strand number 29 (Figure 4.1) in each of the long-span girders (Span 2) and to strand number 9 (Figure 4.8) in the two short girders (Span 1). In each case the load cell was placed directly behind the strand chuck at the dead end anchor. Unfortunately, the readings proved too unreliable to be used.

4.3 GAGE PREPARATION

Prior to casting, calibration tests were performed on the VWSGs, stress gages, potentiometers and LVDTs. All calibration tests were performed in air only, except for the VWSGs, which were calibrated in both air and concrete. The air calibration numbers for each gage closely matched the calibration number given by the manufacturers. The calibration test for the VWSG embedded in a 152 x 304 mm (6 x 12 inch) cylinder proved inaccurate due to the end effects on the cylinder.

Each gage was tagged with an individual label and color to help facilitate field instrumentation and monitoring. Field manuals were made for each type of instrumentation location. These manuals had matching tags, which were marked next to a figure identifying gage locations within the girders. The instrumentation team practiced using these manuals and gages on a 1.83 meter (6 foot) mock-up of the girder reinforcing cage. Steel was placed in every location that would be encountered in the

field in an effort to discover any problems prior to field installation. Photographs were taken of the installed gages in the mock-up and then placed in the manuals to help provide a visual picture of how the gages would be installed in the girder. This was necessary because the same installation team members were not available for all girders.

4.4 MONITORING PROGRAM

During fabrication, the jacking stress, release stress, and strand slipback were measured for the Test Girder and five bridge girders. Temperature, strain distributions at midspan and 1.52 meter (5 foot) locations, and midspan camber were monitored during fabrication. Monitoring continued at the bridge site for three years from the time of girder fabrication.

4.4.1 Concrete Strains and Temperatures

Concrete strain and temperature were monitored using vibrating-wire strain gages. Table 4.2 shows the frequency of strain and temperature readings in the Test Girder and production girders.

Table 4.2. Frequency of Strain and Temperature Readings

Girder	Time	Reading Interval
Test Girder	Until Destress	15 minutes
	During Destress	1 minute
	Until Approximately 6 Months After Casting	1 hour
	As Long As Possible	6 hours
Production Girders	Until Destress	15 minutes
	During Destress	1 minute
	Until 6 Months After Casting of Deck	1 hour
	At 6 Months After Casting of Deck	intense 36 hour monitoring
	Until End Of Project	6 hours

4.4.2 Strand Slipback

Strand slipback was measured in the Test Girder, two of the long bridge girders (Span 2), and one short bridge girder (Span 1)(Sections 4.1.2 and 4.2.2). Transfer of the stress from the prestressing strands occurred in stages, the number of which depended on the girder. Readings from the potentiometers were taken before transfer and again after each destressing stage. Table 4.3 lists the number of destressing stages in each girder and the strands that were monitored (Figures 4.1 and 4.8).

Table 4.3. Strand Monitored for Slip-Back and Number of Destressing Stages

Girder	Destressing Stages	Strands Monitored
Test Girder	18	1,2,13,14,25,26,27,32,35,40
2A	10	5,6,13,14,25,26,27,32,35,40
2B	10	6,13,14,25,26,27,32,35,40
1A	14	1,4,5,8,9,10,13,14

4.4.3 Girder Camber

Camber for girders A, B and C in Span 1, and all five girders in Span 2 was measured periodically using a surveyor's level. Level readings continued for three years after casting. Table 4.4 shows the schedule for camber measurements with the level.

Table 4.4. Schedule of Level Readings

Time of Reading	Test Girder	Bridge Girders
Before Transfer	•	•
During Transfer (after each transfer stage)	•	•
As Permitted in Yard		•
Before Shipment		•
Once Every Other Week until Slab Casting		•
Slab Casting		•
Approximately 1,3,6 Months		•
Approximately 1,2,3 Years		•

During construction, an automated stretched-wire system was installed on the instrumented girders (1A, 1B, 1C, 2A, 2B and 2C) as often as construction permitted. After construction was completed, the automated stretched-wire system was permanently attached to the instrumented girders. Camber readings from each of these girders was taken at the same frequency as the concrete strains and temperatures.

4.4.4 Strand Stress

A load cell was attached to one 15 mm (0.6 inch) prestressing strand on both the Test Girder and all five of the production girders. Strand force was measured after jacking and again before transfer. As mentioned in Section 4.2.4, these measurements were unreliable.

CHAPTER 5
OBSERVED BEHAVIOR

This chapter presents the observed behavior of the SR18/SR516 bridge girders. The discussion is organized into two sections. Section 5.1 discusses the behavior of the girders from the time of casting until the time of destressing. Section 5.2 discusses the service behavior of the girders after destressing.

5.1 CASTING THROUGH DESTRESSING

Before destressing the instrumented girders, strength measurements were made on 100 x 152 mm (4 x 8 inch) diameter cylinders that had been subjected to the same temperature history as the embedded thermocouple. For these cylinders, Table 5.1 lists the casting dates, average slump, hours of curing, maturity and the average compressive strengths measured by Central Premix Prestress Co. For a given mix design, maturity values (Lew and Reichard 1978) can be calculated as

$$\text{Maturity} = \int \left(T_i(t) + 12.2\right) dt \qquad (5.1)$$

where $T_i(t)$ = temperature (°C) at time t

t = time

For all six sets of cylinders, the measured compressive strength exceeded the specified strength of 51 MPa (7400 psi), but it took approximately 24 hours to reach this target. As expected, the cylinders with the longest curing times (cylinders for Test Girder and 2A) also had the highest compressive strengths.

Table 5.1. Match-Cured Cylinder Data

Girder	Casting Date	Average Slump (mm)	Curing Time for Cylinders (hours)	Cylinder Maturity (°C-hrs)	Average Strength (MPa)
TEST	12/11/96	108	26.75	1394	56.2
1A	4/2/97	121	23.25	1170	53.7
1C	4/2/97	121	23.25	1170	53.7
2A	3/6/97	111	26.75	1394	55.2
2B	3/10/97	105	23.75	1202	52.2
2C	3/12/97	127	23.0	1154	51.7

5.1.1 Temperature

Figure 5.1 shows the measured temperature histories for the midspan of Girder 2B, from casting through destressing. The temperature histories during casting for the remaining instrumented girders are provided by Barr (1998). For the bridge girders, the time shown as the abscissa of the plot starts when the first bridge girder was cast (March 6, 1997).

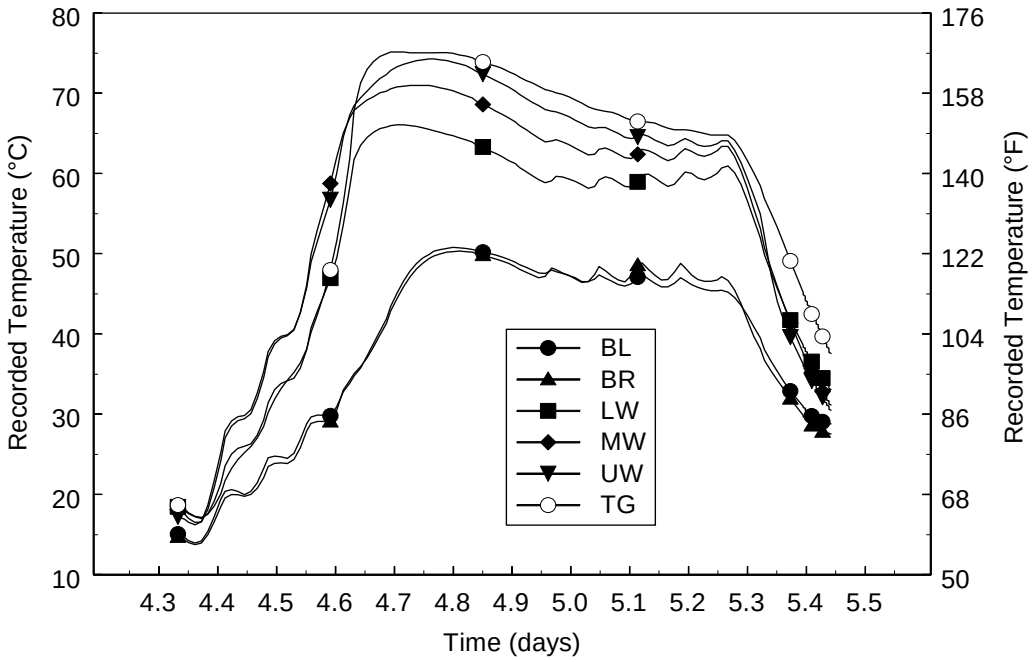

Figure 5.1. Casting Temperatures at Midspan of Girder 2B

Figure 5.1 shows the variation of concrete temperature with time. The temperatures were coldest when the concrete was first cast but heated up as the curing process began. The ripples correspond to activation and de-activation of the automatic steam system. Immediately after casting, the cement hydration had not started, so steam heat was needed to heat the concrete to the target temperature. Thereafter, the hydration reaction was sufficient to maintain the target temperature until approximately 15 hours after casting, when steam was again needed. At day 5.25 (25.5 hours after casting), the steam was turned off, and the forms were removed, which resulted in a temperature decrease.

The temperature varied substantially over the height of the girder. The concrete's temperature was lowest at the bottom and highest at the top. The maximum temperature

difference between the top and bottom was nearly 25°C (45°F) in each girder. This variation can be attributed to the girders' being cast outside during winter, so the cold ground cooled the bottom of the girder. In addition, the steam heat rose to the top of the insulated blanket over the forms.

Figure 5.3 compares the temperature histories for the BL gages at midspan in each of the girders that were instrumented. Because the thermocouple was placed lower in Girder 2B than in the other girders, Girder 2B experienced the highest peak temperature. The peak temperature for the other two long girders (2A and 2C) was the lowest.

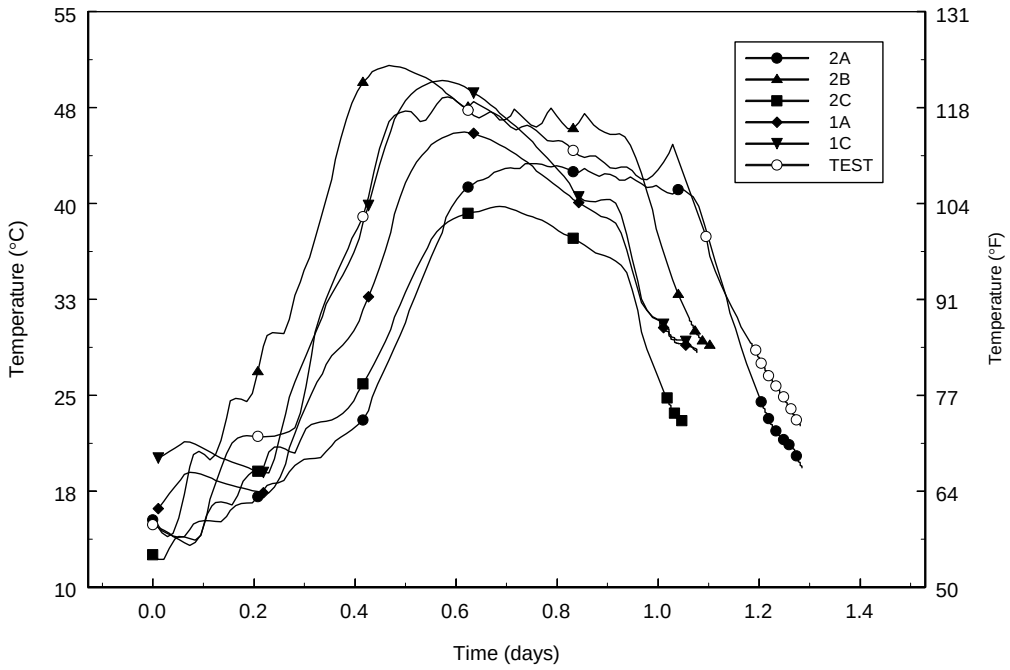

Figure 5.3. Midspan Temperatures in Instrumented Girders: Gage BL

5.1.2 Concrete Maturity

The temperature variation during curing may have significantly affected the concrete strength when the prestressing tendons were released. For the purposes of determining the release strength of the concrete in the girder, the contractor tested two 102 x 203 mm (4 x 8 inch) cylinders that had been connected to the Sure-Cure system (Table 5.1). Since the thermocouple for the Sure-Cure system was usually placed at the mid-height of the girder, the concrete at the bottom of the girder was cured at lower temperatures than the concrete in the cylinders. The lower curing temperatures in the bottom of the girder would be expected to result in concrete that was weaker than that of the cylinders. This effect can be significant, since the highest stress in the girder is at the bottom.

Destressing was usually completed approximately two hours after the cylinders were tested, so at the end of destressing, the concrete strength adjacent to the thermocouple was somewhat higher than the values listed in Table 5.1. Using the temperature histories from gages BL and BR, the maturity of the concrete at the cgp at the time of destressing was calculated using Equation 5.1. The computed maturities for the concrete located at the elevation of the bottom gages for the instrumented girders are listed in Table 5.2.

Table 5.2. Girder Concrete Maturity at cgc at Destressing

Girders	**1A**	1C	2A	2B	2C
Curing Time at Destressing	24.25	24.25	28.25	25	24
Maturity (°C-hrs)	1330	1360	1470	1620	1270

Girder 2B had the highest maturity, because it was subjected to the highest temperature. Girder 2A had the next highest maturity, because it was cured for the longest time.

5.1.3 Strains

The strain histories measured during curing and destressing for the midspan cross-section in Girder 2B are shown in Figure 5.4. Compressive strains are negative.

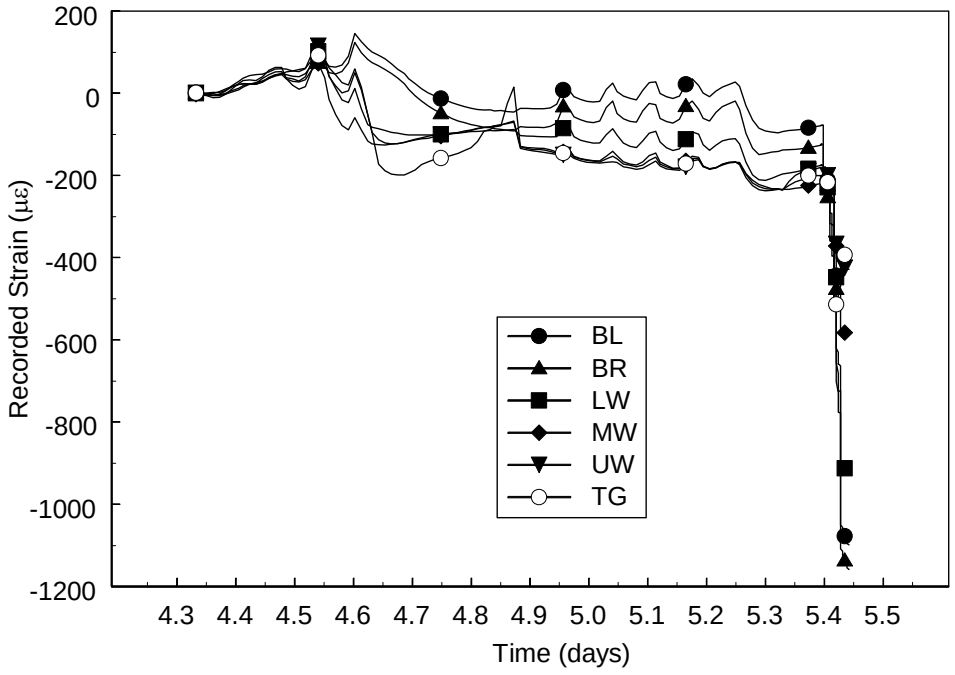

Figure 5.4. Casting Strains at Midspan of Girder 2B

The strains shown are the values recorded by the datalogger. Theoretically, the internal configuration of the VWSG is such that a gage suspended freely in air and heated will record no change in strain. However, for a gage embedded in concrete, the total and nonthermal strains must be derived from the recorded values. In particular, the total and nonthermal strains can be obtained using Equations 5.2 and 5.3 respectively.

$$\varepsilon_{total} = \varepsilon_{recorded} + \Delta T * \alpha_{gage} \quad (5.2)$$

$$\varepsilon_{nonthermal} = \varepsilon_{recorded} + \Delta T * (\alpha_{gage} - \alpha_{conc}) \quad (5.3)$$

where ε_{total} = strains due to all causes, including temperature

$\varepsilon_{nonthermal}$ = strain due to all non-thermal causes, including stress, creep and shrinkage

$\varepsilon_{recorded}$ = strain values recorded with datalogger

ΔT = temperature change from time at which the concrete hardens

α_{gage} = coefficient of thermal expansion of VWSG

α_{conc} = coefficient of thermal expansion of concrete

No corrections were made to the recorded strains, because the values of α_{conc} and α_{gage} were not known with sufficient certainty. The gages were made of stainless steel, and the coefficients of thermal expansion of steel and concrete are similar. If they were identical, Equation 5.3 shows that the recorded strain would be equal to the nonthermal strain.

The early strain histories for the other girders are similar to those shown in Figure 5.4 (Barr 1998), except for the UW and MW gages at the midspan of Girder 1C, and the LW and MW at the midspan of Girder 2A. The UW and MW gages at the midspan of Girder 1C recorded large tensile strains during curing, but functioned correctly afterwards. The LW and MW gages at the midspan of Girder 2A ceased to function when Central Premix Prestress Co drilled a hole through the web of the girder and unintentionally severed the gage cables.

Ripples in the strain measurements (Figure 5.4) correspond to the ripples in the temperature histories (Figure 5.1) and were caused by the activation of the steam. If the steam heated the entire girder uniformly, and if α_{gage} were equal to $\alpha_{concrete}$, then no ripples should be visible. A nonlinear temperature profile would lead to induced stresses, but since they would have to be self-equilibrating, some should be compressive and some tensile. All the recorded strains became simultaneously more tensile as the steam heat

was applied, so the gages' response cannot have been induced by stress alone. The other probable excitation is thermal. Thus it is likely that α_{gage} and $\alpha_{concrete}$ differed.

The abrupt change in strain at 5.45 days is a result of releasing the prestressing strands. The destressing process lasted about two hours for Girder 2A and about one hour for each of the other instrumented girders.

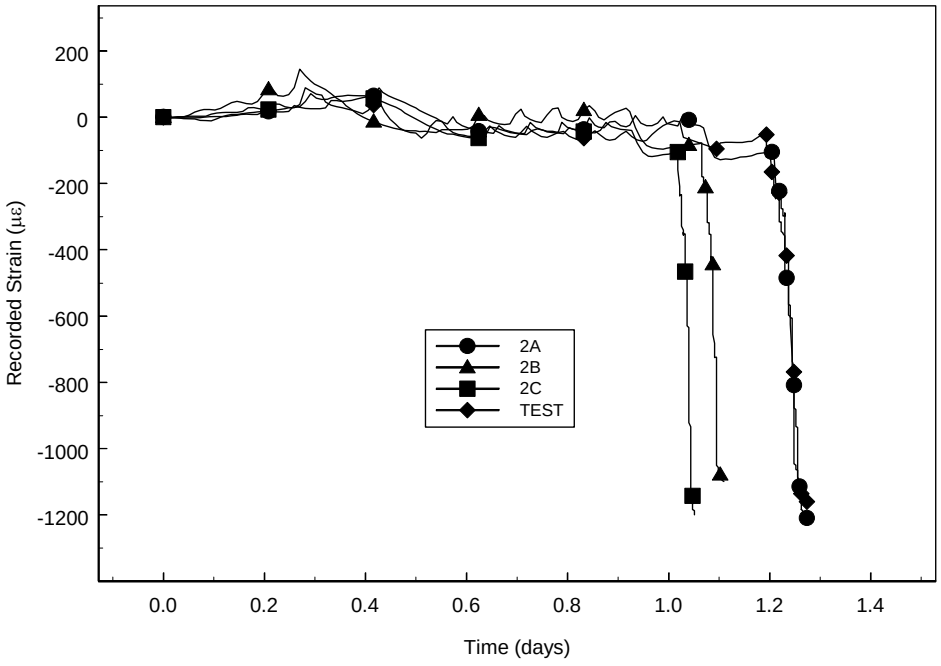

Figure 5.5. Midspan Strains in Most Highly Stressed Girders: Gage BL

Figure 5.5 compares the BL gage strain readings during curing and destressing of the four most highly stressed girders. The abrupt change in strain shows the effect of destressing. The differences in time at destressing reflect the different times for which the girders were cured (Table 5.2). At the end of destressing, the bottom compressive strains in girders 2A, 2C and the Test Girder were within 4.5 % of each other. The strain in Girder 2B after destressing was less than that in the other girders, possibly because it

was cured at a higher temperature. The strain in Girder 2A was the largest, because the destressing operation lasted the longest, so more creep occurred.

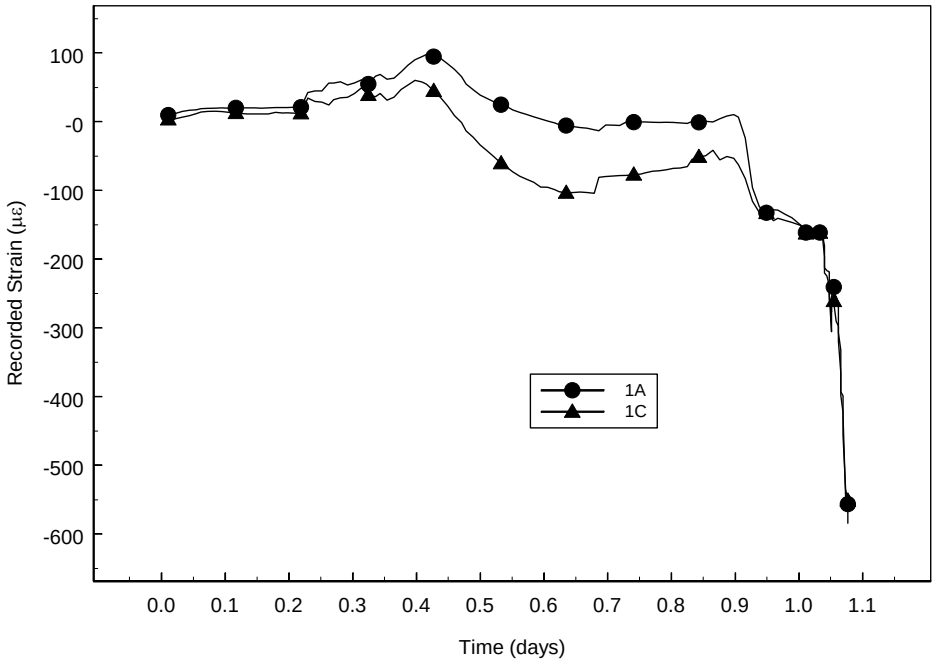

Figure 5.6. BL Gage Strain Comparison of Span 1 Girders

Figure 5.6 shows the BL strains during curing and destressing for the instrumented girders in Span 1. Girders 1A and 1C were cast and destressed in the same bed at the same time, therefore the curing times at destressing were identical. The difference between the strains in these two girders at the end of destressing was 4.2 %. The magnitude of strain after destressing for the girders in Span 1 was less than half that of the girders in Span 2, because the girders contained fewer strands.

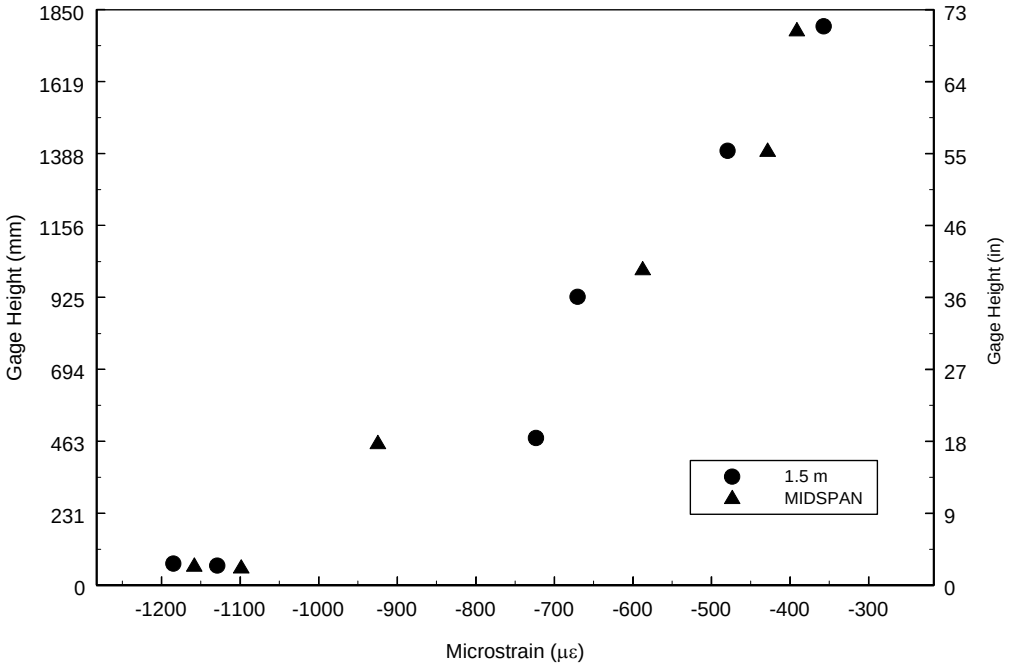

Figure 5.7. Cross-Sectional Strains in Girder 2B after Destressing

Checking whether plane sections remain plane after destressing can help evaluate the consistency of the VWSGs readings. Figure 5.7 shows the strains in Girder 2B immediately after destressing at midspan and at the 1.5 meter (5 foot) location.

At midspan the strain distribution is nearly linear, except for the top gage. At the 1.5 meter (5 foot) cross section, the strain distribution is also nearly linear, other than the gage 18 inches from the bottom (LW) and the top gage. This discrepancy for gage LW at the 1.5 meter (5 foot) cross-section is typical of the other instrumented girders (Barr 1998). During destressing the end of the girder was lifted with lifting loops located near the 1.5 meter (5 foot) cross-section. Stress concentrations caused by these lifting loops could account for the nonlinear strain profile at the 1.5 meter (5 foot) location.

5.1.4 Camber

Camber during destressing was measured with both a surveyor's level and a stretched-wire system for each of the girders, except for the Test Girder and Girder 2A, for which only the stretched-wire system was used. Because the level readings and the stretched-wire readings were taken from marks 0.91 meters (3 feet) from the ends of the girders, adjustments were made to the level readings using the deflection equation for the girders to get a deflection relative to the end of the girder. Table 5.3 lists the cambers after destressing for each instrumented girder.

Table 5.3. Camber Measured after Destressing

Device	1A	1C	2A	2B	2C	Test Girder
Level (mm)	3.6	4.6	N/A	66.5	67.8	N/A
LVDT (mm)	1.5	6.4	63.5	65.3	66.0	2.29
Difference	+2.1	-1.8	---	+1.2	+1.8	---

The camber measurements for the Span 2 girders were much larger than those for the girders in Span 1 for both the level and stretched-wire system. The differences between the camber measurements for the level and stretched-wire system were approximately the same as the estimated accuracy of the instruments (±1mm).

Figure 5.8 shows the cambers measured during each stage of destressing for Girder 2B. The strands in the web were cut in stages 1 through 4. Between stages 4 and 5 one end of the girder was lifted to prevent the concrete from crushing at the skewed corners as the girder cambered upward. The change in camber readings between these two stages is thought to be a result of the lifting of the end. During stages 5 through 10 the bottom flanges were released. Similar trends were found for the other instrumented girders (Barr 1998).

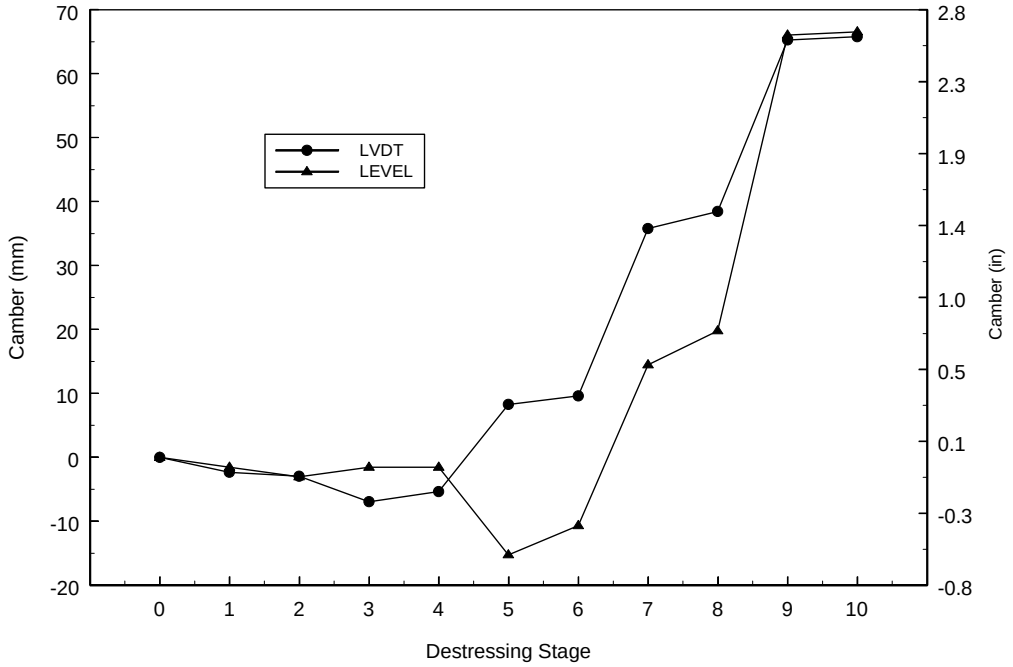

Figure 5.8. Camber During Destressing in Girder 2B

5.1.5 Transfer Length

Voltage readings were taken from potentiometers attached to prestressing strands in girders 1A, 2A and 2B using a hand held digital voltmeter. The voltage readings were converted into end-slip readings by multiplying them by the gage factor. The end slip measurements for Girder 2B are shown in Figure 5.9. Strands 27 and 35 were located in the web and were destressed during stages 1 to 4. The others were bottom flange strands and were destressed during stages 5 to 10.

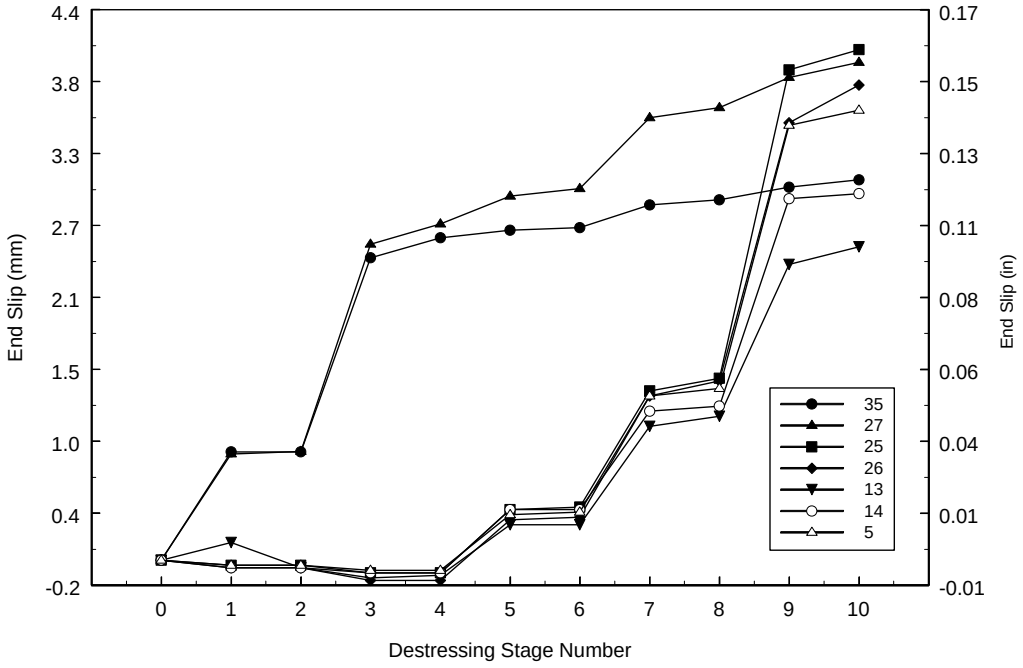

Figure 5.9. End Slip Measurements of Girder 2B

Transfer lengths were computed from strand slip measurements in girders 1A, 2A and 2B. The two quantities are related by Equation 5.3 (Logan 1997).

$$L_{tr} = (2 * \Delta * E_p) / f_{pi} \qquad (5.3)$$

where L_{tr} = transfer length

Δ = measured end slip

E_p = elastic modulus of strand =196.5 GPa (28,500 ksi)

f_{pi} = initial prestress (GPa) directly after transfer, just beyond the transfer zone

= 1.22 (2A and 2B), 1.32 (1A)

The transfer lengths calculated from measured end slips are shown in Figure 5.10. The strand locations are shown in Figure 4.1.

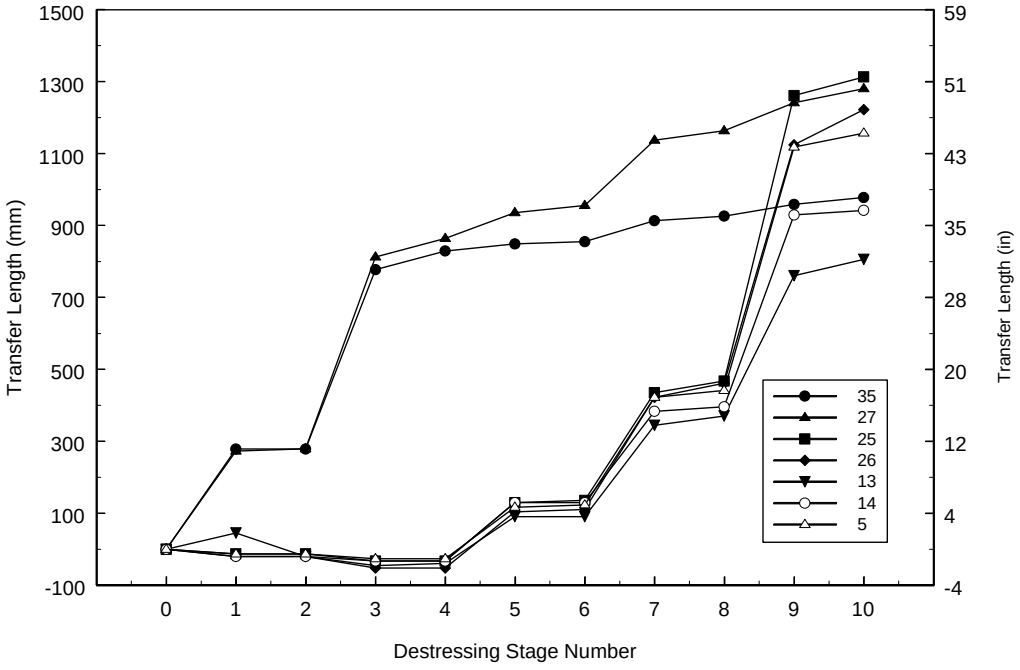

Figure 5.10. Calculated Transfer Lengths During Destressing of Girder 2B

End-slip measurements ended after destressing was completed. Research has found that some additional end slip can occur after destressing is complete (Logan 1997). Therefore, Figure 5.10 represents a minimum value for the actual transfer length. The transfer lengths for the other instrumented girders are presented in Barr (1998). No correlation between size of slip back and location of strand was found.

Figure 5.11 summarizes all the transfer length data. Nineteen of the twenty four instrumented strands exceeded the transfer length value of 60 strand diameters predicted by the AASHTO Specification (AASHTO 1994). Because the vertical component of the prestressing force in the harped strands is used to help resist shear stresses, an increase in

the transfer length near the supports could cause shear cracking problems. In addition, cracking near the supports is more likely to occur because the reduction of axial force due to the longer transfer length will increase the principal stresses. Cracking in the transfer zone has been shown (Russell and Burns 1996) to cause anchorage failure in the strand. When bond failure occurs, the tension force in the strand is lost and the concrete's contribution to shear is reduced.

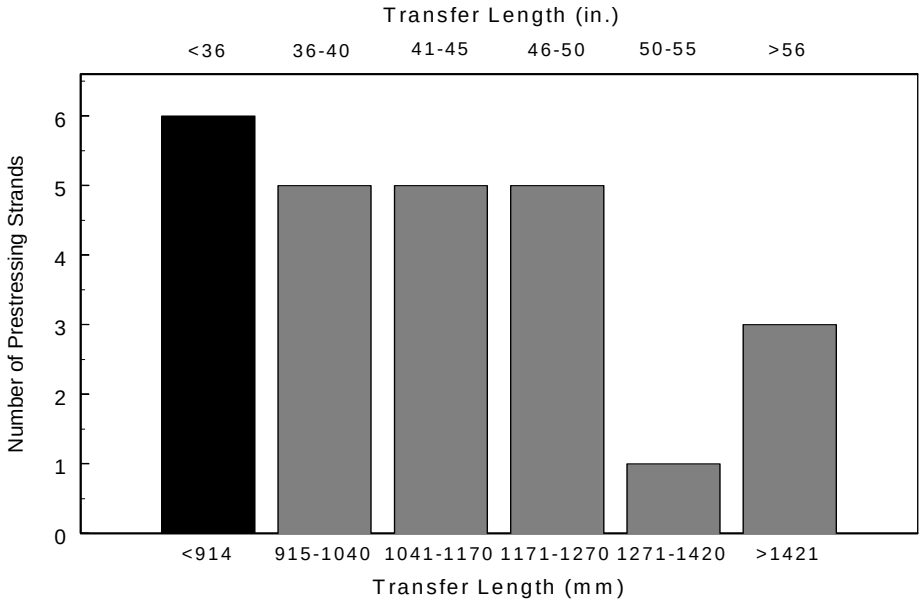

Figure 5.11. Summary of Calculated Transfer Lengths

5.2 SERVICE CONDITIONS

This section presents the observed behavior of the girders for a period of three years after the girders were taken from the casting bed.

5.2.1 Temperature

Figure 5.12 shows the temperature histories of the midspan gages in Girder 2B. The gaps in the data between days 55 through 70, 460 through 475, 825 through 855 and

986 through 1006 represent time intervals during which the equipment was not taking readings.

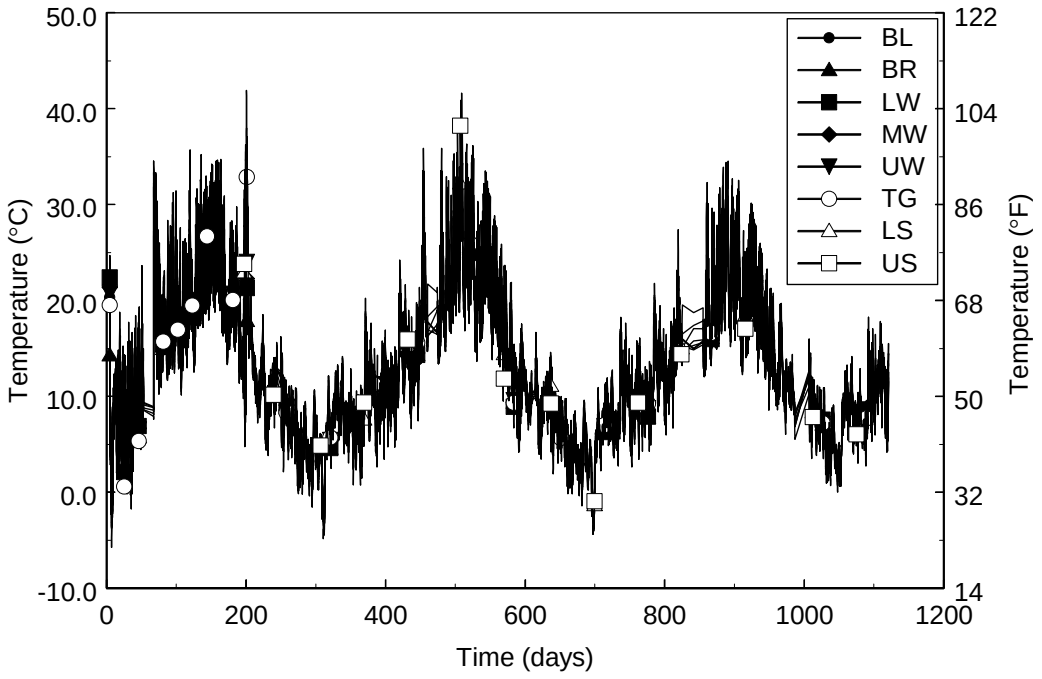

Figure 5.12. Service Temperatures at Midspan of Girder 2B

The thermistors in the VWSGs performed extremely well after casting. They provided readings without fail, and those readings followed all expected trends. In general, the temperatures were colder during the winter and hotter during the summer months (Figure 5.12). They also read hotter during the day and colder at night. Before the slab was cast, the temperature during the day was always highest at the top gage (TG). After the slab was cast, the temperature was highest in the upper slab gage (US). The gages in the exterior girders, both in the yard and after erection, registered higher temperatures than the interior girders. This difference is attributed to the sun shining on the exterior face of the girders. The daily temperature cycles are represented with sharp

peaks in Figure 5.12. The daily temperature variations in the girders diminished starting at day 200, which corresponds to the day of the deck casting.

Figure 5.13 shows a typical daily temperature history for the midspan of Girder 2B drawn with a larger time scale. The three peaks shown are for September 4, 5 and 6 of 1997. The bridge deck was not in place at the time, and readings were being taken hourly. As expected, the top gage (TG) measured the highest temperature during the day. As a result of the safety deck being above the bottom two gages (BL and BR), but below the web gages (LW, MW, UW), the heat from the road below made the bottom gages hotter than the web gages. The extreme temperatures in the top gage (TG) and bottom gages (BL and BR) also occurred earlier than those in the web. The maximum temperatures occurred at 5:00 P.M., while the minimum temperatures usually occurred between 6:00 and 7:00 A.M. The daily temperature plots for the other instrumented girders were similar and are provided by Barr (1998).

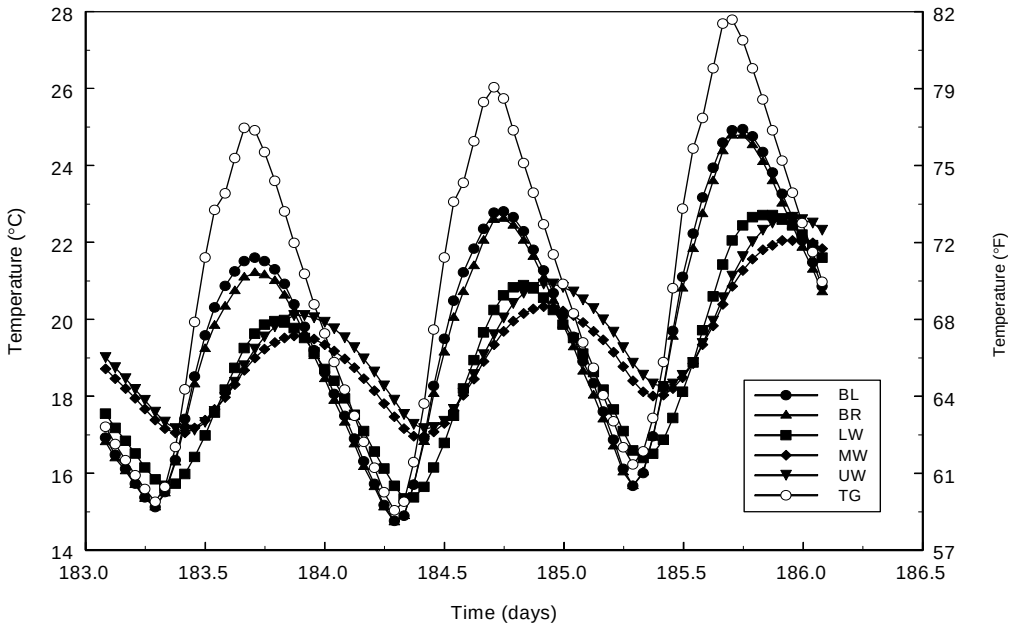

Figure 5.13. Typical Temperature Variation at Midspan in Girder 2B

5.2.2 Strains

With the exception of the days mentioned in Section 5.2.1, strain readings were taken continuously after casting. Figure 5.14 shows the strain histories for the midspan of Girder 2B.

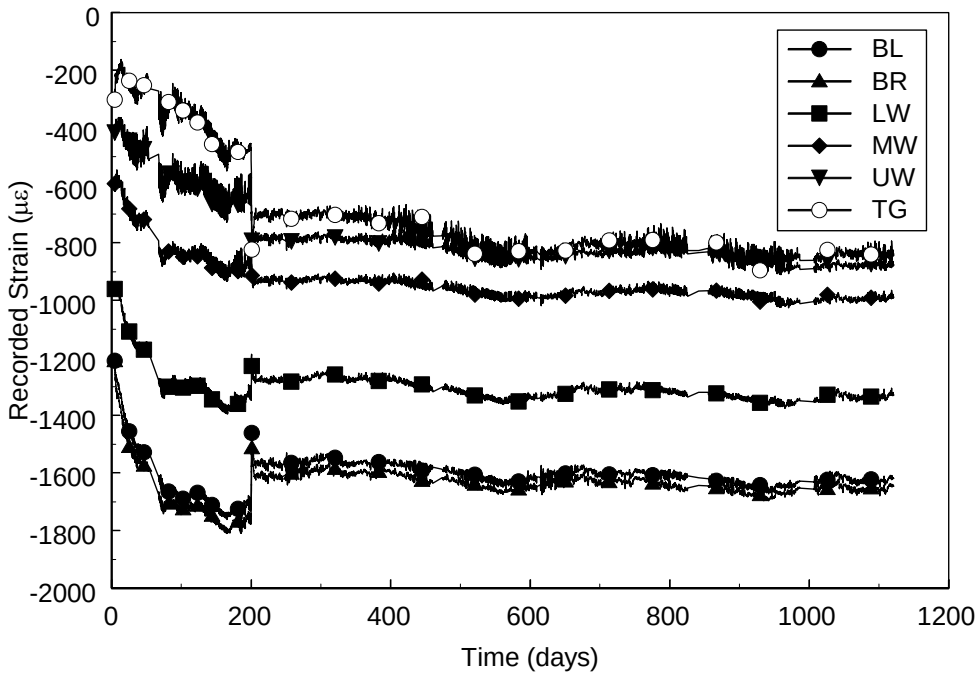

Figure 5.14. Service Strains at Midspan of Girder 2B

The changes in measured strains are attributed to creep and shrinkage in the concrete, relaxation of the strand and casting of the bridge deck. The gages towards the bottom of the girder experienced the largest change in strain, as a result of the high stresses there. The change in strain measurements for the top gage was smaller, because the stresses were smaller. A small increase in strain occurred after transportation (days 55 to 70). This increase is thought to have been a result of the removal of wooden blocks, which supported the girder in the yard. They provided some frictional resistance at the supports, which in turn led to a positive end moment and reduced camber. Once the girders were lifted off the supports, the girders were free to camber and the bottom strains increased.

The abrupt change in strain on Day 200 corresponds to the deck casting. The strains in gages BL, BR and LW decreased while strains increased in gages MW, UW and TG. As expected, the change in strain was largest in the top (TG) and bottom (BL and BR) gages. After Day 200 the stress in the concrete was nearly zero at the bottom flange, and because nearly all of the shrinkage in the concrete and relaxation in the strand had already occurred, the increase in strains after this time was attributed to differential shrinkage (Section 2.8). The distribution of the recorded strains remained approximately linear during this time. Figure 5.14 also shows that during the first 100 days the bottom gages experienced much more change in strain than during any other period of time for the girder. A slight increase in bottom strain occurred after the slab was cast. This trend is consistent with the fact that the rates of creep and shrinkage decrease with time and the stress in the bottom of the girder after the slab casting was almost zero.

The cross-sectional strains at three times during the service life of Girder 2B are shown in Figure 5.15. The 200-day data is directly before casting of the deck. The measured data show a strain distribution that is nearly linear. This finding agrees with the assumptions of Euler-Bernoulli beam theory and thus provides verification that the gages were working correctly.

The distribution of strain is slightly nonlinear, in that the strains in the upper gages are larger than the values that would fit a linear profile. This tendency follows the same trend as was found at destressing (Figure 5.7). This trend is consistent with the other instrumented girders (Barr 1998)

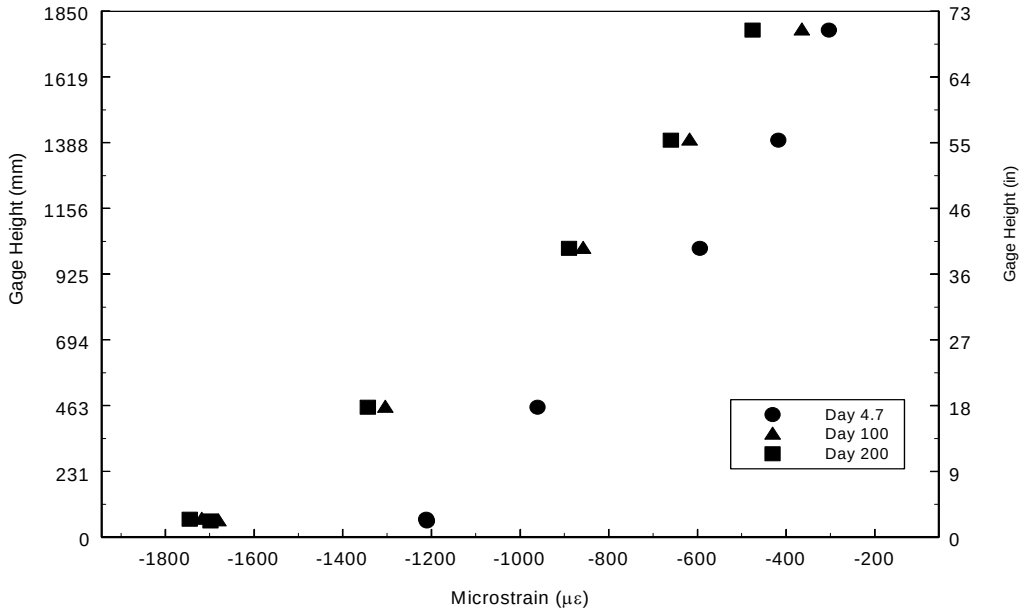

Figure 5.15. Cross-Sectional Strains at Midspan of Girder 2B

Figure 5.16 shows strain measurements that were recorded in the deck concrete of Girder 2B. The gages from the other deck gages showed similar results. The readings start at day 200, which is the casting day for the deck concrete.

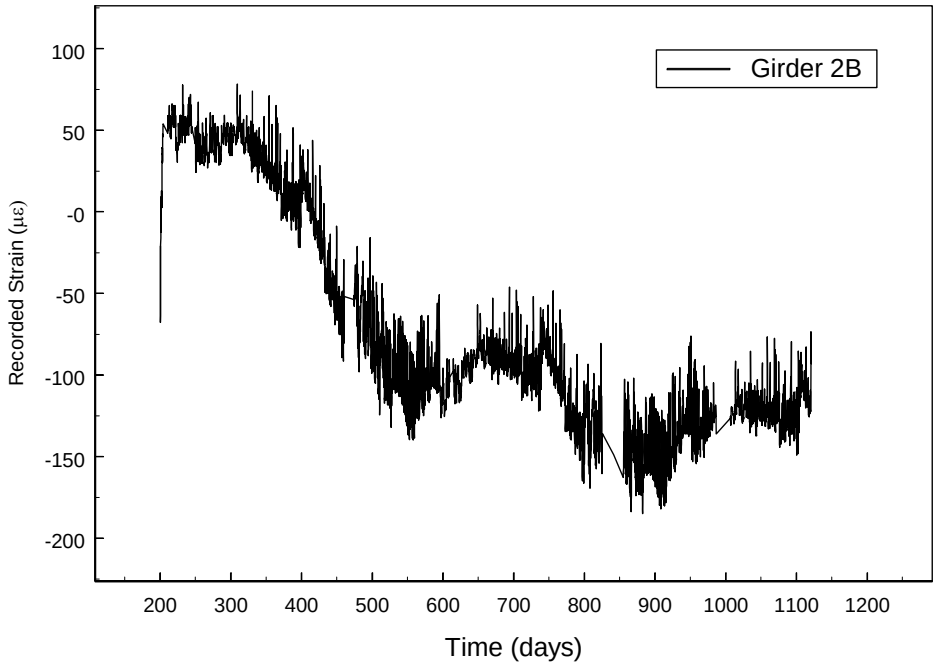

Figure 5.16. Deck Strains for Girder 2B

All deck gages had an initial strain reading of around +50 microstrain that decreased to about –125 microstrain. This change in strain of -175 microstrain is smaller than the free shrinkage strain of –830 microstrain that was measured on material samples in the laboratory (Barr et al. 2000). Although the measured deck shrinkage strain is smaller, this magnitude of strain is consistent with experimental results measured on two half-scale continuous girders by Mattock (1961). He found that the deck shrinkage strain was -245 microstrain. Reasons for the difference include restraint by the deck reinforcement and by the girder.

5.2.3 Camber

The camber histories for all five girders in Span 2 are shown in Figure 5.17. Each reading was made using the surveyor's level. Each camber reading was corrected to account for the various end conditions using Euler-Bernoulli beam theory.

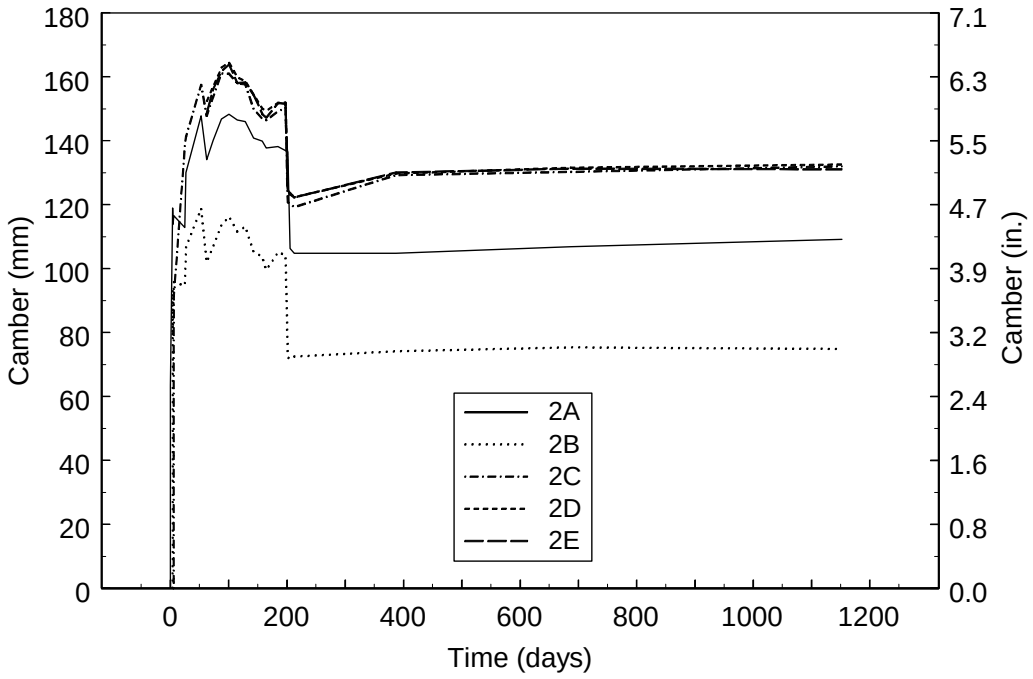

Figure 5.17. Camber Histories for Span 2 Girders (Surveyor's Level)

Before day 53, readings were taken at Central Premix Prestress Co. Because those level readings were taken as time permitted, a number of readings were taken during the day, when thermal effects were the largest. As a result, camber readings taken in the precast yard are affected by creep, shrinkage, the girder location and the time of the day when the readings were taken. In particular, Girder 2C was exposed to the most sun, and therefore, temperature affected its camber more than that of girders 2A and 2B. The first reading after the girders were erected was taken on day 63.

All the girders deflected downward by 10 to 20 mm (0.4 to 0.8 inches) between the last reading in the yard and after erection (day 53 and 62) (Figure 5.17). The level readings on days 53 were taken on a sunny afternoon at 3:30 P.M., and therefore included some thermal camber. The readings on day 62 were taken at 5:30 A.M., which led to minimal thermal camber. The difference in camber between days 53 and 62 is therefore thought to be a result of thermal camber, the magnitude of which is consistent with values after the girders were erected (Figure 5.21).

In addition to the instrumented girders, camber readings were also taken on Girders 2D and 2E on the night that the girders were erected. After the girder erection, camber readings were taken approximately every two weeks. The slight dips in the curves of Figure 5.17 between the readings on days 101 and 114 are related to the casting of the intermediate diaphragms.

The cause for the decline in the camber readings between days 128 and 164 is unclear, however the bottom foot of the pier diaphragms was cast around day 130. The girders had projecting end reinforcement and strand extensions, on some of which strand chucks were mounted to add anchorage, so pouring part of the pier diaphragm connected them in both tension and compression. The restraint to creep and shrinkage at the ends of the girders from this concrete is a plausible explanation for the observed decrease. The sudden drop in camber near day 200 corresponds to the deck casting. Each girder in Span 2 deflected about 25.4 mm (1 inch) during casting of the deck. The camber increased slightly after the slab was cast.

The camber histories for the instrumented girders in Span 1 are shown in Figure 5.18. Each reading was taken with a surveyor's level. Transportation, erection, diaphragm casting and deck casting occurred on the same days as for the girders in Span 2. Camber on Girder 1B was measured starting on day 73. Camber values could not be taken on the night of erection. The deck casting caused each girder to deflect 3 mm (1/8 inch). There was also almost no change in the Span 1 girders' camber after the deck was cast.

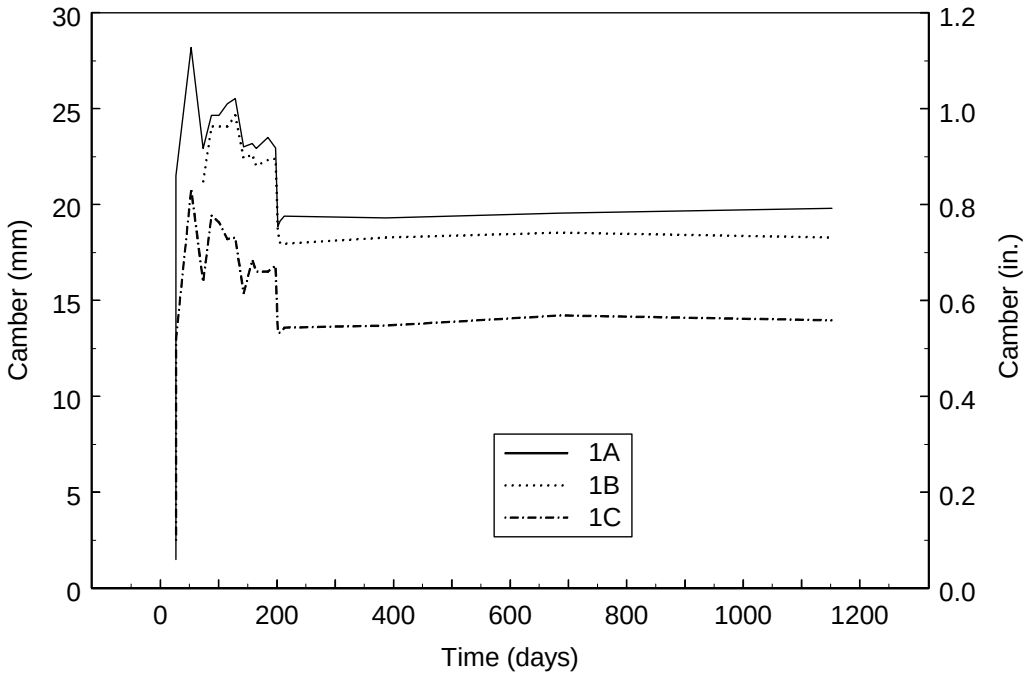

Figure 5.18. Camber Histories for Span 1 Instrumented Girders (Surveyor's Level)

Level readings were also taken on both Span 1 and Span 2 girders approximately every two hours on June 5 (day 89) in order to obtain a daily camber history. The first set of level readings was taken at 9:30 A.M., and the last readings were taken at 8:30 P.M. Figure 5.19 shows the variation in measured camber for each girder throughout the day for both spans. For Girders 1A and 1C the maximum variations in camber were 2.5 and 3.6 mm (0.1 and 0.14 inches) respectively. Girders 2A, 2B and 2C had maximum changes in camber of 9.4, 9.4 and 10.7 mm (0.37, 0.37, and 0.42 inches) respectively. The change in camber during the day is believed to be a result of the temperature gradient in the girders.

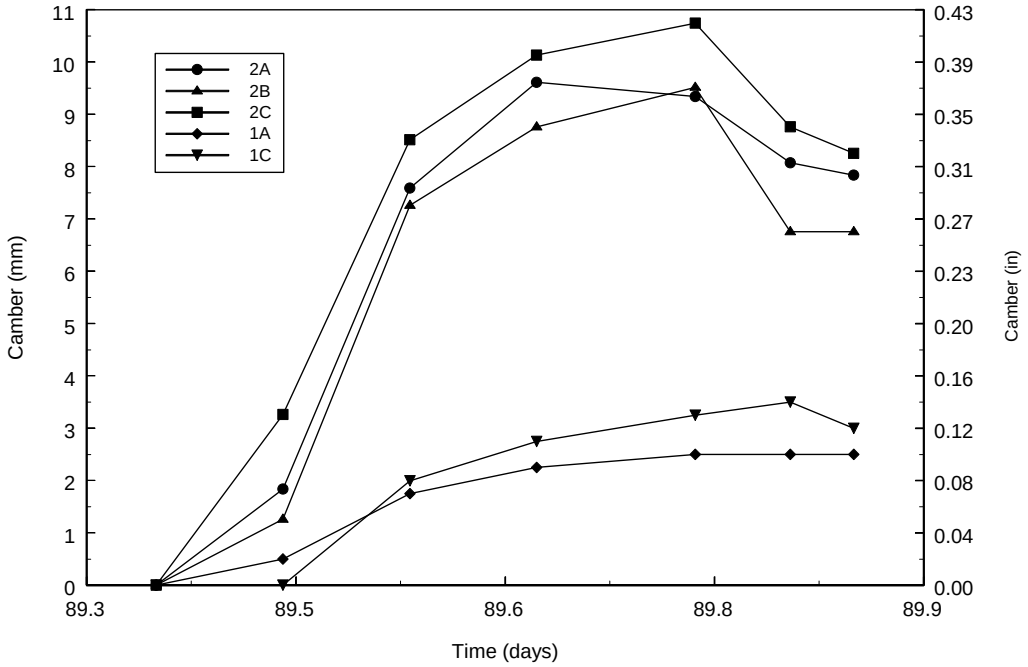

Figure 5.19. Camber versus Time on June 5 (Surveyor's Level)

Due to the likelihood of the stretched-wire system being damaged by construction activities during construction of the bridge, it was only installed for a short period of time before casting the deck. Figure 5.20 shows the camber readings taken during September 4, 5 and 6, 1997 for girders 2B and 2C. On those days, the LVDT for Girder 2A was being repaired, therefore that stretched-wire system was not installed. Daily camber variations range from 15 to 20 mm (0.6 to 0.8 inches). The daily change in camber is a result of the variations in temperature gradient in the girders. The temperature variations for girders 2B and 2C during these three days can be seen in Figures 5.13. Each temperature plot shows a daily change in temperature that corresponds to the change in camber. The temperatures for these two girders are similar, as are the changes in camber. The minimum camber occurred at 6:00 A.M., and the maximum camber occurred at 3:00

P.M. This observation contrasts with the finding in Section 5.2.1 that the maximum temperature at the top occurs approximately at 5:00 P.M. The difference in times of peaks is attributed to the fact that the greatest temperature gradient, on which the camber depends, may not occur at the same time as the maximum top temperature. The relative smoothness of the camber curves and the fact that the values for the two girders are so nearly identical suggest that little frictional resistance existed in the Stretched-Wire System and that the new slides worked well. The reason for the slight roughness in the Girder 2B curve near its minimum is unknown. It is possible that this phenomenon is related to pulley friction.

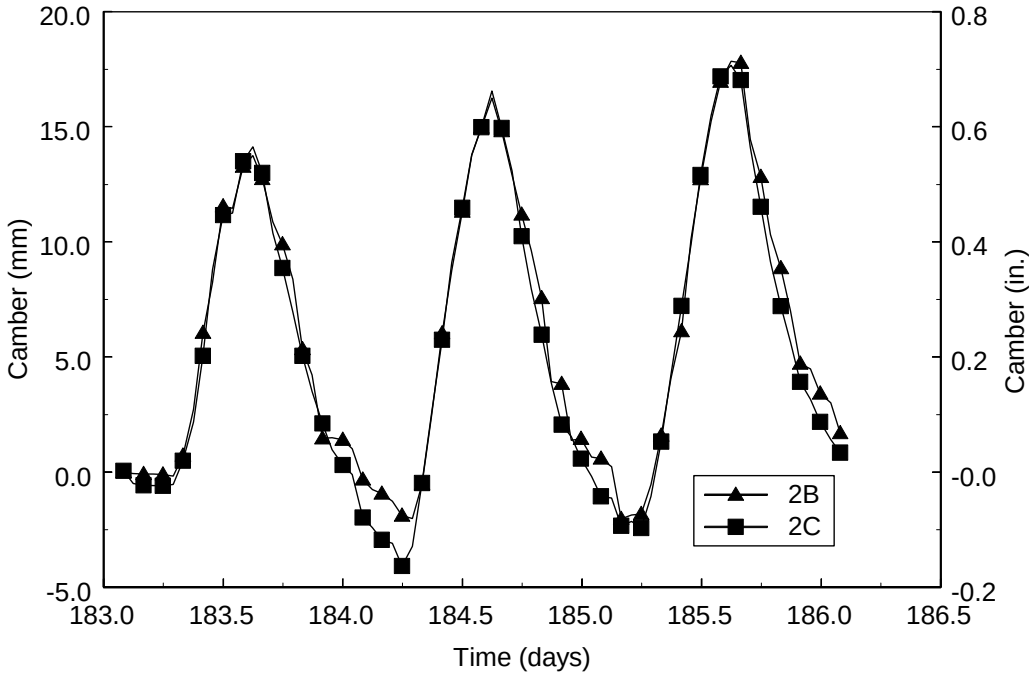

Figure 5.20. Daily Camber Readings for Span 2 (Stretched-Wire System)

As expected, the camber was largest in the afternoons (at approximately Day 183.7, 184.7 and 185.7). Figure 5.21 shows the daily camber values for the instrumented

girders in Span 1. Girder 1B did not have any internal instrumentation and therefore the temperature distribution is unknown, but it might reasonably be expected to be the same as that in the longer girders at the same time, shown in Figure 5.13. The highest camber values were recorded in Girder 1C, and the smallest were recorded in Girder 1A. The temperature plots show that Girder 1A had a hotter bottom flange, and thus a smaller temperature gradient than Girder 1C. The difference in thermal gradients is the likely explanation for the difference between the cambers of these two girders. The bottom temperature in Girder 1B could reasonably lie between these two girders and would therefore produce intermediate camber values.

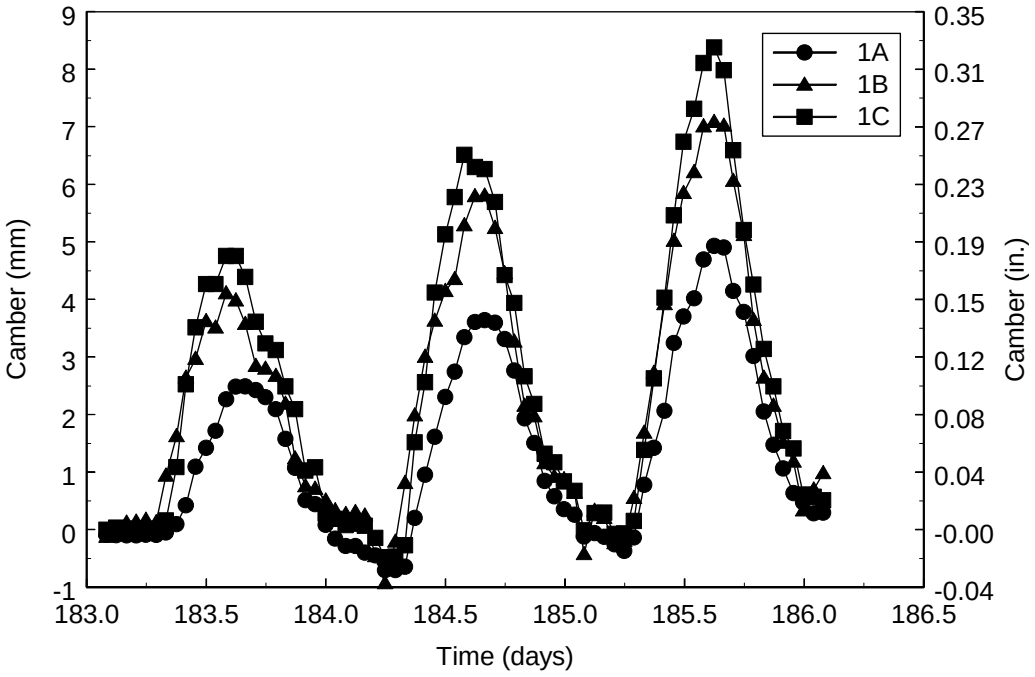

5.21. Daily Camber Readings for Span 1 (Stretched-Wire System)

CHAPTER 6

OBSERVED PRESTRESS LOSSES

This chapter discusses the prestress losses observed in the instrumented girders. Prestress losses occur due to elastic shortening of the concrete (Section 6.1), and shrinkage and creep of the concrete (Section 6.2). Additional changes in prestress occur due to deck casting (Section 6.3) and relaxation of the prestressing strands (Section 6.4).

6.1 ELASTIC SHORTENING AND EARLY CREEP

After release of the strands, the compressive strain in the concrete at the centroid of the prestressing strand cgc is composed of three parts: (1) axial strain due to prestressing force, (2) bending strain due to eccentricity of prestressing force and (3) bending strain due to self weight. As the concrete shortens, the tendons that are bonded to the adjacent concrete also shorten. This shortening of the tendons reduces the prestressing force. Equation 6.1 relates the change in concrete strain to the change in prestressing stress due to elastic shortening.

$$\Delta f_{pES} = Ep * \Delta \varepsilon c \qquad (6.1)$$

where Δf_{pES}= change in steel stress due to elastic shortening

E_p = modulus of elasticity of prestressing steel (196.5 GPa (28,500 ksi) from manufacturer)

$\Delta \varepsilon_c$ = change in strand strain at release

Elastic shortening losses in the prestressing strands were estimated by measuring the strain in the concrete near the centroid of the prestressing strands (gages BL and BR) and multiplying this strain by the modulus of elasticity of the prestressing steel

(Equation 6.1). Figure 6.1 shows a typical strain history near the prestressing centroid (76 mm (3 inches) from the bottom) during destressing.

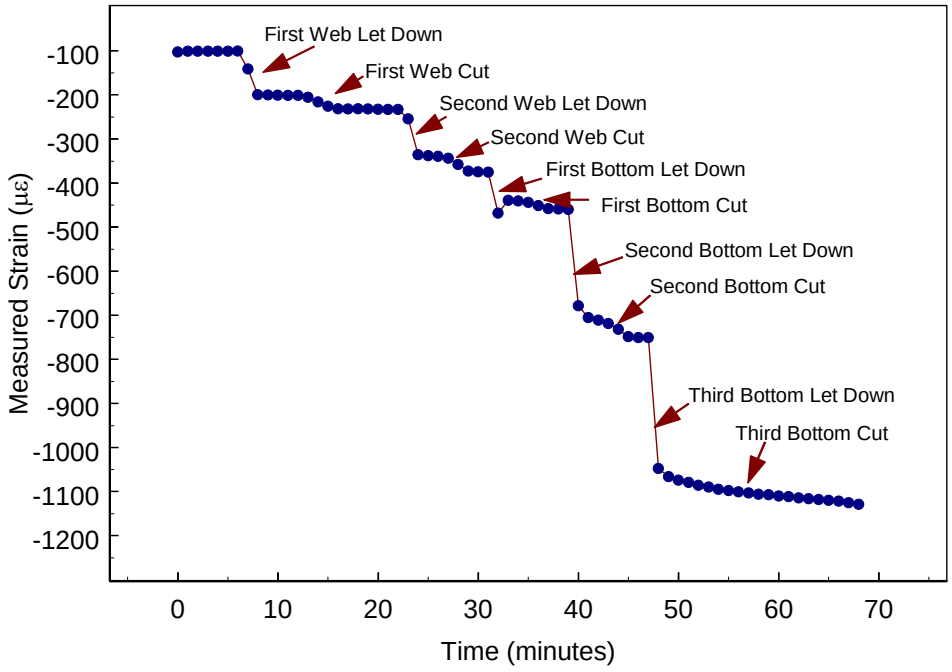

Figure 6.1. Strain History for Prestressing Centroid During Destressing at Midspan of Girder 2B

Figure 6.1 shows that the strains increased abruptly when the live-end strands were let down. They increased further as the dead-end strands were cut and between the destressing stages. This increase in strain between stages is attributed to creep in the concrete during the destressing operation, which typically lasted about 1 hour. The change in strain due to early creep was estimated as the strain changes that occurred between destressing operations.

Table 6.1 lists the stress losses attributable to creep during destressing for the instrumented girders. Girder 2A experienced the largest creep during destressing, which is reasonable, because it also took the longest to destress (2 hours). Girders 2B and 2C experienced similar creep values. The creep values for girders 1A and 1C were also similar to each other.

Table 6.1. Early Creep Losses During Destressing

	1A	1B	2A	2B	2C
Change in Strain (με)	49	58	156	106	107
Stress Loss (MPa)	9.7	11.7	30.3	20.7	20.7
Destressing Time (minutes)	72	72	121	68	52

The values for early creep strain (Table 6.1) were subtracted from total strain during destressing to estimate the strain due to elastic shortening only. Table 6.2 lists the elastic shortening losses computed in this way for each of the instrumented girders.

Table 6.2. Elastic Shortening Losses In Instrumented Girders

Girder	1A	1C	2A	2B	2C
Change in Strain (με)	374	353	982	920	985
Stress Loss (Mpa)	73.1	69.6	193	181	194
Maturity (°C-hrs)	1330	1360	1470	1620	1270

The elastic shortening losses were similar for the two short girders (1A and 1C). For the short girders, the mean elastic shortening loss (71.7 MPa (10.4 ksi)) corresponds to 5.1 percent of the jacking stress 1396 MPa (202.5 ksi).

For the long girders, the mean loss (189 MPa (27.4 ksi)) corresponds to 13.5 percent of the jacking stress. As with the short girders, the elastic losses were similar to each other for the three long girders. For each long girder, the elastic loss was within 5% of the mean.

For each of the instrumented girders, the maturity at the time of destressing at the centroid of the prestressing strand was calculated using Equation 5.1 (Table 5.2). As shown in Table 6.2, Girders 1A and 1C had similar maturity values as expected, because they were cured together. Girder 2C had the lowest maturity value followed by girders 2A and 2B. This trend is consistent with the expectation that, the lower the maturity value, the larger the elastic shortening, but the effect was small.

6.3 GIRDER CREEP AND SHRINKAGE

Creep is the time-dependent flow of concrete caused by its being subjected to stress. This deformation, which occurs rapidly at first and then decreases with time, can be several times larger than the deformation due to elastic shortening. Creep has been found to depend on the mix proportions, humidity, curing conditions and maturity of the concrete when first loaded (Nilson 1987). The deformation due to creep causes a shortening of the prestressing strands, which decreases the strand stress.

Shrinkage of the concrete consists of basic and drying shrinkage. Basic shrinkage is caused by hydration of the cement and is independent of boundary conditions. Drying shrinkage is caused by evaporation of excess water and is unrelated to load application or thermal effects. Concrete mixes contain more water than is needed for the hydration of the cementitious material, and this excess water evaporates in time. Drying of the concrete due to the evaporation of the excess water is accompanied by a reduction in volume. The rate of volume reduction occurs initially at a high rate and later diminishes with time.

Shrinkage is affected by many parameters, including mix proportions, type of aggregate, type of cement, curing time, time between the end of external curing and the application of prestressing, and environmental conditions (Nawy 1989). As was the case

for creep, shrinkage of the concrete shortens the prestressing strands, which reduces prestressing force.

The change in strain in the prestressing strands due to creep and shrinkage was computed by subtracting the strain due to elastic shortening (Table 6.2) and deck casting (Table 6.4) from the average change in strain at the prestressing centroid. Figure 6.2 shows the change in strain attributable to creep and shrinkage of the girder concrete and differential shrinkage of the deck at midspan of each instrumented girder.

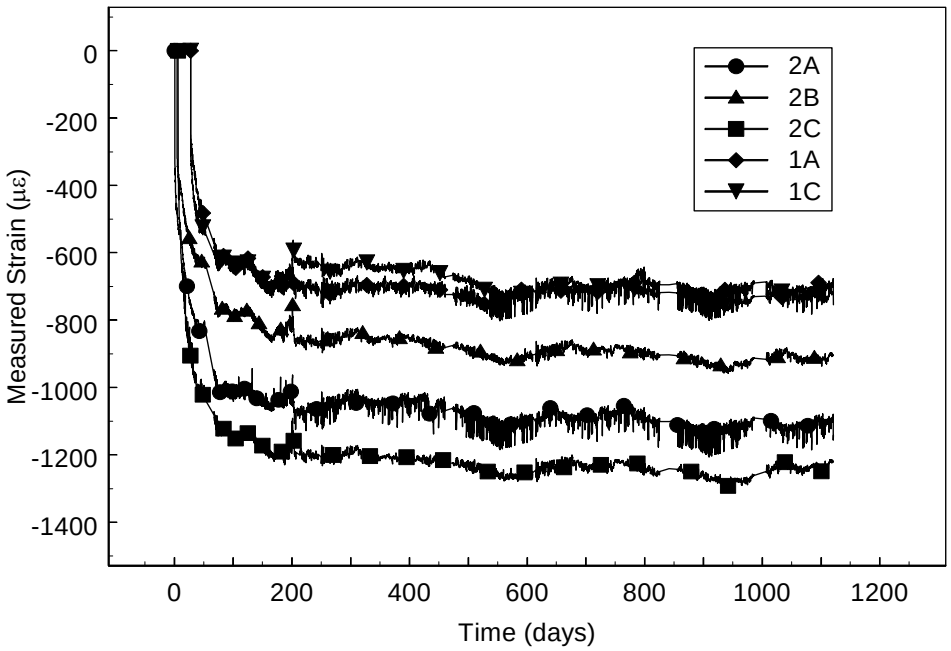

Figure 6.2. Change in Strain at Tendon Centroid Due to Creep and Shrinkage

Figure 6.2 shows that the two instrumented girders in Span 1 (1A and 1C) experienced similar changes in strain due to creep and shrinkage. The total strain due to creep and shrinkage at three years is provided in Table 6.3. The girders in Span 2

experienced different values of creep and shrinkage strain. In particular, Girder 2C experienced the largest change in strain, followed by Girders 2A and 2B.

Tables 6.3. Losses Due to Creep and Shrinkage (Three Years)

Girders	1A	1C	2A	2B	2C
Change in Strain (με)	688	722	1090	904	1230
Stress Loss (MPa)	135	142	214	178	241
Maturity at Destress (°C-hrs)	1330	1360	1470	1620	1270

Theoretically, the change in strain due to shrinkage of the concrete should be the same for all five girders, because each girder has the same cross-sectional dimensions and concrete mix. Edge girders 1A and 2A might be expected to shrink more, because they were exposed to the sun; however this increase in shrinkage is thought to be small. Therefore the differences between the strain measurements in Figure 6.3 are likely due to differences in creep. Since the mix proportions were the same for each girder, the differences between the girders in spans 1 and 2 can be attributed to the different levels of prestress. However, the differences in loss among the Span 2 girders likely result from differences in maturity at the time of destressing. As was the case with the elastic shortening losses (Table 6.2), the creep and shrinkage losses in Span 2 were largest for the girder that was the least mature at release (Girder 2C).

The change in stress at midspan due to creep and shrinkage was calculated by multiplying the change in strain (Figure 6.2) by the modulus of elasticity of the prestressing strands (Equation 6.1). Figure 6.3 shows the prestress loss due to creep and shrinkage. The same trends that were observed in Figure 6.2 are repeated in Figure 6.3.

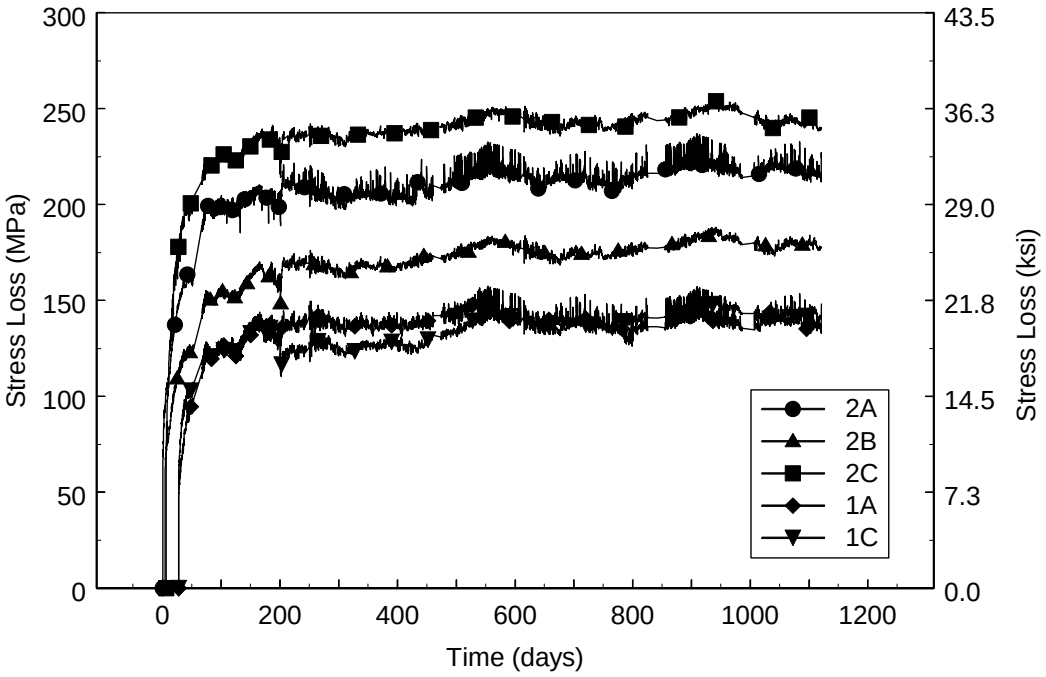

Figure 6.3. Prestress Losses Due to Creep and Shrinkage

The change in strain after deck casting, which can be attributed mainly to differential shrinkage, is listed in Table 6.4. The average change in stress, after the deck casting, was 20.2 and 29.2 MPa (2.9 and 4.2 ksi) for the Span 1 and Span 2 girders. These losses correspond to 1.4 and 2.1 percent of the jacking stress.

Table 6.4. Losses Due to Creep and Shrinkage After Deck Casting

Girders	1A	1C	2A	2B	2C
Change in Strain (με)	79.1	126	174	146	126
Stress Loss (MPa)	15.5	24.8	34.2	28.7	24.8
% of Total Creep and Shrinkage Strain	11.5	17.5	16.0	16.2	10.2

6.4 CASTING OF BRIDGE DECK

At day 200, the prestressing strands experienced an abrupt change in strain due to casting of the deck. This change in strain increased the prestressing force. The casting started at 7:30 in the morning and finished at 4:00 in the afternoon. Figure 6.4 shows the strain history of Girder 2B from about one week before casting until about one week after casting. The strains in the lower gages (BL, BR and LW) became more tensile, Gage MW had almost no change in strain because it was near the girder neutral axis, and the strains in the upper gages (UW and TG) became more compressive. The heat of hydration from the deck is believed to have caused the top gage (TG) to record higher compressive strains than the upper web gage (UW) for a short period after the casting, but after the hydration finished, the top gage recorded lower compressive strains than any other gage.

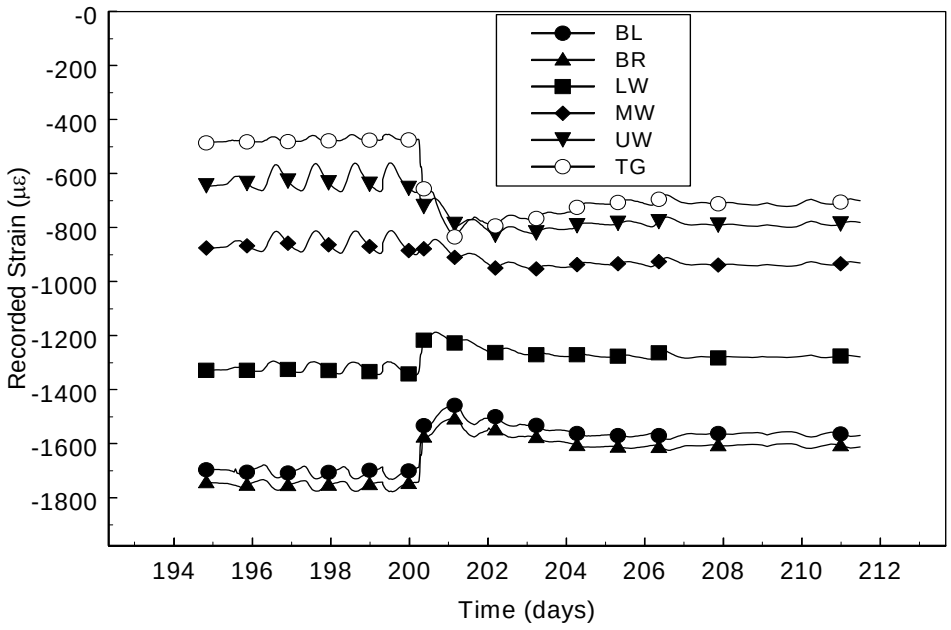

Figure 6.4. Girder 2B Deck Casting Strains

The change in stress due to the deck casting was calculated by multiplying the change in strain by the modulus of elasticity of the prestressing strand (Equation 6.1). Table 6.5 lists the measured gain in strand strain at midspan due to the deck casting and the corresponding calculated change in strand stress. Casting of the deck caused a smaller change in stress in the interior girders (1C, 2B and 2C) than in the exterior girders (1A and 2A). This result was surprising, because the tributary slab width for each of the girders is approximately the same.

Table 6.5. Increase in Strand Stress at Midspan Due to Deck Casting

Girder	1A	1C	2A	2B	2C
Measured Change in Strain (με)	77.9	49.5	204	193	175
Change in Strand Stress (Mpa)	15.3	9.72	40.1	37.9	34.4

6.4 RELAXATION

Intrinsic relaxation in a prestressing strand is the loss of stress while the strand is stretched and maintained at a constant length. This reduction in strand stress continues almost indefinitely, although the rate diminishes with time. Intrinsic relaxation losses depends on the type and grade of prestressing steel, on time and magnitude of initial stress, and on temperature (Nilson 1987). Low relaxation strand is used almost exclusively today, and such strand was used for this project.

Prestress loss due to relaxation of the strand in the instrumented girders could not be measured independently from other losses, so intrinsic relaxation test data performed at room temperature for typical 15 mm (0.6 inch) prestressing strand was obtained from the manufacturer, Sumiden Wire Products Corporation. Equation 6.2 provides an empirically based estimate, calibrated against Sumiden test data, of the loss in stress due to intrinsic relaxation with time for the 15 mm (0.6 inch) strand used in the instrumented girders.

$$\Delta f_{pRE} = \frac{\left[0.147 * \ln(t*24) + 0.796\right] * f_{pj}}{100} \qquad (6.2)$$

where Δf_{pRE} = change in stress due to intrinsic relaxation

ln = natural logarithm

f_{pj} = jacking stress

t = time (days) starting at 1/24

The reduced relaxation coefficient procedure (Section 2.9) was applied to the intrinsic relaxation in order to obtain a more accurate estimate of the relaxation losses. The measured values of stress loss due to creep and shrinkage (Figure 6.3) were used to obtain the reduced relaxation coefficient for each instrumented girder.

Figure 6.5 shows a plot of stress loss due to relaxation (using Equation 6.2 with Equation 2.45) versus time for the prestressing strands used in the instrumented girders, which were pretensioned to 1396 MPa (202.5 ksi). The time shifts between curves represent differences in casting times. The difference in relaxation values for the strands result from different reduction coefficients (Section 2.9) calculated using the different creep and shrinkage values measured in the girders. The Span 1 girders experienced the largest relaxation losses, primarily because they were not stressed as highly as the Span 2 girders and experienced lower creep losses. The relaxation losses ranged from 18.5 to 24.3 MPa (2.68 to 3.52 ksi), which was between 1.3 to 1.7 percent of the jacking stress.

Although the precaster installed a load cell behind the anchor chucks of one web strand, its readings were too unreliable to check the relaxation values. Even if the load cell readings had been reliable, stress changes due to thermal expansion would have made verification difficult.

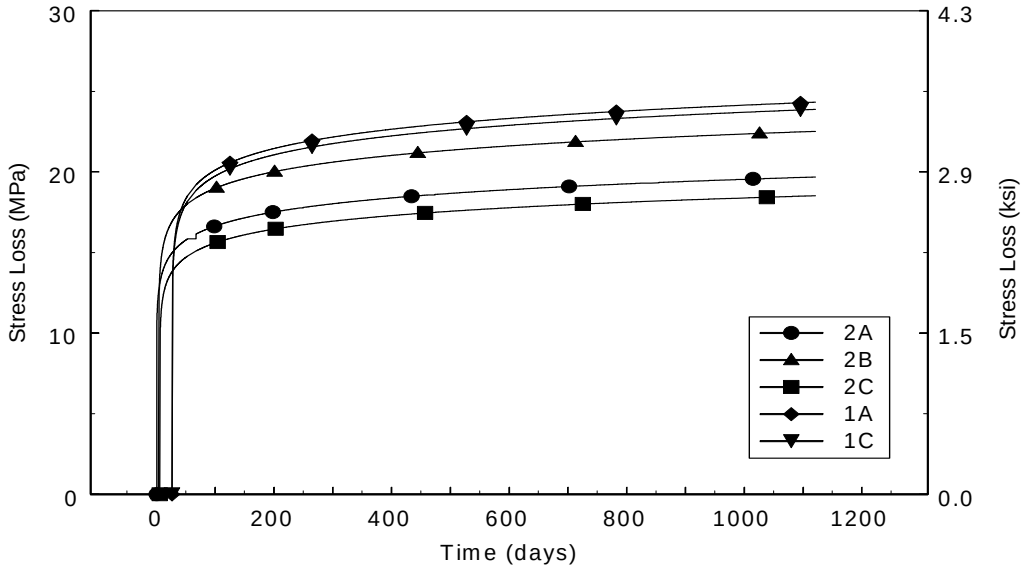

Figure 6.5. Stress Loss Due to Relaxation

6.5 SUMMARY OF OBSERVED PRESTRESS LOSSES

Figure 6.6 provides a summary of the prestress losses estimated in the previous sections. The gain in prestress due to the deck casting (Section 6.3) was subtracted from the total change in stress for each girder.

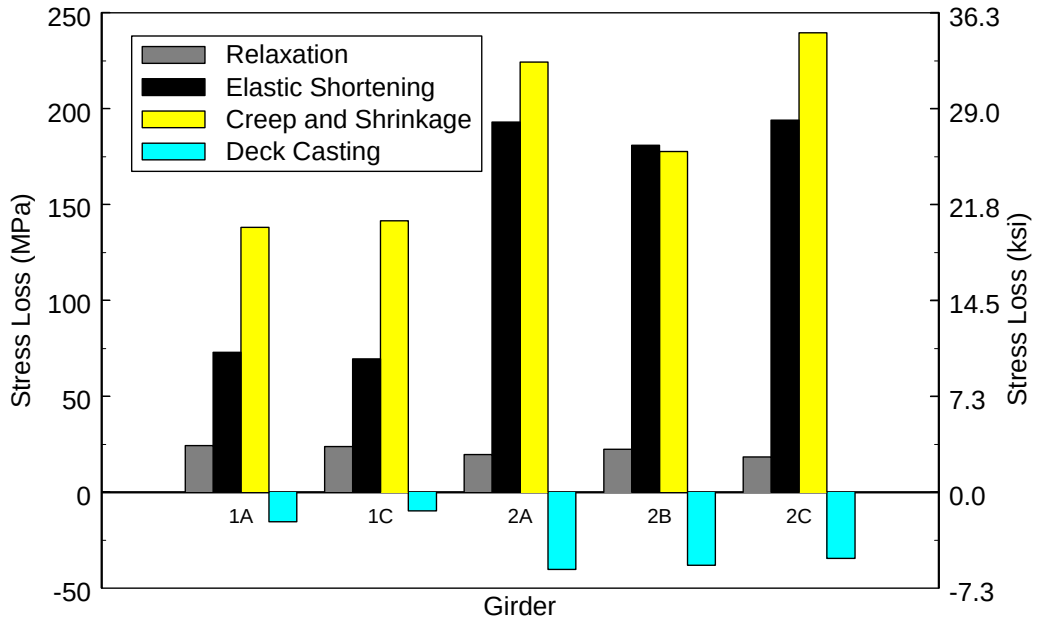

Figure 6.6. Summary of Observed Prestress Losses

The losses due to relaxation, elastic shortening, and shrinkage and creep are nearly identical for the two girders in Span 1 (girders 1A and 1B). This similarity is expected since the girders were cast, cured and destressed together. For the girders in Span 1, the losses due to elastic shortening are approximately half the magnitude of the losses due to shrinkage and creep.

As expected, the losses were much larger in Span 2. The creep and shrinkage losses for Girders 2A and 2C were significantly larger than the elastic shortening losses. For Girder 2B, the elastic shortening losses was almost equal to the creep and shrinkage losses. For all instrumented girders, the relaxation losses were small, and casting of the deck increased the strand stress.

Table 6.6 lists, at three years, the total prestress losses for the instrumented girders and the corresponding percentage of jacking force.

Table 6.6. Total Observed Prestress Losses at Three Years

	Span 1			Span 2			
Girder	1A	1C	Average	2A	2B	2C	Average
Total Loss (MPa)	220	225	223	397	343	418	386
Percent Jacking Stress	15.7	16.1	15.9	28.4	24.5	29.9	27.6

CHAPTER 7

COMPARISON WITH OBSERVED PRESTRESS LOSSES

In this chapter, the observed values of prestress losses (Chapter 6) are compared with values calculated using the recommended PCI General Method (PCI 1975) and AASHTO LRFD Specifications (AASHTO 1994). The material properties used in these methods were based on design equations, rather than measured values, in order to simulate the estimates that would be made during design.

The PCI General Method is a time-stepping algorithm, in which the incremental loss of prestress in each time interval is calculated using the total stress at the start of the interval (Section 2.6). The total stress is then updated before calculating the incremental loss in the next interval. For the AASHTO Refined Method, the total prestress loss at the end of the service life is calculated in a single step. The AASHTO Refined Method was modified into a time-history method in this chapter by multiplying the ultimate prestress loss predicted by the AASHTO method by creep and shrinkage coefficients provided in the AASHTO Specifications (Section 2.3).

7.1 ELASTIC SHORTENING

In this section, the measured elastic shortening losses in the instrumented girders (1A,1C, 2A, 2B and 2C), and the elastic shortening losses predicted using the AASHTO LRFD Specifications (1994) and the PCI General Method (1975) are compared. The predicted elastic shortening losses were calculated using the guidelines presented in Section 2.2 (AASHTO LRFD Specifications) and Section 2.6 (PCI General Method). The measured elastic shortening losses were reported in Section 6.2.

The assumed value of the modulus of elasticity at transfer (E_{ci}) greatly affects the calculated elastic shortening loss. According to the AASHTO LRFD Specifications (1994), E_{ci} should be calculated as

$$E_{ci} = 0.043 w^{1.5} \sqrt{f'_{ci}} \quad \text{(MPa)} \qquad (7.1)$$

where E_{ci} = modulus of elasticity at release of the prestressing strands
= 37.9 GPa (5500 ksi) using Equation 7.1
w = unit weight of concrete, 2480 kg/m^3 (0.155 kcf) WSDOT design value
f'_c = concrete compressive strength at release (51.0 MPa (7.4 ksi))

However, this equation, which is also used in the ACI Building Code (ACI 1995), has been found (Nawy 1996) to overestimate the elastic modulus for high-strength concrete, so the ACI 363 Committee Equation, which is specifically for high-strength concrete, was used as a second means to calculate the modulus of elasticity (ACI 363, 1990).

$$E_{ci} = \left(3320\sqrt{f'_{ci}} + 6900\right)\left(\frac{w}{2320}\right)^{1.5} \quad \text{(MPa)} \qquad (7.2)$$

For the values of w and f'_c listed in Equation 7.1, E_{ci} is equal to 33.8 GPa (4900 ksi) using Equation 7.2. This value is 11% lower than the value computed with Equation 7.1.

Figure 7.1 compares the predicted elastic shortening losses using the PCI and AASHTO methods with the measured elastic shortening losses for the girders in Span 2. A unit weight of 2480 kg/m^3 (0.155 kcf) was used for all the calculated values. In the figure, the word in the parentheses indicates the source of the equation that was used to calculate the elastic modulus. For example, PCI (AASHTO) means that the value was computed using the PCI method for losses and the AASHTO equation for E_{ci}.

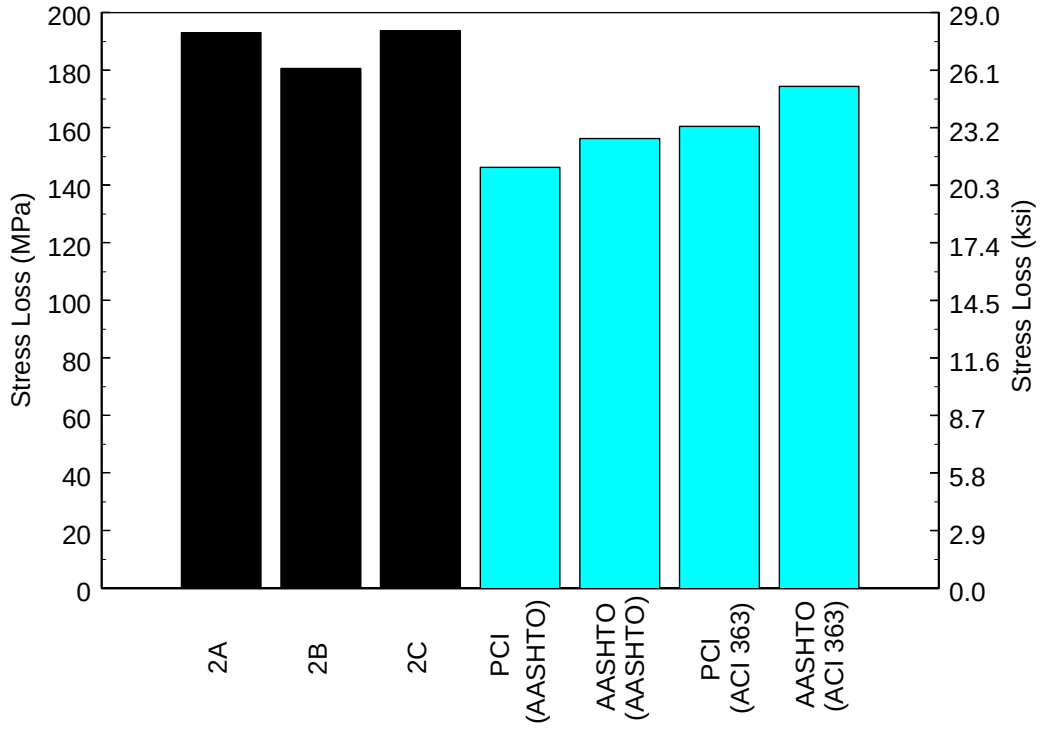

Figure 7.1. Observed and Computed Elastic Shortening Losses for Span 2 Girders

The average measured elastic shortening loss for the Span 2 girders was 189 MPa (27.4 ksi). Regardless of the equation used to calculate the initial elastic modulus (Equation 7.1 or 7.2), the average measured loss exceeded the predicted loss using either the AASHTO LRFD Method (AASHTO 1994) or the PCI Method (PCI 1975). The difference between the measured and calculated losses was larger when the elastic modulus was calculated with the equation in the AASHTO LRFD Specifications (1994). This finding would seem to confirm previous research (Nawy 1996) that Equation 7.1 overestimates the elastic modulus for high-strength concrete. Even if the modulus of elasticity was calculated using the ACI 363 Equation (ACI 1990), the elastic shortening losses were still underestimated.

Compared with the PCI exact method, the approximate AASHTO LRFD Method predicts elastic shortening losses that were closer to the measured losses. This result does not indicate that the AASHTO method is better than the PCI method. Because the same elastic modulus was used for both methods, the difference lies in the calculation of the initial prestress force. The AASHTO method approximates the initial stress after transfer as $0.7f_{pu}$ (1300 MPa (189 ksi))(Equation 2.3). This value is higher than the measured initial prestress stress (1396–189 =1207 MPa (202.5-27.4 = 175 ksi)). Essentially, the AASHTO result is closer to the measured losses only because it overestimated the initial prestress.

Figure 7.2 shows the measured and predicted elastic shortening losses for Span 1 using a unit weight of 2480 kg/m^3 (0.155 kcf). The same notation that was used in Figure 7.1 is used in 7.2.

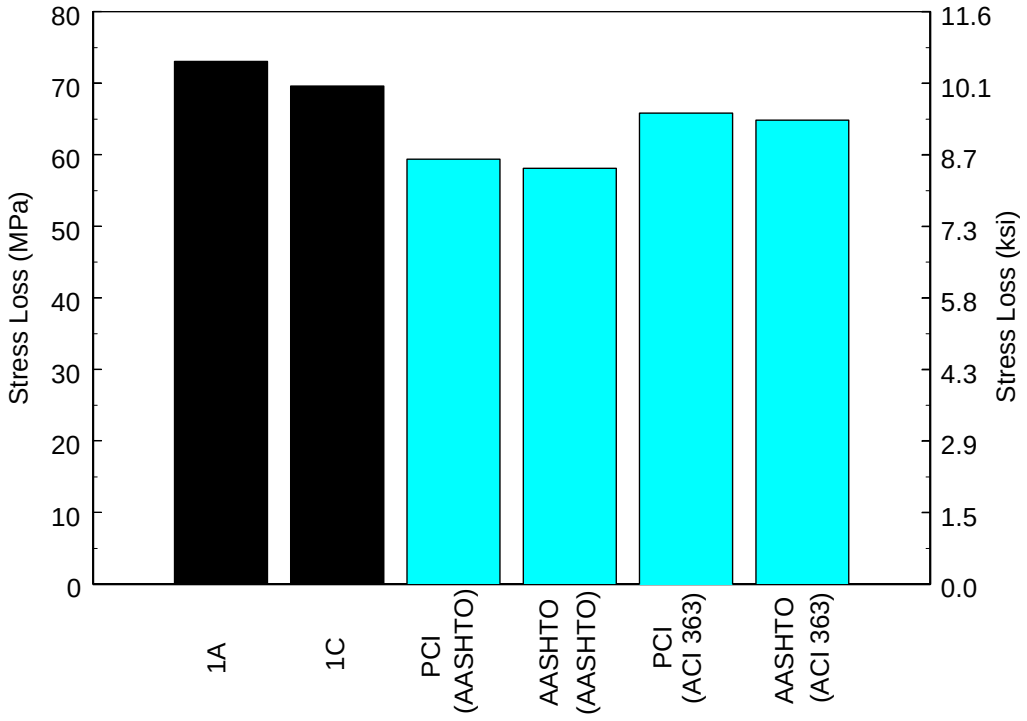

Figure 7.2. Observed and Predicted Elastic Shortening Losses for Span 1 Girder

For the Span 1 girders, the average measured loss was 71.3 MPa (10.3 ksi). The losses are smaller than those in Span 2, because fewer prestressing strands were used. In Span 1, the PCI and AASHTO methods again underestimated the measured elastic shortening losses. As with the Span 2 girders, the predicted elastic shortening losses were closer to the measured losses when the elastic modulus was calculated with the ACI 363 equation (Equation 7.2).

The elastic shortening losses predicted using the AASHTO LRFD Method and the PCI Method were within 2% of each other, with the PCI Method predicting slightly higher losses. For Span 1, the AASHTO method now predicts lower losses than the PCI method, because the approximated initial prestress (1300 MPa (189 ksi)) is now lower than the actual prestress (1396 - 71.3 = 1325 MPa (202.5 – 10.3 = 192 ksi)).

Two explanations are possible as to why the measured elastic shortening is higher than the predicted: (1) either the calculated elastic modulus was larger than the actual elastic modulus or (2) the estimated values of early creep losses was too low (Section 6.1).

Part of the discrepancy between measured and predicted losses can be attributed to using too high a value for the unit weight of concrete. The WSDOT used a value of 2480 kg/m^3 (0.155 kcf) for the unit weight of the concrete. The unit weight of the concrete measured by Central Premix Company was 2400 kg/m^3 (0.150 kcf), which is 3% lower. If the measured unit weight had been used in design, the calculated modulus of elasticity would have decreased by 5%.

Table 7.1 lists the average observed and predicted elastic shortening losses as a percentage of the total jacking stress for unit weights of 2480 kg/m^3 (0.155 kcf) and 2400 kg/m^3 (0.150 kcf). Table 7.1 shows that, when the measured value of concrete unit weight (2400 kg/m^3 (0.150 kcf)) was used, the predicted elastic shortening losses were closer to the average measured values.

Table 7.1. Elastic Shortening Loss as a Percentage of Jacking Stress

	Average Measured	PCI (AASHTO E_c)	AASHTO (AASHTO E_c)	PCI (ACI 363 E_c)	AASHTO (ACI 363 E_c)
w = 2480 kg/m^3					
Span 1	**5.1**	**4.3**	**4.2**	**4.7**	**4.6**
Span 2	**13.5**	**10.5**	**11.2**	**11.5**	**12.5**
w = 2400 kg/m^3					
Span 1	**5.1**	**4.5**	**4.4**	**4.9**	**4.9**
Span 2	**13.5**	**10.9**	**11.8**	**12.0**	**13.1**

Using the PCI exact method for the girders in spans 1 and 2, a modulus of elasticity of 31.0 GPa (4500 ksi) and 28.3 MPa (4100 ksi) respectively would be required to produce the measured observed elastic shortening losses. This value is even smaller than the elastic modulus calculated using the ACI 363 Equation (32.2 MPa (4670 ksi)) with a unit weight of 2400 kg/m^3 (0.150 kcf). Although smaller than the predicted elastic modulus with the ACI 363 equation, the required elastic modulus for spans 1 and 2 falls within the range of measured elastic modulus values from the material samples (Barr et al. 2000a).

The other possible explanation as to why the elastic shortening losses were higher than the predicted losses, was that the procedure for estimating early creep losses during destressing produced values lower than the actual ones. In Section 6.1, early creep was defined as any change in strain that occurred between destressing stages. Separating the individual destressing stages from the total destressing time is believed to have been done with reasonable accuracy. However, it is also reasonable to assume that some creep did occur during the destressing stages.

The early creep during the destressing stages was estimated for each of the instrumented girders. For example, for Girder 2B (Figure 6.1) the total minutes during destressing (68) were divided into estimated minutes that elastic shortening occurred (17)

and estimated minutes during which early creep occurred (51 minutes). The estimated change in stress during the destressing stages could be calculated as the ratio of time attributed to elastic shortening over the total destressing time, multiplied by the estimated change in stress due to early creep losses (Table 6.1) (i.e. 17/68*20.7 = 5.2 MPa for Girder 2B). For the instrumented girders, the estimated change in stress due to early creep loss during the destressing stages was between 2 to 3% of the measured elastic shortening losses. Because these values are small, it is believed that the difference between the measured and calculated elastic shortening losses is more likely due to a smaller elastic modulus value than was calculated with equations 7.1 and 7.2.

7.2 SHRINKAGE

Changes in prestress due to shrinkage stem from two sources. The first source is shrinkage of the prestress girder. The second source occurs in a composite girder in which differential shrinkage between the deck and girder concrete changes the strand stress. The AASHTO Refined Method (AASHTO 1994) and the PCI General Method (PCI 1975) provide guidelines for calculating changes in stress due to girder shrinkage but do not provide procedures for calculating stress changes due to differential shrinkage.

The loss of stress due to shrinkage alone could not be identified in the instrumented girders, because it was not possible to separate the effects of shrinkage and creep. For the AASHTO and PCI methods, Figure 7.3 compares the calculated prestress losses due to shrinkage for the girders in Span 1 and Span 2. Note that the Span 1 girders were cast approximately 27 days after the long Span 2 girders.

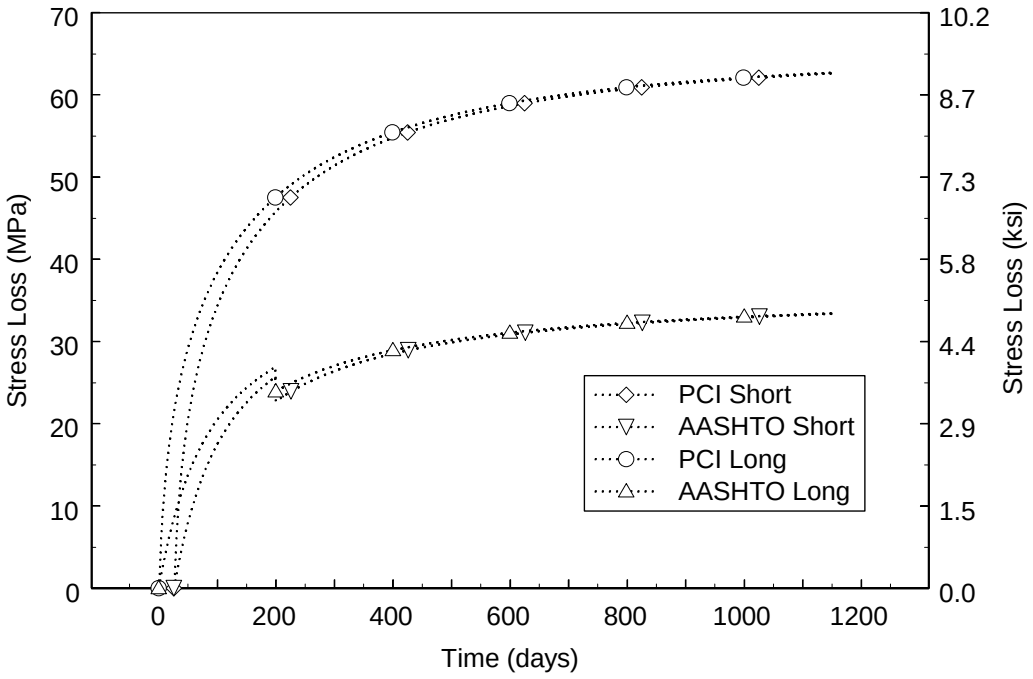

Figure 7.3. AASHTO and PCI Shrinkage Loss Predictions

Figure 7.3 shows that the methods predict ultimate stress losses due to shrinkage that are similar for the two spans, as expected, but the ultimate shrinkage losses predicted by the two methods differed greatly. The PCI method predicts an ultimate shrinkage loss of 63 MPa (9.1 ksi) at 3 years, while the AASHTO method predicts an ultimate loss of 35 MPa (5.0 ksi). For the AASHTO Method, the jump in the shrinkage stress loss when the deck was cast is due to a change in the parameter (k_s) that was used to make the ultimate stress loss time dependent (Section 2.3). This parameter affects the rate of loss, but not the ultimate value. The AASHTO LRFD refined method is the simpler method, because the ultimate loss is only a function of the humidity. The PCI method is more complex; the shrinkage losses are a function of the elastic modulus, volume-to-surface ratio and time since curing.

7.4 CREEP

The prestress losses due to creep in the concrete were calculated using the PCI (Section 2.6) and AASHTO methods (Section 2.3). Figures 7.4 and 7.5 show the prestress losses due to creep for the girders in spans 2 and 1 respectively.

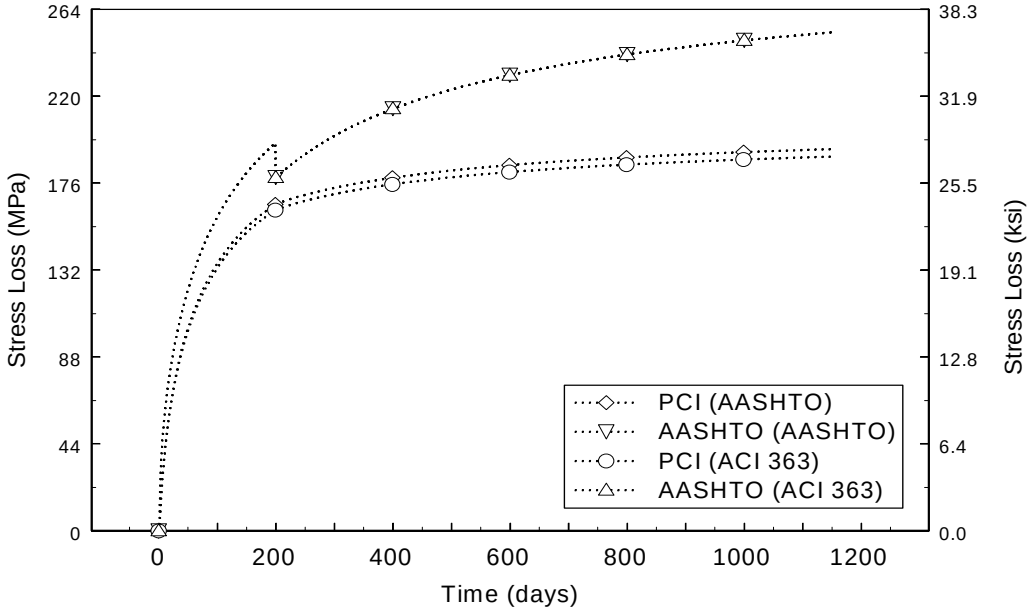

Figure 7.4. Computed Prestress Losses Due to Creep in Span 2 Girders

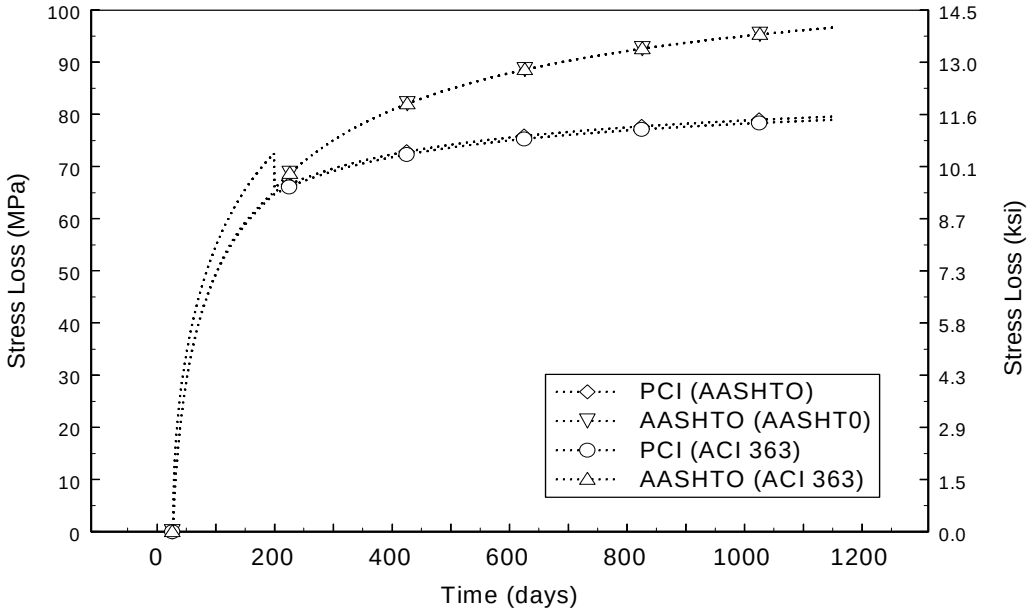

Figure 7.5. Computed Prestress losses Due to Creep in Span 1 Girders

The AASHTO LRFD Specifications (1996) predict a stress loss due to creep that is higher than that predicted by the PCI method, regardless of span. Both methods predict initially high rates of losses through the first 100 days after which the rate of stress loss decreases. The choice of equation for estimating the elastic modulus barely affected the creep losses computed in the PCI General Method (1975). One would expect there to be less stress loss due to creep if the elastic shortening loss increased (because the aplied force would be lower), which is what happened in the PCI Method. In the AASHTO LRFD Method (1994) the calculated creep loss was independent of the elastic modulus used. This result is expected for this method. If the approximate method of calculating f_{pi} is used (Section 2.3), f_{cgp} will not change even though the elastic modulus changes.

7.5 CREEP AND SHRINKAGE

The combination of changes in strain due to creep and shrinkage was measured in the instrumented girders (Section 6.3). The calculated prestress losses due to girder shrinkage (Section 7.3) and creep (Section 7.4) using the AASHTO LRFD Specifications (1994) and the PCI General Method (1975) were summed to obtain the combined creep and shrinkage losses (Section 7.5.1). The portion of creep and shrinkage losses that are believed to have resulted from differential shrinkage are presented in Section 7.5.2.

7.5.1 Total Creep and Shrinkage Losses

Figure 7.6 shows the observed and predicted combined creep and shrinkage losses for the girders in Span 2.

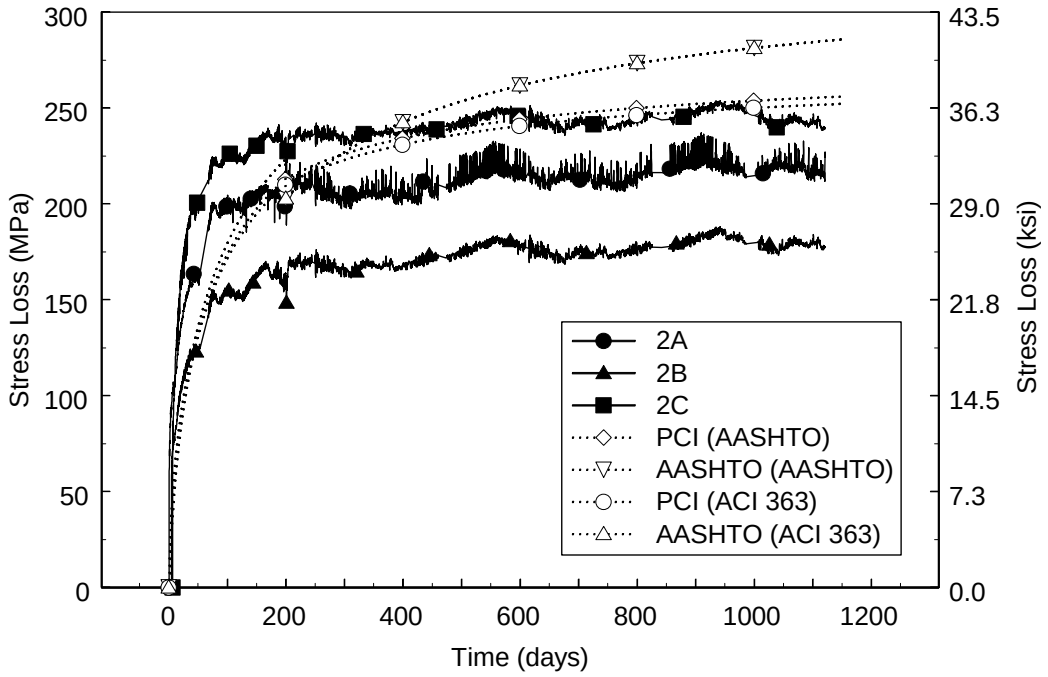

Figure 7.6. Observed and Predicted Creep and Shrinkage Losses for Span 2

The creep and shrinkage losses predicted using the AASHTO and PCI methods exceeded the measured creep and shrinkage losses at three years for all three long girders. At three years, the PCI Method was 19% higher than the average measured creep and shrinkage losses, while the AASHTO Method was 34% higher. Both PCI and AASHTO methods produced similar results, regardless of the choice of elastic modulus equation.

The combination of creep and shrinkage losses was also computed for the instrumented girders in Span 1. Figure 7.7 shows the observed and predicted creep and shrinkage losses for the girders in Span 1.

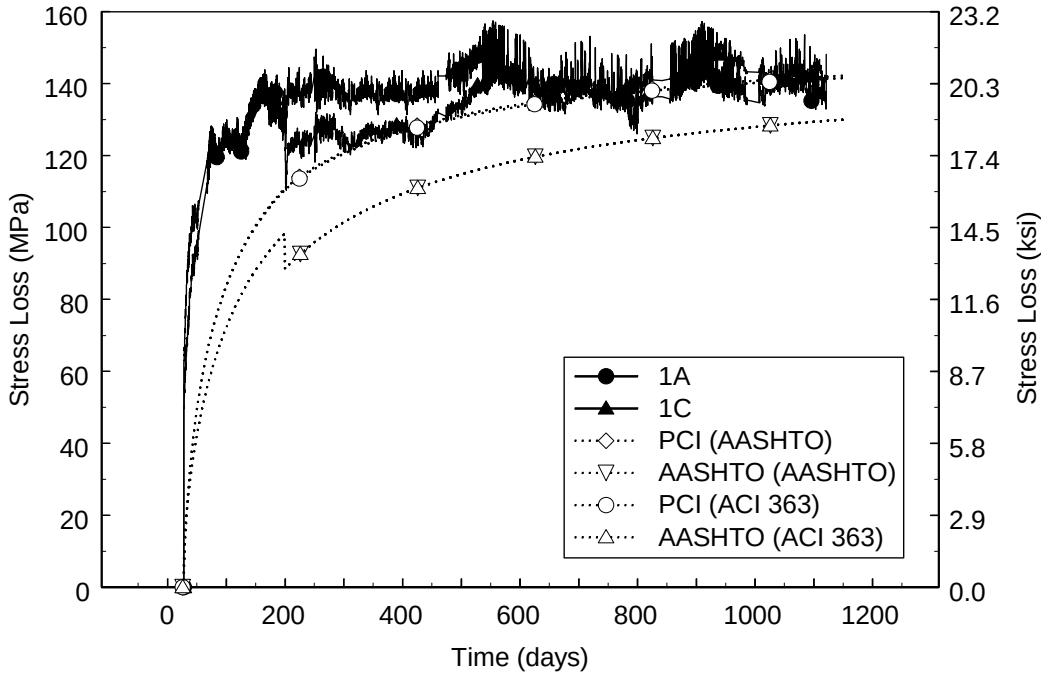

Figure 7.7. Observed and Predicted Creep and Shrinkage Losses for Span 1

For Span 1, the predicted values are lower than the observed values throughout the first three years of the girders' life. The discrepancy was largest initially but

therefore diminished with time. The PCI method predicts a creep and shrinkage loss that is closer to the measured values than the AASHTO method. The PCI predicts shrinkage and creep prestress losses that were about 2% lower than the average measured losses, while the AASHTO method was 10% lower at three years. Table 7.2 lists the creep and shrinkage losses at three years as a percentage of the initial jacking force.

TABLE 7.2. THREE YEAR CREEP AND SHRINKAGE LOSSES AS PERCENT OF THE JACKING STRESS

Girder	Average Observed	PCI (AASHTO E_c)	AASHTO (AASHTO E_c)	PCI (ACI 363 E_c)	AASHTO (ACI 363 E_c)
Span 1	10.4	10.4	9.4	10.3	9.4
Span 2	15.3	18.8	20.6	18.5	20.6

7.5.2 Differential Shrinkage

The deck was placed 200 days after casting the first bridge girder, and under service conditions, the stress at the bottom of the girder was designed to be low (-0.89 MPa (0.13 ksi))(Table 3.6). Therefore, any changes in strand stress after deck casting can reasonably be attributable to differential shrinkage. After the deck was cast, the spans were connected by casting a pier cap between them that contained considerable top reinforcing steel. Analyses of data from a live-load test (Barr et al. 2000b) indicates that the girders behaved as though they were continuous. Figure 7.8 shows the change in strand stress for the Span 2 girders (2A, 2B and 2C) for the first 30 days starting after the deck was cast (Day 200). It was computed from the measured changes in strain in the bottom flange. Most of the stress changes occurred within the first week after casting and leveled off after about 30 days.

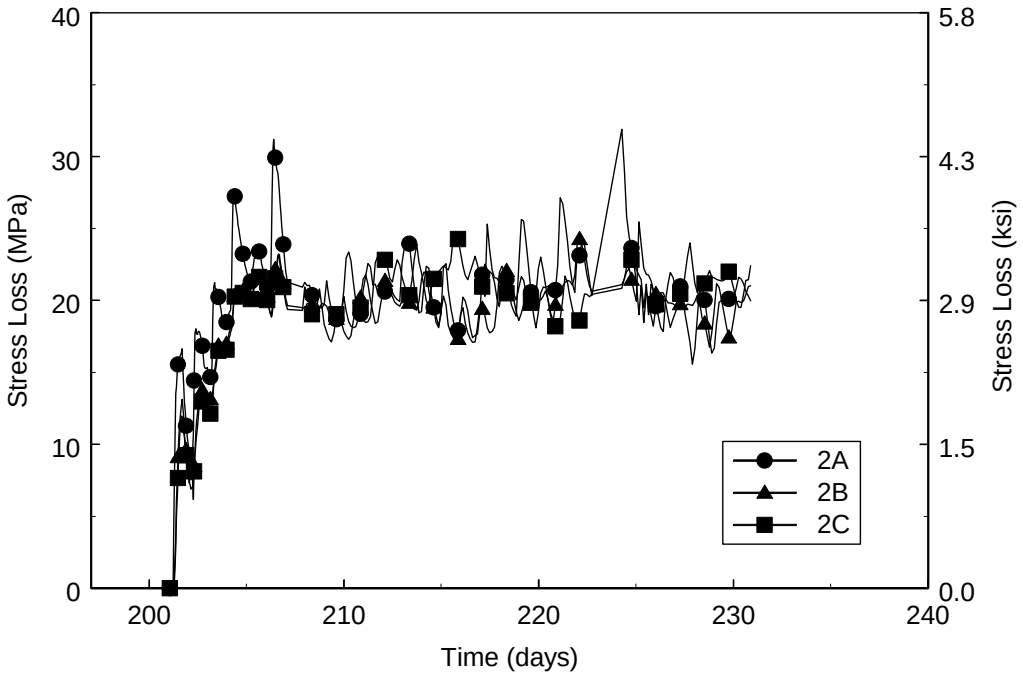

Figure 7.8. Change in Strand Stress After Deck Casting

The effect of differential shrinkage was analyzed according to the procedure outlined in Section 2.8 considering the SR18/SR516 Bridge as a three-span continuous bridge. In these calculations, the values for free shrinkage strain (ε_{sh}) (-830 microstrain), girder modulus of elasticity (E_g) (37.9 GPa (5500 ksi)) and deck modulus of elasticity (E_d) (35.2 GPa (5100 ksi)) were all taken from concrete samples taken at the time of casting (Barr et al. 2000a). The deck concrete had a specified compressive strength of 27.6 MPa (4000 psi), so a creep coefficient (C_c) of 2.9 was used in the calculations (Nilson 1991).

The measured response of the SR18/SR516 Bridge to differential shrinkage was compared to the calculated response through strain measurements. A change in strain of -125 microstrain due to differential shrinkage was calculated to occur in the deck

concrete. This is close to the –175 microstrain that was measured in the deck (Figure 5.16). Table 7.3 compares the measured changes in strand stress after deck casting with the changes in stress predicted by modeling the girders as simply supported and continuous.

Table 7.3. Strand Loss Due to Differential Shrinkage

	Average Observed	Simply Supported	Continuous
Span 1	14.1	-17.9	26.7
Span 2	20.6	-17.9	35.7

Assuming continuous girders, the prestress loss was calculated to be 35.7 MPa (5.18 ksi) in the Span 2 girders. This value is close to the average measured change in strand stress in the Span 2 girders of 20.6 MPa (3.0 ksi). If the girders had been simply supported, the predicted change in stress would have been a stress gain of –17.9 MPa (-2.6 ksi).

The average prestress loss for the girders in Span 1 was 20.1 MPa (2.9 ksi). This value is also close to the predicted loss of 26.7 MPa (3.87 ksi) for a continuous beam. The stress gain for the Span 1 girders is the same as the Span 2 girders for the simply supported condition, because the change in stress due to differential shrinkage does not depend on the span length for a simply supported girder.

7.6 RELAXATION

In this section, the reduced intrinsic relaxation losses from the manufacturer (Section 6.4) are compared with the relaxation losses predicted by the AASHTO LRFD Specifications (1994) and the PCI General Method (1975). The procedure for calculating relaxation loss throughout time is described in Section 2.3 for the AASHTO Refined Method and Section 2.6 for the PCI General Method. A comparison of the relaxation losses for the girders in Span 1 and Span 2 are shown in Figures 7.9 and 7.10

respectively.

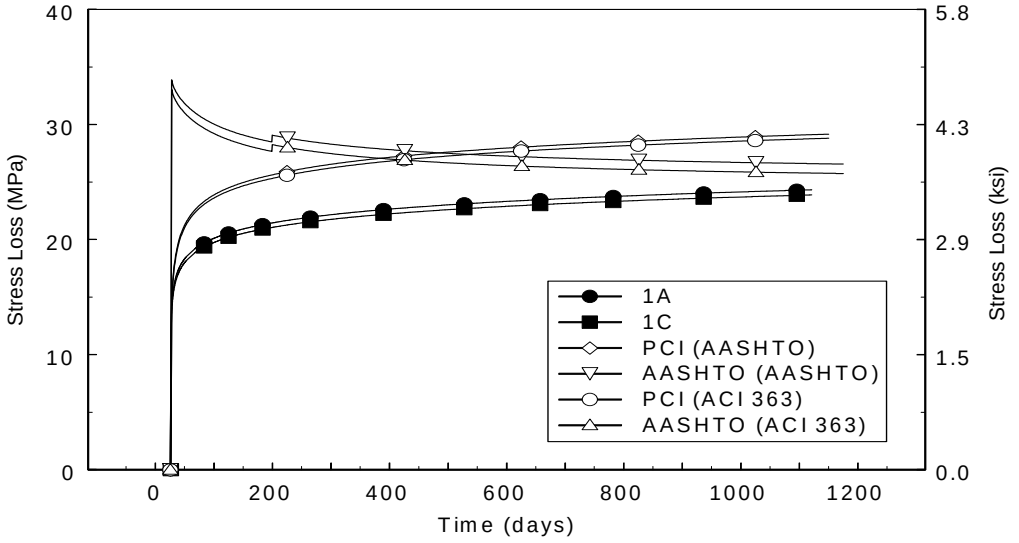

Figure 7.9. Observed and Predicted Relaxation Losses in Span 1

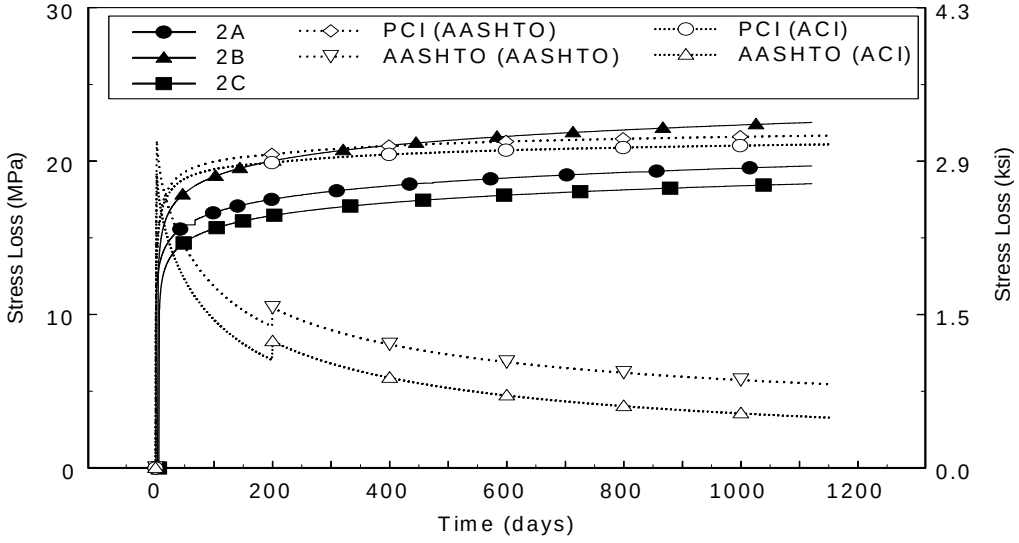

Figure 7.10. Observed and Predicted Relaxation Losses in Span 2 Girders

In general, there was less relaxation loss for the Span 2 girders than the Span 1 girders. This result was expected, because the sustained strand stress was lower in Span 2.

The PCI method predicts a loss that varies with time in a manner that resembles the measured data. For Span 2, the values also lie within the scatter band of the measured data. For Span 1, the predicted values are about 25% higher than the measured.

The AASHTO method suggests a loss that, after transfer, decreases with time. This prediction is counterintuitive and arises from the fact that the method is really intended for calculation of prestress loss only at one time (e.g., the end of service life) rather than continually over time. However, its use as a time-dependent function has been suggested by Lwin and Khaleghi (1996). The jump in relaxation loss at day 200 is a result of the change in volume-to-surface ratio when the deck is cast. This change in volume-to-surface ratio causes a jump in the creep and shrinkage coefficients (Equations 2.9 and 2.11 respectively), which in turn, causes a jump in the relaxation loss (Equation 2.13).

The relaxation loss predicted with the AASHTO LRFD Specifications is small for the Span 2 girders. According to the AASHTO LRFD Equation (Equation 2.13), the relaxation loss will become smaller as the elastic shortening, creep and shrinkage losses increase and, in extreme cases, could even become negative. Table 7.4 lists the values for the relaxation prestress losses, as a percentage of the jacking stress, for the two methods and the reduced intrinsic manufacturer's data at 3 years.

Table 7.4. Predicted Relaxation Loss as a Percentage of Jacking Stress at 3 Years

Girder	**Average Observed**	PCI (AASHTO E_c)	AASHTO (AASHTO E_c)	PCI (ACI 363 E_c)	AASHTO (ACI 363 E_c)

Span 1	1.7	2.1	1.9	2.1	1.8
Span 2	1.4	1.6	0.4	1.5	0.2

7.7 DECK CASTING

In this section, the measured change in stress due to the deck casting is compared with the predicted change in stress. The PCI General Method and the AASHTO LRFD Method use a simply supported equation to estimate the change in stress due to deck casting (Equation 2.36), the only variable that was changed in this section was the elastic modulus of the concrete (either Equation 7.1 or 7.2). In addition to implementing the PCI and AASHTO methods, the change in stress was also calculated using a two-degree of freedom model (Section 2.7) that was developed for the SR18/SR516 Bridge with the elastic modulus values calculated with Equations 7.1 and 7.2. The girder concrete was assumed to have a compressive strength of 68.9 MPa (10 ksi) at the time the deck was cast. Although the compressive strength was higher (Barr et al. 2000a) the value of 68.9 MPa (10 ksi) would be what a designer would use.

Figure 7.11 shows the average measured and the calculated change in stress for the girders in Spans 1 and 2. Table 7.5 lists the calculated and average measured changes as a percentage of total jacking stress due to deck casting.

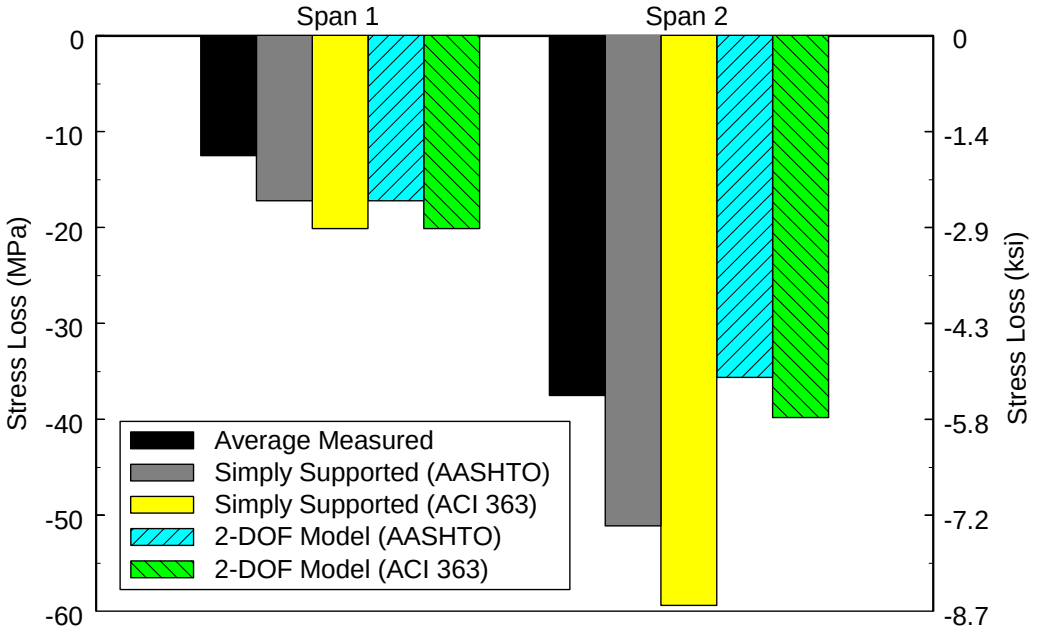

Figure 7.11. Comparison of Average Changes in Stress During Deck Casting

Table 7.5. Stress Losses During Deck Casting

	Average Observed	Simply Supported (AASHTO E_c)	Simply Supported (ACI 363 E_c)	2-DOF Model (AASHTO E_c)	2-DOF Model (ACI 363 E_c)
Span 1	12.5	17.2	20.1	17.2	20.1
Span 2	37.5	51.1	59.4	35.6	39.8

When the girder was modeled as simply supported, the changes in stress were over predicted, regardless of which equation was used to calculate the elastic modulus.

The changes in stress due to deck casting for the simply supported girders were more closely predicted when the AASHTO equation for the modulus of elasticity was used. The AASHTO equation compared more closely with the measured values because it predicted a high value for the elastic modulus, which reduced the changes in stress.

To predict more accurately the changes in stress due to deck casting, a partially restrained end condition, such as the one used in the two-degree-of-freedom model explained in Section 2.7, would have to be used. According to the results from this model, the one-foot strip of concrete significantly affected the behavior of the Span 2 girders. This strip of concrete inhibited the rotation of the Span 2 girders and caused the girders to behave more as fixed girders than as simply supported girders. Using the two-degree-of-freedom model, the predicted changes in prestress for the Span 2 girders were within 6% of the measured values, regardless of the equation used to calculate the elastic modulus. However, the predicted stress change in the Span 1 girders was unchanged because the elastomeric bearing at the abutments were very flexible compared with the girder, so they offered almost no restraint to girder end rotation.

7.8 TOTAL PRESTRESS LOSSES

The total prestress losses due to relaxation of the prestressing strand, elastic shortening, shrinkage, creep and deck casting were added to obtain the total prestress losses. Figure 7.12 shows the observed and predicted total prestress losses for the Span 2 girders.

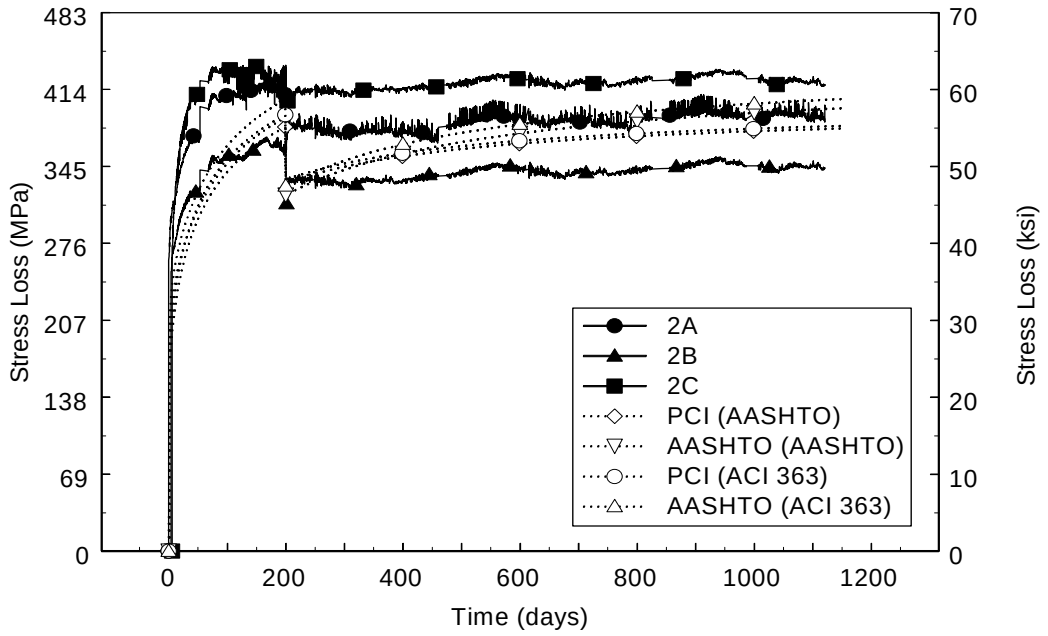

Figure 7.12. Total Prestress Losses for Span 2 Girders

Figure 7.12 shows that the total observed prestress losses for Span 2 girders are reasonably well predicted by the AASHTO LRFD Specifications (1994) and the PCI General Method (1975). The AASHTO method predicts total prestress losses that are slightly higher than the PCI method, mainly because the computed elastic shortening losses are larger. The total losses are slightly larger for the AASHTO method when the ACI elastic modulus equation was used, but the PCI method predicted nearly identical losses at three years, regardless of which elastic modulus equation was used.

Figure 7.13 shows the total observed and predicted prestress losses for the Span 1 girders. The total observed prestress losses for the Span 1 girders are higher than the losses predicted for both the PCI and AASHTO methods. The difference between the observed and predicted values is larger at first and diminishes with time. The PCI method predicts a total prestress loss that is slightly higher than the AASHTO method.

Table 7.6 lists the total prestress losses at three years as a percentage of the initial jacking stress.

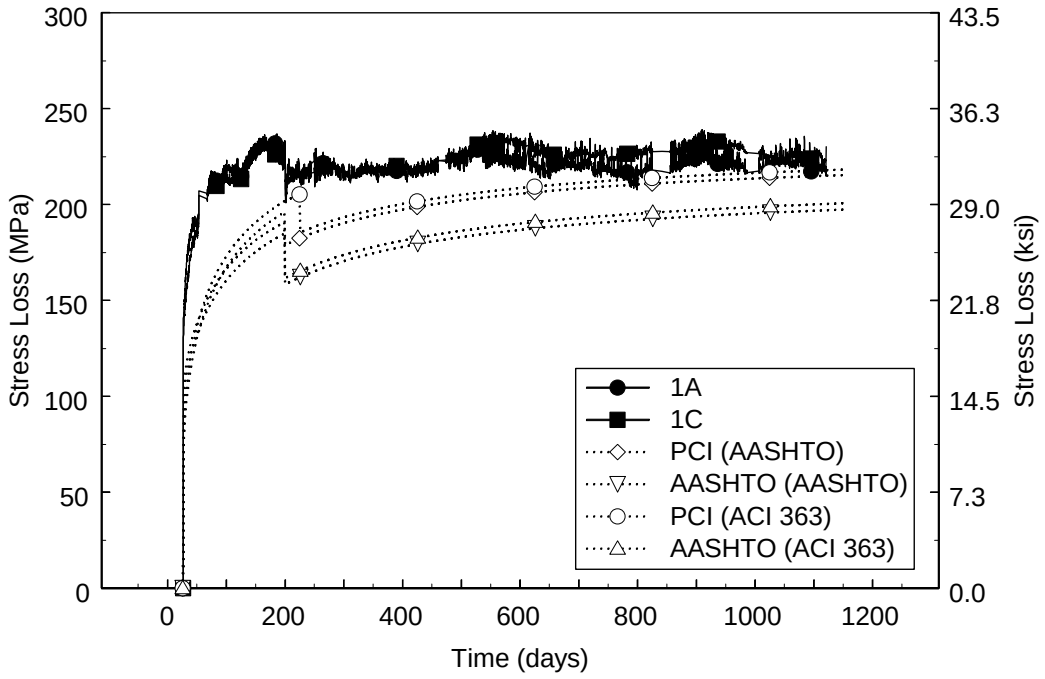

Figure 7.13. Total Prestress Losses for Span 1 Girders

Table 7.6. Total Prestress Losses at 3 Years as Percentage of Jacking Stress

Girder	Average Observed	PCI (AASHTO E_c)	AASHTO (AASHTO E_c)	PCI (ACI E_c)	AASHTO (ACI E_c)
1A	16.3	15.5	14.2	15.7	14.4
2A	27.6	27.2	28.5	27.3	29.1

The total prestress losses predicted using the AASHTO LRFD Specifications (1994) and the PCI General Method (1975) were close to the average total measured losses. However, this agreement is not a result of the methods accurately predicting each of the individual components. Instead, the total changes in prestress compared well, because some predictions were too low (e.g., elastic shortening) and others were too high (e.g., creep and shrinkage, relaxation and deck casting).

Table 7.7 summarizes the measured changes in stress for each of the instrumented girders and the calculated changes in stress at three years for each of the methods investigated in this chapter.

Table 7.7. Observed and Calculated Prestress Losses at Three Years (MPa)

Loss	Girder	1A	1C	Avg.	2A	2B	2C	Avg.
Total	PCI (AASHTO E_c)	216		216	380			380
	AASHTO (AASHTO E_c)	198		198	398			398
	PCI (ACI 363 E_c)	219		219	382			382
	AASHTO (ACI 363 E_c)	202		202	406			406
	Observed	230	223	227	396	343	418	386
Elastic Shortening	PCI (AASHTO E_c)	59.4		59.4	146			146
	AASHTO (AASHTO E_c)	58.1		58.1	157			157
	PCI (ACI 363 E_c)	65.8		65.8	161			161
	AASHTO (ACI 363 E_c)	64.9		64.9	174			174
	Observed	73.1	69.6	71.4	193	183	194	190
Creep and Shrinkage	PCI (AASHTO E_c)	145		145	262			262
	AASHTO (AASHTO E_c)	131		131	287			287
	PCI (ACI 363 E_c)	144		144	258			258
	AASHTO (ACI 363 E_c)	131		131	287			287
	Observed	148	142	145	224	178	240	214
Relaxation	PCI (AASHTO E_c)	29.4		29.4	21.7			21.7
	AASHTO (AASHTO E_c)	26.5		26.5	5.4			5.4
	PCI (ACI 363 E_c)	28.9		28.9	21.1			21.1
	AASHTO (ACI 363 E_c)	25.7		25.7	3.2			3.2
	Observed	24.3	23.9	24.1	19.7	22.5	18.5	20.2
Deck Casting	AASHTO E_c	-17.2		-17.2	-51.1			-51.1
	ACI 363 E_c	-20.1		-20.1	-59.4			-59.4
	Observed	-15.3	-9.7	-12.5	-40.1	-37.9	-34.4	-37.5

7.9 ESTIMATED EFFECT OF USING HPC ON PRESTRESS LOSSES

Many researchers have speculated that using HPC will decrease prestress losses. In this section, the estimated effect of using HPC on elastic shortening (Section 7.9.1) and creep losses (Section 7.9.2) are investigated.

7.9.1 Estimated Elastic Shortening Losses for HPC

The form of Equations 7.1 and 7.2 show that the use of HPC is likely to increase the elastic modulus. For example, if the equation to calculate the elastic modulus is in the form of

$$E_{ci} = C_1(f'c)^r \tag{7.3}$$

then an increase in f'c will increase E_{ci}. However, if the concrete stress at transfer is controlled by the bottom compression, causing a stress at the cgp of C_2f'c, the elastic shortening loss will be in the form of Equation 7.4.

$$\Delta f_{pES} = \frac{C_2 f'c}{C_1(f'c)^r} = \frac{C_2}{C_1} f'c^{(1-r)} \tag{7.4}$$

Values of r recommended by various authors (ACI 363 1990, Ahmad and Shah 1995, ACI 318 1995, Nawy 1996 etc) lie in the range of 0.3 to 0.50. Therefore the elastic shortening loss will rise with some power, greater than or equal to 0.5, of the compressive strength.

7.9.2 Expected Creep Losses for HPC

The effect of using HPC on creep loss depends on the relationship between the creep coefficient (C_C) and the concrete compressive strength (f'c). The creep coefficient is defined as

$$C_c = \frac{\varepsilon_{cr,ult}}{\varepsilon_{el}} \tag{7.5}$$

where C_c = creep coefficient

$\varepsilon_{cr,ult}$ = ultimate concrete strain due to a sustained stress

ε_{el} = strain due to elastic shortening

Equation 7.4 provides an expression for the initial change in prestress force due to elastic shortening. The loss due to creep, Δf_{pCR}, is usually assumed to be proportional to the initial change in stress, Δf_{pES}, and the creep coefficient.

$$\Delta f_{pCR} \approx C_c \Delta f_{pES} = \frac{C_2}{C_1}\left[C_c f'c^{(1-r)}\right] \tag{7.6}$$

Thus, Δf_{pCR} is proportional to $C_c f'c^{(1-r)}$. In general, C_C is believed to fall with increasing concrete compressive strength (f'c), but the rate at which it falls is open to question. For example, data from Nilson (1991) is given in Table 7.8.

Table 7.8. Typical Creep Parameters (Nilson 1991)

f'c (MPa)	C_C
20.7	3.1
27.6	2.9
41.4	2.4
55.2	2.0
68.9	1.6
82.7	1.4

A best-fit power curve using the data in Table 7.8 was obtained from a log-log plot and is shown in Figure 7.14.

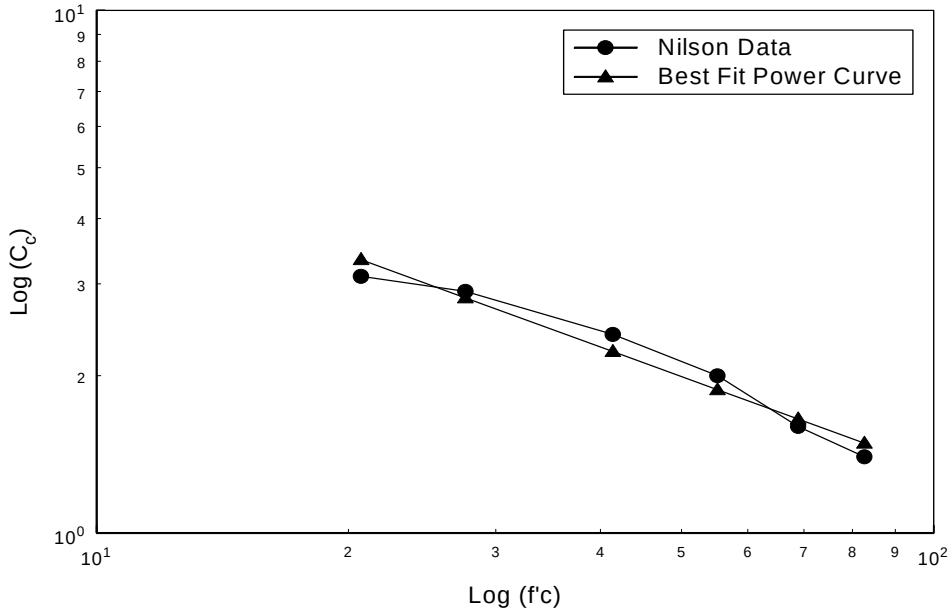

Figure 7.14. Best Fit Power Curve for Creep Coefficient vs. Compressive Strength

The equation for the-best fit power curve is in the form shown in Equation 7.7.

$$C_C = a(f'c)^{-p} \tag{7.7}$$

where a = 19.6

p= 0.5843

If Equations 7.6 and 7.7 are combined, the stress loss due to creep can be written as

$$\Delta f_{pCR} = \frac{aC_2}{C_1}\left[f'c^{(1-r-p)}\right] \tag{7.8}$$

Figure 7.15 shows the normalized creep loss as a function of concrete compressive strength (f'c) for various (1-r-p) values. The normalized creep loss is defined as the creep loss associated with a 34.5 MPa (5 ksi) concrete.

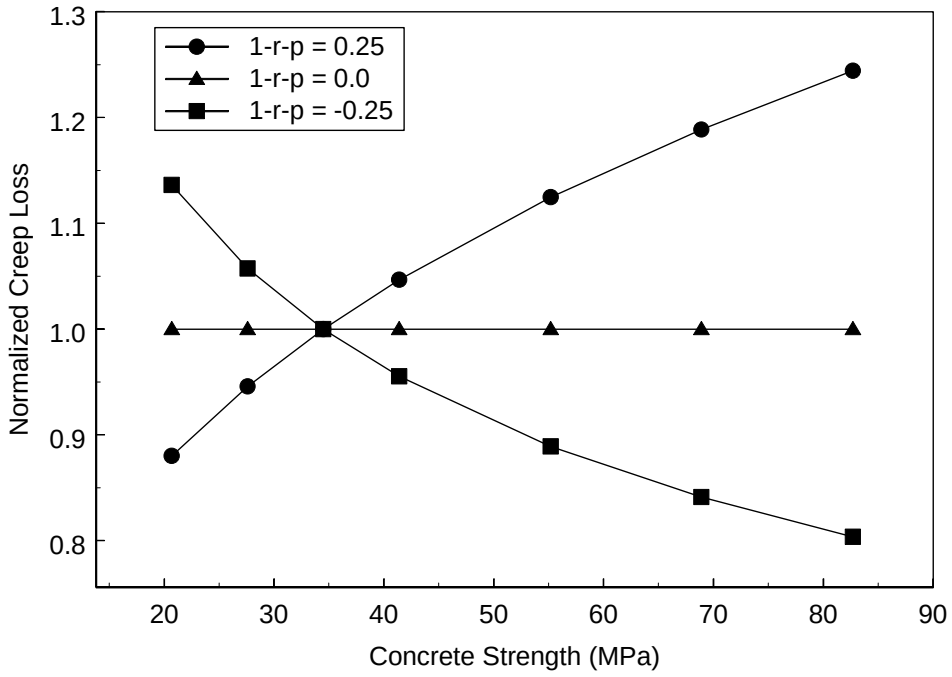

Figure 7.15. Normalized Creep Loss versus Concrete Strength

Figure 7.15 shows that the creep loss for a prestressed concrete girder would be expected to decrease for stronger concrete if the value of (1-r-p) is less than zero. The Euro-International Concrete Committee (CEB) Model (Macgregor 1997) assumes that p in Equation 7.8 is 0.5. The combination of r = 0.5 (Equation 7.1) with p = 0.5 (CEB Model for creep) (MacGregor 1997) would lead to the conclusion that the creep loss is independent of concrete strength. However, Nilson's values for the creep coefficient (p = 0.58) combined with r = 0.5 (Equation 7.1) suggest that the creep loss would actually increase with compressive strength. If the value of r is actually less than 0.5, as

some authors have suggested (Ahmed and Shah 1985), then one would expect the creep loss to decrease with increasing concrete compressive strength. This trend is opposite to the trend in the AASHTO LRFD Specifications (AASHTO 1994) as shown in Equation 2.6 which predicts a decrease in prestress loss due to creep with an increase in compressive strength. This analysis shows that loss of prestress cue to creep depends on factors that may counteract each other as the concrete strength is changed. High strength concrete may result in either more or less prestress loss than that found in conventional concrete, depending on the properties of the mix and the details of the analytical model used to describe the behavior. Therefore the use of HPC should not be assumed automatically to decrease the prestress loss due to creep.

CHAPTER 8

COMPARISON OF CALCULATED AND OBSERVED CAMBERS

In this chapter, observed and estimated values of camber are compared. In Section 8.1, the observed values of total girder camber (Section 5.2.3) are compared with estimated values calculated using the recommended PCI multipliers (PCI 1992). The observed camber due to differential shrinkage is compared with predicted camber in Section 8.2.

8.1 PCI METHOD (1992)

The PCI method (PCI 1992) for estimating long-term camber consists of applying long-term deflection multipliers to the immediate elastic deflections. The upward and downward components of the immediate elastic deflection are separated, because the upward component due to prestressing will be influenced by both creep and prestress loss, whereas the downward component will be influenced by creep alone. Equation 8.1 calculates the initial downward deflection at midspan due to the weight of a simply supported girder.

$$\Delta_{sw} = \frac{5 * w_{sw} * L^4}{384 * E_{ci} * I} \tag{8.1}$$

where Δ_{sw} = downward deflection due to self weight

w_{sw} = self weight of girder (0.012 KN/mm for ρ=2480 kg/m^3 (0.0670 kips/in. for ρ=155 lbs/ft^3))

L = girder span

E_{ci} = modulus of elasticity at transfer

I = girder moment of inertia (228x10^9 mm^4 (547,000 in^4))

The initial upward camber is caused by the eccentric prestressing force after transfer. Equation 8.2 predicts the upward midspan camber after transfer for a prestressed girder with two harping points.

$$\Delta ps = \frac{P * L^2}{8 * Eci * I}\left[ec + (ee - ec)\frac{4}{3}\frac{a^2}{L^2} \right] \qquad (8.2)$$

where Δ_{ps} = camber due to prestressing force

P = prestressing force in tendons after transfer

e_c = eccentricity of prestressing strand at midspan

e_e = eccentricity of prestressing strand at end

a = distance from end of girder to harping point

According to the PCI method, the deflection of a girder before slab casting is estimated by applying PCI multipliers of 1.80 to the upward elastic deflection caused by prestressing and 1.85 to the downwards elastic deflection caused by girder weight (PCI 1992).

The deflection after slab casting is the deflection before slab casting plus the downward deflection due to the casting of the deck. The equation for the downward deflection due to the casting of the deck is the same as Equation 8.1, except that the weight of the girder is replaced by the tributary weight of the slab (0.014 KN/mm (0.082 kips/inch)), and the initial elastic modulus is replaced with the girder modulus at deck casting.

The predicted long-term camber values are obtain by multiplying the camber due to the prestressing force by 2.2, the deflection due to self weight by 2.4, the deflection due to deck casting by 2.3 and the deflection due to any superimposed dead load by 3.0.

8.2 CALCULATED AND MEASURED CAMBERS

Figures 8.1 and 8.2 show the PCI estimated cambers and the cambers measured with a surveyor's level. The measured cambers were discussed in Section 5.2.3. The predicted camber was calculated at transfer, before the slab was cast, after the slab was cast, and at service for the Span 1 and Span 2 girders. The modulus of elasticity was calculated using the equation in the AASHTO LRFD Specifications (AASHTO 1994) with a concrete compressive strength of 51.0 Mpa (7.4 ksi) for the deflection at release and 68.9 MPa (10 ksi) for the deflection at the time the slab was cast.

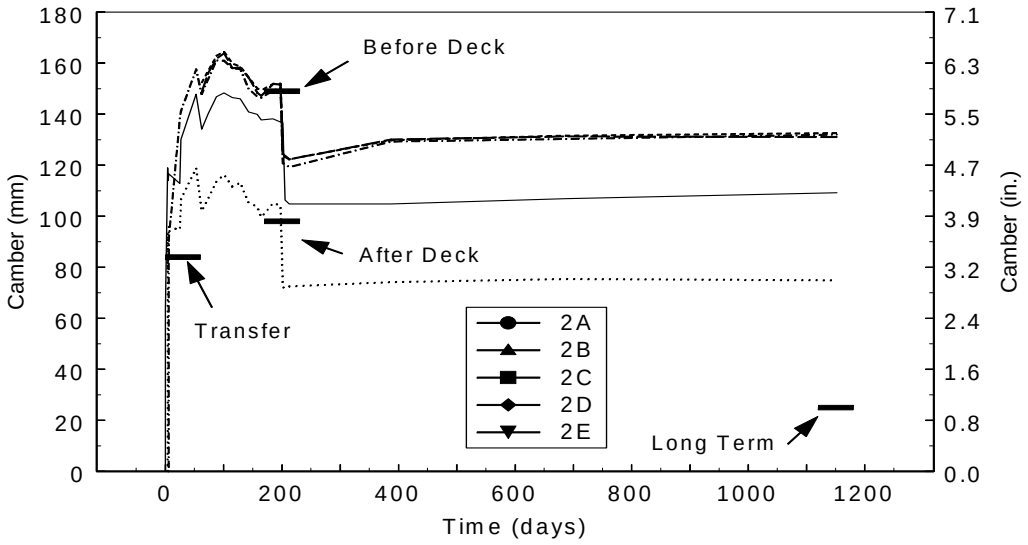

Figure 8.1. Comparison of Calculated and Measured Cambers for Span 2

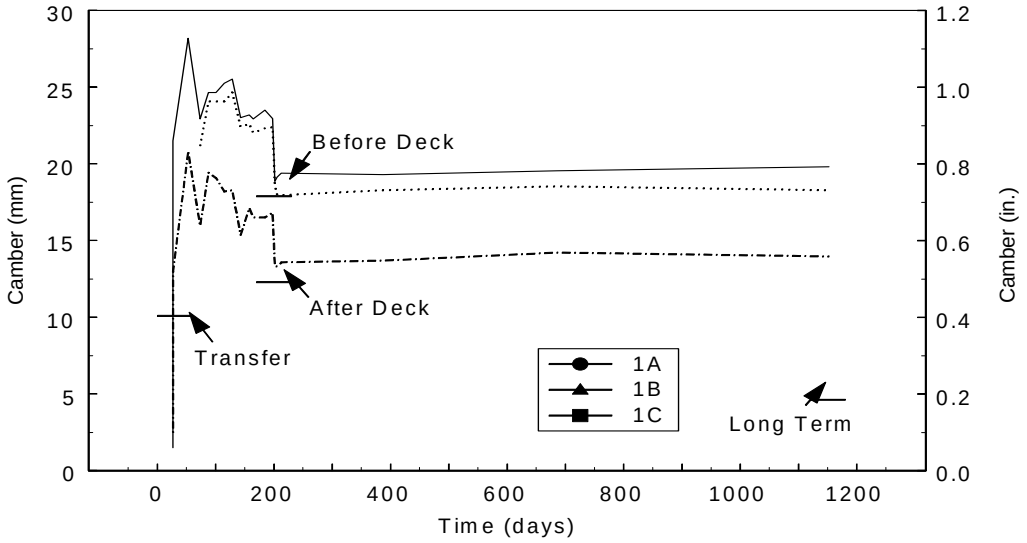

Figure 8.2. Comparison of Calculated and Measured Cambers for Span 1

Table 8.1 compares the average girder camber values measured in Span 1 and Span 2 with the predicted PCI camber values using elastic modulus values calculated with both the AASHTO LRFD Specification (1994) equation (Equation 7.1) and the ACI 363 (ACI 1990) equation for high-strength concrete (Equation 7.2).

Table 8.1. Comparison of PCI Predicted and Measured Cambers (mm)

	Time	Average Measured	AASHTO E_c	Predicted/ Measured	ACI E_c	Predicted/ Measured
Span 2	Transfer	68	84	1.23	104	1.53
	Before Deck	130	149	1.15	184	1.42
	After Deck	100	98	0.98	120	1.20
	Long Term	105	25	0.24	26	0.25
Span 1	Transfer	4	10	2.5	12	3.0
	Before Deck	21	18	0.86	22	1.05
	After Deck	17	12	0.71	15	0.88
	Long Term	17	5	0.29	5	0.29

The PCI method for calculating deflections overestimated the deflection for both Span 1 and Span 2 girders at transfer, regardless of the choice of elastic modulus equation. In general, the discrepancy between the average measured camber and the estimated PCI camber was larger when the elastic modulus from ACI 363 (ACI 1990) was used. However, the elastic modulus calculated using ACI 363 expression for E_c is the most similar to that measured on material samples in the lab. Other possible explanations for the lower camber measurement are:

- the temperature gradient present during curing influenced the initial camber
- the prestress force was somehow smaller than estimated

The temperature gradient present during curing could account for some of the difference in measured and predicted cambers at release. The change in concrete temperature at the top of the girder was the largest after the steam was turned off and the forms were removed (Figure 5.1). The top of the girder would therefore contract causing,

a downward deflection. This downward deflection would be superimposed onto the initial camber and the net camber would therefore be lower than expected.

Another possible explanation of the low initial camber is that the strand force was reduced as a result of curing temperature. This could occur if strand stress is reduced by expansion of the strand due to the high curing temperatures, or an increase in relaxation loss due to the high curing temperature. A reduction in prestress force would decrease the initial camber.

The long-term deflection was consistently underpredicted by the PCI multipliers, regardless of the source of elastic modulus. For the Span 2 girders, the long-term camber was only 23% of the camber estimated using the elastic modulus from the AASHTO LRFD Specifications (1994) and only 12% of the camber estimated using the elastic modulus from ACI 363 (1990). Most of the error was caused by inaccurate prediction of the effects of the slab weight.

8.2 CAMBER DUE TO DIFFERENTIAL SHRINKAGE

For a simply supported girder, the deflection due to differential shrinkage can be calculated as

$$\Delta_{DS,SS} = -\frac{\phi_{DS} L^2}{8} \tag{8.3}$$

where $\Delta_{DS,SS}$ = deflection due to differential shrinkage of simply supported girder

ϕ_{DS} = curvature of composite system caused by differential shrinkage

$$= \frac{-Q_d e_d}{(EI)_{comp}}$$

Q_d = restraint force

$= -A_d E_d \varepsilon_{sh}$

A_d = cross-sectional of deck

E_d = young's modulus of deck concrete

ε_{sh} = free shrinkage strain

e_d = distance from centroid of composite system to centroid of deck

L = length of girder

$(EI)_{comp}$ = flexural stiffness of composite system

Figure 8.3 shows the primary, secondary and total curvatures of a continuous three span bridge subjected to differential shrinkage.

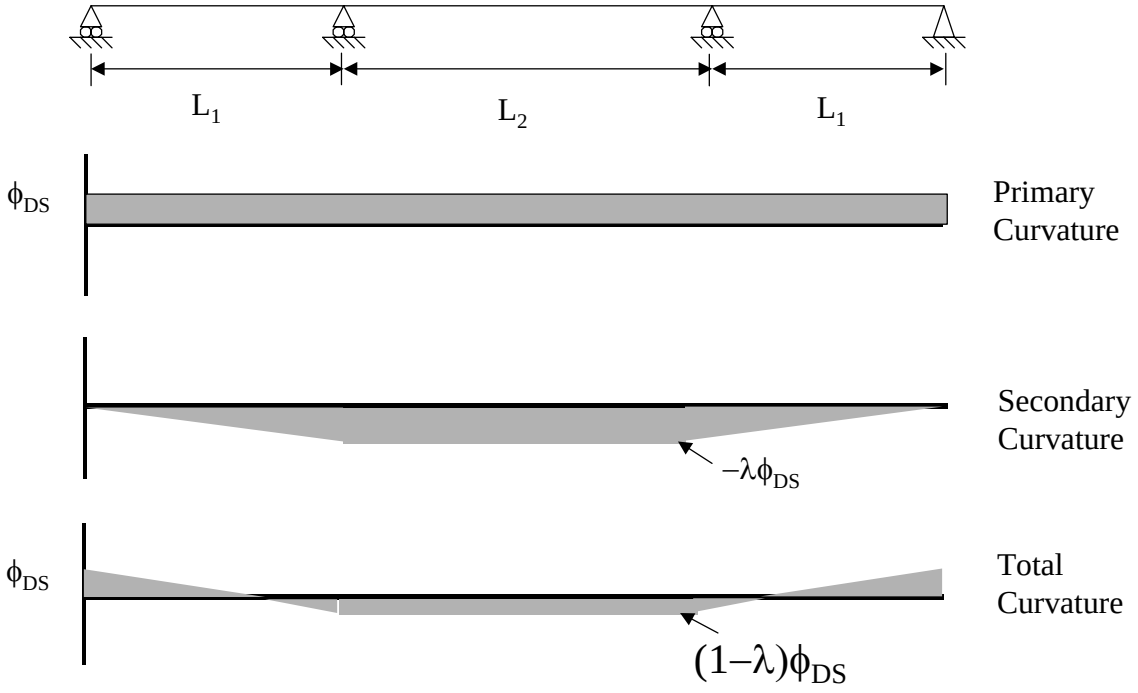

Figure 8.3. Curvature Diagram for Three-Span Bridge

The total curvature for a three-span bridge subjected to differential shrinkage was obtained by summing the primary and secondary curvatures that are induced due to the differential shrinkage. The secondary curvature factor, λ, is given as

$$\lambda = \frac{L_1 + L_2}{\left(\frac{2}{3}L_1 + L_2\right)} \tag{8.4}$$

where λ = secondary curvature factor

L_1 = length of Span 1

L_2 = length of Span 2

The deflection at midspan of Span 2 can be calculated as

$$\Delta_2 = \frac{(1-\lambda)\phi_{DS}{L_2}^2}{8} \tag{8.5}$$

where Δ_2 = deflection at midspan of Span 2 (positive is downwards). The deflection at midspan of the spans 1 and 3 can be calculated as

$$\Delta_1 = \phi_{DS}{L_1}^2\left(\frac{\lambda}{16} - \frac{1}{8}\right) \tag{8.6}$$

The predicted and measured camber changes attributable to differential shrinkage are listed in Table 8.2. The material properties used to obtain the calculated values are the same as those used in Section 7.5.2.

Table 8.2. Comparison of Camber Due to Differential Shrinkage at Three Year

	Span 1	Span 2
Average Measured **(**mm**)**	-0.44	-6.4
Predicted (Simply Supported) **(**mm**)**	15.4	42.5
Predicted (Continuous) **(**mm**)**	6.6	-5.9

The continuous model provided the best prediction of camber for both spans. In Span 2, the predictions were very close. In Span 1, the predictions were within 6 mm, but, because the measured cambers were so small, the relative accuracy was poor.

The continuous model is a simplification of the true structure, but a more complex model was not used because of lack of reliable material data (i.e. the rate of creep and shrinkage). Characteristics to be taken into account in a more complex model should include

- Changes in the structural confirmation over time. For example, the deck was cast in the spans first, and was made continuous over the piers two weeks later.
- Translational and rotational restraint at the interior supports provided by the flexural stiffness of the columns.

CHAPTER 9

CONCLUSIONS

This research focused on evaluating the effectiveness of using High-Performance Concrete (HPC) in precast, prestressed concrete girders. HPC was used in the fabrication of fifteen W74MG girders for a bridge located in Washington State (SR18/516 Overcrossing). The use of HPC permitted WSDOT engineers to reduce the number of girder lines from seven to five. To obtain the required prestressing force, while maintaining the minimum 50 mm (2 inch) strand spacing needed for bond, the prestressing strands size was increased from the normal 12.7 mm diameter to 15.2 mm diameter (0.5 in. to 0.6 in. diameter).

Five bridge girders were instrumented and monitored for three years. The observed behavior of the instrumented bridge girders was compared with the behavior predicted with current design methods. This chapter summarizes the research and its conclusions.

9.1 FABRICATION

The fabricator used externally applied steam to attain the required release strength of the concrete as rapidly as possible. Nonetheless, the average curing time until the start of destressing was slightly over 25 hours for each of the five instrumented girders (Table 5.2). This rapid curing raises two problems. First, requiring a high concrete strength at release may force the fabricator to implement a two-day fabrication cycle. The economic impacts of this choice should be considered during design. Second, curing at high temperature improves the short-term strength needed at release, but detracts from the long-term strength. The need for high strength at release is not in question, but the real needs for high, long-term strength should be carefully assessed.

During the steam curing, the internal concrete temperatures varied approximately 25 °C (45 °F) over the depth of the girder (Figure 5.1). The lowest temperatures were recorded at the bottom of the girders, which consequently had the lowest maturity and, by

implication, the lowest concrete strength. This finding is significant, because it means that the weakest concrete was located where the compressive stress was the highest. This temperature gradient is likely to be most significant in girders that are cast outdoors during the winter.

The fabricator used a thermocouple in the girder that was connected to a Sure-Cure system to monitor concrete strength prior to strand release. The thermocouple was placed at mid-height for all of the girders (except Girder 2B, in which it was placed 457 mm (18 inches) from the bottom of the girder). Consequently, the concrete at the bottom of the girder was weaker than the concrete in the cylinders connected to the Sure-Cure system. Again, this finding is significant, because it means that the most highly stressed concrete may have been weaker than the concrete in the Sure-Cure cylinders.

Twenty-four strands were instrumented to measure end slip. For nineteen of these strands, the computed transfer length exceeded the 914 mm (36 inches) predicted by the AASHTO prediction method (AASHTO 1994). The unexpected long transfer length would be expected to decrease the shear strength of the girders.

9.2 OBSERVED PRESTRESS LOSSES

Table 9.1 lists the average observed and calculated (using the PCI General method or the AASHTO LRFD Method) prestress losses for the five instrumented girders after three years.

Table 9.1. Comparison of Prestress Losses after Three Years

Losses	Calculation Method	Span 1		Span 2	
		MPa	% of Observed	MPa	% of Observed
Total	PCI (AASHTO E_c)	216	94	380	98
	AASHTO (AASHTO E_c)	198	86	398	103
	PCI (ACI 363 E_c)	219	95	382	99
	AASHTO (ACI 363 E_c)	202	88	406	105
	Average Observed	230	100	386	100
Elastic Shortening	PCI (AASHTO E_c)	59.4	84	146	77
	AASHTO (AASHTO E_c)	58.1	81	157	83
	PCI (ACI 363 E_c)	65.8	92	161	85
	AASHTO (ACI 363 E_c)	64.9	91	174	92
	Average Observed	71.4	100	190	100
Creep and Shrinkage	PCI (AASHTO E_c)	145	100	262	122
	AASHTO (AASHTO E_c)	131	90	287	134
	PCI (ACI 363 E_c)	144	99	258	121
	AASHTO (ACI 363 E_c)	131	90	287	134
	Average Observed	145	100	214	100
Relaxation	PCI (AASHTO E_c)	29.4	121	21.7	107
	AASHTO (AASHTO E_c)	26.5	109	5.4	27
	PCI (ACI 363 E_c)	28.9	119	21.1	104
	AASHTO (ACI 363 E_c)	25.7	106	3.2	16
	Average Observed	24.3	100	20.2	100
Deck Casting	AASHTO E_c	-17.2	138	-51.1	141
	ACI 363 E_c	-20.1	161	-59.4	164
	Average Observed	-12.5	100	-36.2	100

Some of the features of the observed losses are summarized as follows.

- The total average observed prestress losses for the Span 2 long-span girders (2A, 2B and 2C) constituted 28% of the total jacking stress of 1396 MPa (202.5 ksi).

For the short-span girders (1A and 1C), the total average losses constituted approximately 16% of the total jacking stress.

- The average observed elastic shortening losses for the long-span girders 2A, 2B and 2C constitute approximately 14% of the total jacking stress. For girders 1A and 1C, the elastic shortening loss constitute only 5% of the total jacking stress.
- The average observed creep and shrinkage losses after three years for girders 2A, 2B and 2C constitute 15% of the total jacking stress. For girders 1A and 1C, the average creep and shrinkage losses constitute approximately 10% of the total jacking stress. Between 7% to 14% of the creep and shrinkage losses occurred during destressing. The magnitude of the contribution depended on the time needed for destressing. For a given span length, the magnitude of the creep and shrinkage losses correlated well with the maturity of the concrete at destressing (Table 6.3).
- In general, prestress losses may be higher in HPC girders than in girders made with conventional concrete (Section 7.9). The elastic shortening and creep components dominate the losses. The elastic shortening component will almost certainly be higher because the applied stress will likely increase in direct proportion to the release strength, whereas the Young's modulus (E_{ci}) is usually treated as increasing only with the square root, or even some lower power, of concrete strength. Whether the creep component is larger depends on E_{ci}/C_c, where C_c is the creep coefficient.

9.3 COMPARISON WITH CALCULATED PRESTRESS LOSSES

Losses were calculated using the PCI (1979) and AASHTO methods (1994). The elastic modulus used in each of these methods was calculated according to the AASHTO LRFD Specifications (1994) and the ACI Committee 363 guidelines (ACI 1990). The ACI 363 equation for calculating the elastic modulus was developed specifically for high-strength concrete, but it was calibrated against data with compressive strengths between 35 and 85 MPa (Carasquillo et al. 1980).

The average total observed prestress losses ranged from 13% lower to 5% higher than the total prestress loss calculated with either the PCI method or the AASHTO Method. The calculated total losses are particularly close to the total observed losses when the ACI 363 (ACI 1990) equation was used to calculate the elastic modulus. This apparently good prediction masks poor prediction of the individual components of loss. This result does not suggest that either method would be reliable with other materials and stress states.

On average, the observed elastic shortening losses were found to be 8% to 23% higher than the elastic shortening losses calculated with the PCI and AASHTO methods when the WSDOT design unit weight of concrete of 2480 kg/m^3 (0.155 kcf) was used. If the actual unit weight of concrete was used (2400 kg/m^3 (0.150 kcf)), the predicted elastic shortening losses for both methods increased by 5%. In comparison to the PCI method, the AASHTO method predicted larger elastic shortening losses for the Span 2 girders, but smaller losses for the Span 1 girders.

The observed losses for creep and shrinkage were between 19% lower to 3% higher than the losses calculated with the PCI method. The observed losses for creep and shrinkage ranged from 10% lower to 35% higher than the losses calculated with the AASHTO method. The PCI Method predicted creep and shrinkage losses closer to the average measured losses in comparison to the AASHTO Method. The PCI and AASHTO methods over predicted the creep and shrinkage losses for the Span 2 girders. The AASHTO method under predicted the creep and shrinkage losses for the Span 1 girder, but the PCI method came fairly close to the observed values.

Relaxation loss could not be measured in the girders because it could not be separated from the other time dependent effects. Therefore estimates based on manufacturer's data that were adjusted to take into account elastic shortening, creep and shrinkage were used in place of the measured values. The predicted relaxation losses ranged from 85% lower to 23% higher than the estimated values. Although this relative error is large, the absolute error is still small, because relaxation contributes so little to the total loss. The predicted losses using the AASHTO method differed the most in

comparison to the estimated relaxation losses. The AASHTO method correctly predicts smaller relaxation losses with increasing elastic shortening, creep and shrinkage losses. Theoretically, the relaxation losses predicted using the AASHTO method could become negative under certain circumstances.

The measured magnitude of gain in prestress due to deck casting was on the same order of magnitude as the relaxation losses. The predicted gain in prestress was up to three times larger than the observed change. This discrepancy is attributed to the fact that the SR18/SR516 girders experienced partial longitudinal restraint at the bottom flange level due to concrete that was placed over the piercaps between the girders. This concrete locked the girders to the piercaps and induced longitudinal resistance to the column stiffness.

9.4 CAMBER

Camber was monitored with a stretched-wire system, and intermittently, with a surveyor's level. Both systems were capable of an accuracy of approximately ±1 mm, but the stretched-wire system could only be mounted when no construction activities were taking place. At three years, the cambers for Girders 2C, 2D and 2E were all approximately 132 mm (5.2 inches), while the cambers for girders 2A and 2B were 24 and 57 mm (0.9 and 2.2 inches) lower. The anomalous camber in Girder 2B is thought to be attributable to differences in curing time prior to release. The cambers for the Span 2 girders used up nearly all the elevation tolerance (95 mm (3.75 inches)) built into the lift/pad. At three years, the camber for girders 1A and 1B was about 19 mm (0.75 inches), while the camber in girder 1C was approximately 14 mm (0.55 inches).

During the course of a typical late summer day, the peak-to-peak camber variation in the long girders was approximately 20 mm (0.8 inches). This variation is attributed to daily thermal effects. On the same day, the peak-to-peak thermal camber for the short girders ranged from 5.1 to 8.1 mm (0.2 to 0.32 inches). The minimum and maximum camber readings occurred at 6:00 a.m. and 3:00 p.m., respectively. The minimum and maximum temperature readings for the same day occurred at 4:30 p.m. and 6:15 a.m.

The difference in time between maximum girder temperature and maximum camber is attributed to the fact that the thermal camber depends on temperature gradient rather than absolute temperature. Camber due to temperature gradients will be more of an issue with HPC, since the girders will typically be more slender, and the stresses higher, than girders built with conventional concrete.

9.5 RESEARCH RECOMMENDATIONS

A designer needs to be able to predict the prestress losses and cambers for the concrete mix to be used. Ideally, this prediction is done with an instrumentation program, but performing an instrumentation program for every mix would not be feasible. A more economical approach would be to perform materials testing that could be used to calibrate a prestress loss model. Research is needed to provide the link between creep and shrinkage observed in the laboratory, and creep and shrinkage to be expected in the field.

This study identified the critical need to improve the means of predicting girder creep and shrinkage based on the measured behavior of cylinders. To achieve this goal, it is necessary to closely simulate in the laboratory specimens the curing conditions and time of loading of the girders. Greater consistency between the cylinder and girder strains could be achieved by conducting a laboratory testing program in which the mix proportions, curing conditions, and time of loading were more carefully controlled than was possible in this study. The measured strains appear to be very sensitive to the curing history, age at loading and environmental conditions. Such a study would also permit investigation of the use of maturity as a measure of the intrinsic age of the concrete.

This project was one of several similar projects being performed in several states. The prestress losses and camber values from girders various states need to be compared and efforts made to construct a robust analytical model that will reliably predict prestress losses and camber changes for a wide range of materials and construction conditions.

REFERENCES

ACI MANUEL OF CONCRETE PRACTICE. *PART 1 – MATERIALS AND GENERAL PROPERTIES OF CONCRETE.* DETROIT, MICHIGAN. 1990.

AHMAD, S. H., AND SHAH, S. P. "STRUCTURAL PROPERTIES OF HIGH STRENGTH CONCRETE AND ITS IMPLICATIONS FOR PRECAST PRESTRESSED CONCRETE." *PRESTRESSED CONCRETE INSTITUTE JOURNAL.* VOLUME 30, NO.6, NOVEMBER/DECEMBER 1985.

American Association of State Highway and Transportation Officials. *Standard Specifications for Highway Bridges.* 1st Edition LRFD. Washington, D.C. 1994.

American Concrete Institute (ACI). *Building Code Requirements for Structural Concrete.* Farmington Hills, Michigan. 1995.

Burns, N. H., and B. W. Russell. "Measured Transfer Lengths of 0.5 and 0.6 inch Strands in Pretensioned Concrete Girders." *Prestressed Concrete Institute Journal.* Volume 41, No.5, September/October 1996, pp.44-63.

Barr, P. J. "Behavior of High Performance Prestressed Concrete Girders." Master's Thesis. University of Washington. 1998.

Barr, P. J., Fekete, E., Stanton, J. F., Eberhard, M. O., Janssen, D. "High Performance Concrete in Washington State SR 15/ SR 516 Overcrossing: Final Report on Materials Tests." Washington State Department of Transportation Bridge and Structures Office, report, Olympia, Washington, 2000a.

- Barr, P.J., Stanton, J.F., Eberhard, M.O. "Live Load Distribution Factors for Washington State SR18/SR516 Overcrossing." Washington State Department of Transportation Bridge and Structures office, report WA-RD 477.1, Olympia, Washington, 2000b.

Carrasquillo, R. L., Nilson, A. H., Slate, F. O. "Microcracking and Engineering Properties of High-Strength Concrete." *Report No. 80-1*. Department of Structural

Engineering School of Civil and Environmental Engineering, Cornell University, Ithaca, New York.

Fekete, E. "Prestress Losses in High Performance Concrete Girders." Master's Thesis. University of Washington. 1997.

Ghali, A. and Farve, R. *Concrete Structures Stresses and Deformations.* E & FN Spon. London. 1994.

Goodspeed, C. H., Vanikar, S., & Cook, R. A. "High-Performance Concrete Definition for Highway Structures". *Concrete International*. Volume 18, No.2, February 1996, pp.62-67.

Lew, H. S., and Reichard, T. W. "Prediction of Strength of concrete from Maturity." *Accelerated Strength Testing.* ACI Publication SP-56, American Concrete Institute, 1978, pp.229-248.

Logan, D. "Acceptance Criteria for Bond Quality of Strand for Pretensioned Prestressed Concrete Applications." *Prestressed Concrete Institute Journal.* Volume 42, No.4, March/April, pp.52-90.

Lwin, M. M., and Khaleghi, B. "Time-Dependent Prestress Losses in Prestress Concrete Girders Built of High Performance Concrete (Preprint)." Transportation Research Board. 76th Annual Meeting. January 1997.

FHWA, The National Bridge Inventory. US Department of Transportation, Federal Highway Administration, Washington, D.C. July 1997.

MacGregor, J. G. *Reinforced Concrete Mechanics and Design*. Third Edition. Prentice Hall. New Jersey. 1997.

Nawy, E. G. *Prestressed Concrete A Fundamental Approach.* Prentice-Hall. New Jersey. 1989.

Nawy, E. G. *Fundamentals of High Strength High Performance Concrete.* Longman Group Limited. London. 1996.

Nilson, A. H. *Design of Prestressed Concrete*. Second Edition. John Wiley & Sons. New York. 1987.

Nilson, A. H., Winter, G. *Design of Concrete Structures.* McGraw-Hill Inc. New York, New York. 1991.

PCI Committee on Prestress Losses. “Recommendations for Estimating Prestress Losses.” *Prestressed Concrete Institute Journal.* July/August 1975, pp.44-75.

PCI Industry Handbook Committee. *PCI Design Handbook.* Fourth Edition. Precast/Prestressed Concrete Institute. Chicago. 1992.

Russell, B. W., and Dallas R. R. “Investigation of Standardized Tests to Measure the Bond Performance of Prestressing Strand.” *Prestressed Concrete Institute Journal.* July/August 1997.